Strangeness-exchange interactions at high energies

Irving, Alan C.

STRANGENESS-EXCHANGE INTERACTIONS

AT

HIGH ENERGIES

THESIS SUBMITTED TO

THE UNIVERSITY OF DURHAM

BY

ALAN C. IRVING, B.Sc. (GLASGU.)

FOR THE DEGREE OF DOCTOR OF PHILOSOPHY

DEPARTMENT OF PHYSICS
UNIVERSITY OF DURHAM

DATE: JULY 1972

CONTENTS

ABSTRACT

In Chapter 1 we discuss the importance of a study of high energy strangeness-exchange reactions in elucidating the exchange mechanisms and symmetry properties of meson-baryon scattering. The cross-section and polarisation data for $\bar{K}N \to \pi\Sigma, \Lambda$ and $\pi N \to K\Sigma, \Lambda$ are reviewed in Chapter 2. An exchange-degenerate poles with weak cuts model for the data is proposed, and the resulting successful polarisation and unsuccessful cross-section descriptions are discussed. The model's failure to reproduce the well-known line reversal cross-section inequality at intermediate energies is interpreted in terms of low energy resonance effects.

A unified treatment of non-zero exotic exchange processes and line reversal symmetry violation in terms of Regge-Regge cuts is presented in Chapter 3. After a theoretical appraisal of a multiple scattering approximation for these cuts we present explicit calculations of the exotic strangeness-exchange cross-sections for $K^- p \to \pi^+ \Sigma^-$ and $\pi^- p \to K^+ \Sigma^-$. It is shown that the small size of the data for these is not easily explained. Since we also show that the inclusion of non-leading cuts aggravates the disagreement between data and the leading cuts model, the usefulness of Regge-Regge cut descriptions at intermediate energies is called into question.

In Chapter 4 we propose an alternative method of obtaining, from the data, information about strangeness-exchange amplitudes. It is shown how a study of joint decay correlations can yield an almost complete production amplitude determination. Using the process $\pi^- p \to K^* \Lambda$ as an example, we present an efficient means of accomplishing this and interpret the ensuing numerical results making comparisons with the model of Chapter 2.

Some conclusions are recorded in Chapter 5.

ACKNOWLEDGEMENTS

I thank Dr. Alan Martin for his continuing generous and friendly guidance. My interest in the subject of elementary particle physics owes much to his enthusiastic influence.

I am also grateful to Professor B.H. Bransden and to Dr. C. Michael from whom I have received much assistance and encouragement.

Useful conversations with many of my colleagues in the Departments of Physics and Mathematics at Durham University are acknowledged. I have also benefitted from discussions with Professor V. Barger.

Part of the work presented in this thesis (where noted) was done in collaboration with Drs. M. Abramovich, A.D. Martin and C. Michael. Their co-operation is gratefully acknowledged. I also thank the CERN theory division for hospitality while some of this work was undertaken.

My thanks are due to Mrs. J. Henderson for her careful and patient typing of this thesis.

For the award of a research studentship and travel grants, I thank the Science Research Council.

Finally, I am indebted to my wife Catriona for financial and moral support.

C H A P T E R O N E

I N T R O D U C T I O N

1 : INTRODUCTION

1.1 The elementary particles

In the past two decades an increasing number of so-called elementary particles have been observed in high energy scattering experiments. Subsequent theoretical efforts have been directed towards classifying these into multiplets according to a set of quantum numbers describing their internal symmetry properties, and according to their physical characteristics such as mass and spin. Most of these particles or resonant states can exhibit half-lives and interaction times which are orders of magnitude shorter than those of the typical electromagnetic interactions, and are grouped together as a class and denoted hadrons[1] (or strongly interacting particles). This thesis concerns some aspects of the interactions among members of this class.

Quantum numbers found to be useful, since they correspond to conserved quantities in strong interactions, are parity (P), charge conjugation (C), G parity, baryon number (B), charge (Q), hypercharge (Y), strangeness (S)† and angular momentum (J). The existence of this last quantum number is a direct consequence of Lorentz invariance which assumption forms a cornerstone of the theory of elementary particles physics. The observation that hadrons occur in multiplets of particles e.g. $(\pi^-\pi^0\pi^+)$ possessing similar properties apart from their charge Q, can be explained by invoking a further invariance principle that of isospin (I). In the S-matrix formalism[1] of

†Y and S are not independent - see equation (1.1.1).

particle scattering which we shall adopt, the assumption of isospin invariance is implemented by postulating that the amplitudes which describe particle interactions are invariant under isospin-space rotations of the group SU(2). This assumption has been experimentally well verified as it had been previously in nuclear physics where it was first introduced.

In the same way that observed isospin multiplets were explained in terms of an underlying symmetry principle and its associated group structure, it was suggested by Gell-Mann[2] and Ne'eman[3] that the observed grouping of these isospin multiplets into higher multiplets (in fact singlets, octets and decuplets) of particles with similar properties, be explained by postulating some higher underlying symmetry. In this case the invariance of scattering amplitudes under rotations of the group SU(3) was postulated. The power of the assumption comes in relating the properties of isospin multiplets of different strangness, and a priori unrelated quantum numbers e.g. (K^o,K^+), (π^-,π^o,π^+) and $(K^-,\overline{K^o})$. It therefore gives an underlying meaning to the Gell-Mann Nishijima[4] rule

$$Q = I_3 + \frac{B+S}{2} \qquad (1.1.2)$$

I_3 being the third component of the isospin vector $\underset{\sim}{I}$.

Just why particles only seem to occur in multiplets which are SU(3) singlets octets or decuplets, is not known. The observed result can be reproduced however, by assuming each particle to be formed from combinations of fundamental triplets q and $\bar{q}$ of particles (quarks) which need have no

existence properties other than mathematical. In particular, if we assume mesons are formed from $q\bar{q}$ combinations we find only singlet and octet SU(3) representations may occur - just as is found experimentally. Mesons not expressible as $q\bar{q}$ and baryons as qqq are called exotics[5]. The experimental absence of such exotic particle states has profound implications for S-matrix theory via the concept of duality which will be introduced in the next section.

1.2 Analyticity of scattering amplitudes

In our S-matrix approach the complete information concerning a scattering process is contained in a (complex) scattering amplitude whose modulus-squared represents a probability. The conservation of probability then demands unitarity of the amplitude - a non linear relation among its matrix elements. Following the example of certain field theories it is supposed that intermediate particle or resonant states are to be associated with poles in the scattering amplitude when considered as a complex function of energy. It has so far been found sufficient to demand analyticity of the scattering amplitudes apart from these singularities and those generated from them by the (non-linear) unitarity condition.†

The assumption of analyticity in complex energy obviously imposes powerful constraints on the possible forms of scattering amplitudes, as does that of crossing

† A more precise definition of maximal analyticity of the first kind may be found in reference (1).

symmetry. In appendix 1A the definitions of the t- and u-channel processes which correspond to a given two-body process

$$a + b \longrightarrow c + d \qquad (1.2.1)$$

are given, along with a summary of our choice of kinematic variables. The assumption of crossing symmetry[6] is that the three analytic amplitudes describing the s-, t- and u-channel processes are analytic continuations of each other.

In summary, the unitarity condition together with the analyticity and crossing postulates leads to a picture wherein bound states (particle states below a given threshold) are manifest as poles in the amplitude on the real energy axis below a threshold branch point. Resonant states are seen as second sheet poles in the energy plane whose position describes the resonance width[7].

Resonance poles are clearly reflected in low energy scattering data for the reaction cross-sections. Their position in the energy plane can be reasonably well determined using phase shift analysis techniques[8] at energies near threshold but as one proceeds to energies several proton masses above this the resonant effects are less marked. The onset of smooth reaction cross-sections indicates that the resonances, if any, overlap and the low energy description of a scattering amplitude as a sum of resonance contributions ceases to be useful by itself. Fortunately in this kinematic region the angular momentum analyticity postulate can be of service in providing an analytic form with which to describe the amplitude. How this comes about is described in the following.

Having made a classical partial wave decomposition of the scattering amplitude

$$A(t,s) = \sum_{\ell=1}^{\infty} (2\ell+1) P_\ell(\cos\theta_t) f_\ell(t) \qquad (1.2.2)$$

where t is the total energy squared for the process

$$\bar{c} + a \longrightarrow \bar{b} + d \qquad (1.2.3)$$

we may postulate that the amplitude $f_\ell(t)$ is an analytic function of ℓ, apart from some specified singularities. It is then possible to convert the sum of equation (1.2.2) to a contour integral - the Sommerfeld - Watson transform. The procedure of continuing $f_\ell(t)$ to all complex ℓ was first justified in non-relativistic potential scattering by Regge[9] who showed that the amplitude developed poles (Regge poles) along some trajectories $\ell = \alpha_i(t)$ which for integer $\ell > -\frac{1}{2}$ could be associated with an exchanged "particle", regarded as providing the scattering potential.

The precise relevance of the above paragraph's arguments to fully relativistic elementary particle scattering is not clear but it would seem plausible that if hadronic scattering is controlled by a similar well-behaved (but short-range) potential, such Regge poles may also exist in hadronic amplitudes and be associated with physical particles.

The decomposition (1.2.2) which refers to the t-channel process (1.2.3) is thus expected to be expressible as contour integral term (the background integral) plus contributions from Regge poles of the form[10],

$$R(s,t) \simeq \sum_i \beta_i(t) \frac{1 \pm e^{-i\pi\alpha_i(t)}}{\sin \pi\alpha_i(t)} P_{\alpha_i}(\cos\theta_t) \qquad (1.2.4)$$

The crossing symmetry postulate then allows us to describe the s-channel process (1.2.1) by a similar form and in particular to describe high energy small angle scattering by the parametric form

$$A(s,t) \simeq \sum_i \beta_i(t) \frac{1 \pm e^{-i\pi\alpha_i(t)}}{\sin\pi\alpha_i(t)} s^{\alpha_i(t)} \qquad (1.2.5)$$

for $t/s << 1$ and where as in equation (1.2.4) the $\pm$ refer to the signature[10] of the relevant Regge pole. Obviously this represents a strong prediction for high energy small angle scattering cross-sections and in particular implies a close connection between the amplitude's power law energy dependence and its phase.

As distinct from the resonance description, this parametrisation of the direct channel process (1.2.1) is expected to be useful in the high energy region where resonance effects have died out. However we have supposed the amplitude always to be analytic in energy, and a simple application of the Cauchy theorem[11] to the amplitude expressed in a resonance parametrisation at lower energies and in a crossed-channel exchange parametrisation at higher energies, will therefore strongly correlate the two sets of parameters. The sum-rule thus obtained is known as a Finite Energy Sum-Rule[12] (F.E.S.R.). The assumption that there exists an energy region where the two parametrisations are equally valid and that there exists a class of amplitudes to which the resonance saturation prescription applies, constitute part of the duality assumption.

When the absence of exotic states mentioned in Section 1.1 is demanded of a direct channel resonance-saturated amplitude, exchange degeneracy (E.X.D) of the crossed channel Regge poles is implied[13] and this in turn imposes strict constraints on the phases of related Regge amplitudes. Thus it is seen that the analytic forms allowed in equation (1.2.5) are in many cases very much determined by reasonable theoretical assumptions and it is of interest to attempt phenomenological verification of them.

1.3 Regge poles in high energy scattering

Part of this thesis will be concerned with matching analytic forms such as equation (1.2.5) to the scattering data in an attempt to determine for a given Regge pole (i) the trajectory $\alpha_i(t)$ and residue $\beta_i(t)$ (both supposed real in the scattering region $t<0$ which is below the crossed channel threshold). It has been shown[14] that Regge poles which saturate amplitudes must have factorisable residues. That is, if pole (i) contributes to the processes,

$$\begin{aligned} a + b &\longrightarrow c + d \\ a + b &\longrightarrow a + b \\ c + d &\longrightarrow c + d \end{aligned} \qquad (1.3.1)$$

then, is an obvious notation,

$$\left(\beta_i^{abcd} \right)^2 = \beta_i^{abab} \times \beta_i^{cdcd} \qquad (1.3.2)$$

It is therefore of interest to see whether some structure, e.g. a zero, in β_i^{cdcd} transmitted to β_i^{abcd} via equation (1.3.2)

is found experimentally. An instance of such residue structure is that implied by the presence of the so-called "nonsense" or "sense mechanisms" required by the t-channel angular momentum analyticity when correct account is taken[15] of spin.

An obvious feature of high energy small-angle scattering implied by (1.2.5) is the presence of a forward peak in the scattering cross-section (the modulus-squared of an amplitude) if and only if the cross-channel quantum numbers allow the exchange of a Regge trajectory of particles. This correlation has been well noted in the literature[16] and lends a measure of credibility to the Regge assumptions. Specifically, if $\alpha_i(t)$, say, is the highest trajectory in equation (1.2.5) when plotted in a Chew-Frautschi[17] plot (Re$\alpha(t)$ vs. t) then to a good approximation

$$|A|^2 \approx \beta_i^2(t) s^{2\alpha_i(t)}$$

$$= \beta_i^2(t) \exp\{2\log s(\alpha_o + \alpha_i' t)\} \qquad (1.3.3)$$

where we have assumed for the moment that

$$\alpha_i(t) = \alpha_o + \alpha' t \qquad (1.3.4)$$

i.e. that $\alpha(t)$ is a straight line in a Chew-Frautschi plot. Thus the slope of the exponential peak is expected to decrease logarithmically with s - a characteristic prediction of Regge pole dominance and the straight line trajectory assumption which we might hope to be a reasonable one if we accept as evidence the linearity of baryon resonance spin when plotted against mass-squared (the $t>0$ part of the Chew

Frautschi plot for baryon Regge trajectories). Unfortunately no evidence of linearity in the meson case is available independently.

When considering, as we will later, meson-baryon scattering processes like

$$\pi N \longrightarrow \pi N$$

$$\text{or} \qquad \pi N \longrightarrow K\Lambda \tag{1.3.5}$$

we are able to make use of angular momentum conservation to decompose $|A|^2$ into the incoherent sum,

$$|A|^2 = |N|^2 + |F|^2 \tag{1.3.6}$$

where F is an amplitude corresponding to unit change in the baryon spin state and N to no change. This decomposition is not unique and depends, for example, on the quantisation directions for the baryon's spins. A useful and simple way of quantising the spin is to project it along the particle 3-momentum. This spin projection called the particle helicity and introduced by Jacob and Wick[18] can be used to define two-particle helicity states and hence helicity amplitudes[18] $H_{\lambda_f \lambda_i}$ (λ_i and λ_f are the initial and final baryon helicities in processes (1.3.5)).

The Reggeisation procedure of paragraph 1.2 involved amplitudes for the t-channel (spinless) process which were analytic so that a simple analytic continuation gave the s-channel ones. The correct crossing procedure for the non-analytic helicity amplitudes was given by Trueman and Wick[14] and involves a matrix in helicity space (see

Appendix 1B). For many applications it is more convenient to use a Regge parametrisation of the s-channel helicity amplitudes thus obtained than a parametrisation of the direct analytic continuation of the t-channel helicity amplitudes. Such an application is discussed in Section 1.4. By considering the properties of the helicity crossing matrix† Cohen-Tannoudji et al[20] have summarised the effect of Reggeisation on s-channel amplitudes which turn out to have simple analytic properties. The contribution of a single Regge pole to process (1.2.1) in the arbitrary spin case is[20]

$$T^{s}_{\lambda_c\lambda_d\lambda_a\lambda_b} = (-t)^{\frac{x}{2}} (t_o-t)^{n/2} \beta_{\lambda_c\lambda_d\lambda_a\lambda_b}(t) \frac{1\pm e^{-i\pi\alpha(t)}}{\sin\pi\alpha(t)} \left(\frac{s}{s_o}\right)^{\alpha(t)} \qquad (1.3.7)$$

where s_o is an arbitrary scale factor

$$n = |\lambda_c-\lambda_a-\lambda_d+\lambda_b| \quad = \text{ nett helicity flip.}$$

$$n + x = |\lambda_c-\lambda_a|+|\lambda_d-\lambda_b|$$

$$t_o = t \Big|_{\cos\theta = 1} \qquad (1.3.8)$$

The extra factor $(-t)^{\frac{x}{2}}$ comes from the (dynamical) assumption of an evasive solution[21] for the t-channel Regge pole.

It is parametric forms of this kind which we shall use in later chapters.

† The authors of Reference (20) claim the asymptotic factorisability of the crossing matrix to be a necessary ingredient of s-channel Reggeisations. We disagree with this and give reasons in Appendix 1B.

1.4 Regge poles in meson-baryon processes

In considering $0^-\frac{1}{2}^+ \longrightarrow 0^-\frac{1}{2}^+$ scattering (where the symbols denote the J^P of the participant particles) we have only two independent helicity amplitudes, which have the form

$$T_n^s = (t_o - t)^{\frac{n}{2}} \beta_n(t) \frac{1 \pm e^{-i\pi\alpha(t)}}{\sin\pi\alpha(t)} \left(\frac{s}{s_o}\right)^{\alpha(t)} \qquad (1.4.1)$$

for a single contributing Regge pole. $n(= 0,1)$ is defined in equation (1.3.8). The expressions for the experimental observables are given in Appendix 2A.

Using such formulae, attempts have been made[22,93,94] to describe the near-forward scattering processes involving $\pi^\pm$, $K^\pm$ incoming beams on both proton and neutron targets. The leading non-strange meson Regge trajectories (and their quantum numbers) which have been used to describe some of these are shown in Table (1.4.1).

Process	Exchanges
$\pi^\pm p \longrightarrow \pi^\pm p$	Pf ρ
$\pi^- p \longrightarrow \pi^o n$	ρ
$\pi^- p \longrightarrow \eta^o n$	A_2
$K^\pm p \longrightarrow K^\pm p$	Pfw ρA_2
$K^\pm n \longrightarrow K^\pm n$	Pfw ρA_2
$K^- p \longrightarrow \overline{K^o} n$	ρA_2
$K^+ n \longrightarrow K^o p$	ρA_2

(a)

	J^P	I^G	C	Mass (MeV)
P	2(?)	0^+(?)	+	?
f	2^+	0^+	+	1260
w	1^-	0^-	-	784
ρ	1^-	1^+	-	765
A_2	2^+	1^-	+	1310

(b)

Table (1.4.1)

In this procedure of Regge pole phenomenology several difficulties have been met with. Among these are:

(i) The observed constancy with energy of total and elastic differential cross-sections at momenta between 15-25GeV†, requires the existence of a vacuum trajectory (P) with intercept $\alpha_p(0)=1$. No particle with an SU(3) classification is known to be associated with this trajectory, the Pomeron. This uncertainty makes a Regge pole description of elastic scattering difficult.

(ii) Factorisation of residue structure is not always compatible with a pole dominance model.

(iii) In processes where only one leading exchange is expected, the recoil polarisation from an unpolarised target (see Appendix 2A) is predicted to be zero. In $\pi^- p \longrightarrow \pi^o n$, for example, a substantially non-zero measurement has been reported[23].

(iv) The logarithmic shrinkage noted in Section 1.3 is not always found, indicating the presence of some other exchange contribution.

(v) The high energy total cross-section measurements of $K^{\pm}p$ and $\pi^{\pm}p$ above 30GeV are not compatible with a single dominating vacuum pole (the Pomeron) which would have predicted asymptotic equality of each pair.

(vi) The Sommerfeld-Watson transform for amplitudes with spin exhibits fixed poles at wrong-signature nonsense

† We use units $\hbar = c = 1 = GeV$

points[15] which are not allowed by unitarity[24] in amplitudes saturated by angular momentum plane poles. The presence of cuts in angular momentum would restore compatibility.

Finally in this section, we note that the baryons and meson trajectories involved in the processes of Table (1.4.1) belong to non-strange multiplets. Within this set of reactions, therefore, we are unable to test SU(3) in its most powerful form, that is, when it relates multiplets of differing strangeness, e.g. in

$$\begin{aligned} &\pi^- p \longrightarrow K^o \Sigma^o \\ \text{and} \quad &\pi^- p \longrightarrow K^o \Lambda^o \end{aligned} \tag{1.4.2}$$

p, Λ and Σ^o belong to separate isospin multiplets (unlike p and n). However (1.4.2) are expected to have the same exchange mechanism (see Chapter 2) in much the same way as do

$$\begin{aligned} &K^- p \longrightarrow K^- p \\ \text{and} \quad &K^- n \longrightarrow K^- n \ . \end{aligned} \tag{1.4.3}$$

In paragraph 1.6 the advantages of discussing processes like (1.4.2) will be discussed further.

1.5 Absorption

In Section 1.4 we noted some theoretical and experimental indications that further exchange contributions should be added to those supplied by Regge poles alone.

Historically it was found[25] that one meson exchange models predicted angular distributions too large in magnitude and not strongly enough peaked in the near-

forward direction when compared with data. It was suggested[26] that this forward peak in the data (which looked like "shadow" scattering in an optical analogy) could reflect the existence of the many inelastic final state channels which are expected to be fed primarily from low impact parameter collisions (large momentum transfers). Thus it was thought that the low partial wave (impact parameter $b \simeq \ell/q$) amplitudes should be reduced below the exchange model expectation in order to reproduce this "absorption" effect. Indeed the agreement of data and predictions was improved when this was done[26].

Similar difficulties were encountered with the Regge pole exchange model in describing angular distributions. Although the Regge pole model should already include the effects of absorption (as compared with the one meson exchange) additional absorption[27,28] achieved by suppressing the low partial waves, was found beneficial[28] in that the angular distributions became more peripheral. By peripheral, we mean that in impact parameter space only a finite band of amplitudes contribute significantly to the total scattering amplitude. A typical Regge exchange amplitude before (R) and after (A) absorption is shown in b-space in Figure (1.5.1).

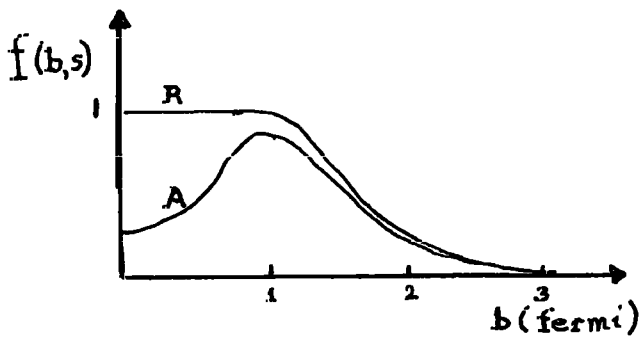

Figure (1.5.1)

Why a more strongly peaked angular distribution is obtained is easily seen with reference to equation (1.2.2). The more rapidly varying $P_\ell(\cos\theta)$ near $\cos\theta = 1$ are those with high ℓ, so that the angular variation of the overall amplitude is then determined by the relative weights of the high and low order polynomals. Suppressing the low f_ℓ amplitudes therefore is expected to increase the angular variation (slope) of the overall amplitude.

The details of how such absorption is achieved in a given reaction will be discussed in Chapter 2 and Appendices. The procedure may be described roughly as adding to the Regge exchange, a b-space convolution of this exchange amplitude and a Pomeron exchange amplitude representing the diffractive part of the associated elastic scattering. In a loose sense this is seen to represent a double Regge pole exchange, probably a cut singularity in the crossed channel ℓ-plane and as such might provide a solution to problem (vi) of Section 1.4. The theoretical implications of this interpretation of the absorptive correction as an angular momentum cut will be discussed briefly in Chapter 3. For the moment we treat absorption simply as a prescription but may loosely describe the corrective term as a "cut" for convenience of notation.

Two distinct philosophies on the construction of pole plus cut amplitudes have arisen:

(i) The basic Regge pole exchange should have the residue structure demanded of it by analyticity in the t-channel (nonsense mechanisms etc.) and by dual schemes

(e.g. exchange degeneracy). Then the unenhanced convolution part should only weakly modify the basic structure given by the pole[29].

(ii) The basic Regge pole should be structureless since analyticity requirements should apply to the complete amplitude. Any structure in the final amplitude is obtained from destructive interference with an enhanced convolution part[30].

The weak cut prescription (i) has proved more successful in describing the dip/no dip systematics of meson-baryon scattering[31], while the strong cut model[30] has had notable successes in photo-induced processes[32] where the small energy dependence of the cross-sections is a problem for pole or weak cut models. Their implications for strangeness—exchange interactions will be discussed in Chapter 2. An extension of such cut models has been to replace the vacuum exchange (Pomeron) by another Regge pole and thus try to explain double charge-exchange processes, for example. Applications like this will be made in Chapter 3.

1.6 Strangeness-exchange processes

The previous sections have shown that in order to develop a dynamical theory of hadronic physics, it is necessary to identify the exchange forces and their underlying symmetries. Useful concepts which provide a framework within which to operate have been listed:-

(a) Regge pole exchange and possible absorptive corrections.

(b) The duality assumptions.

(c) SU(3) symmetry.

In order to investigate these phenomenologically (i.e. by constructing models to compare with experiment) it is advantageous to select a set of reactions for which there exists as complete a set of data as possible, and whose Regge exchanges span complete SU(3) multiplets. Ambiguities in an analysis are reduced by choosing each reaction in the set such that it involves as few exchanges and as few spin amplitudes as possible†. Reactions of the type

$$PB \longrightarrow PB \qquad (1.6.1)$$

where P is a pseudoscalar ($J^P=0^-$) meson and B an octet baryon ($\frac{1}{2}^+$), satisfy these criteria well. The non-strange exchange mediated subset listed in Table (1.4.1) have been well studied whereas the following strangeness exchange reactions have been less so,

$$\begin{aligned} \bar{K}N &\longrightarrow \pi Y \\ \pi N &\longrightarrow KY \end{aligned} \qquad (1.6.2)$$

where N is a nucleon and Y a hyperon (Λ or Σ). The only expected exchanges in (1.6.2) are the K*(890) (the $J^P = 1^-$ SU(3) octet partner of the ρ and ω) and the K*(1420) (the $J^P = 2^+$ partner of the A_2 and f). These mesons have natural parity since they have $P = (-)^J$. Only two

† An exception to this is discussed in Chapter 4.

spin amplitudes are involved, e.g. s-channel helicity flip and non-flip. Since Λ is an isospin singlet and Σ an isospin triplet in the same SU(3) baryon octet, a chance occurs of testing SU(3) symmetry for vertex couplings. The helicity flip amplitude is seen to dominate[29] in ρ or A_2 exchange processes (witness the forward cross-section turnover in $\pi^- p \to \pi^o n$) so that the non-flip amplitude is not well-determined. The absence of a forward turnover in reactions (1.6.2) gives the hope of a dominant and hence well-determined non-flip helicity amplitude. Also since the Λ and Σ^+ decays are not parity conserving, the spin state of the final state baryon (the polarisation) is simply analysed experimentally[33], leading to a more complete set of measurements than is readily obtainable for the processes of Table (1.4.1).

There are further theoretical reasons for examining processes (1.6.2) which are henceforth denoted as a class by H.C.E.X. (Hyper-Charge Exchange, or equivalently strangeness exchange) reactions. s-channel processes of the form

$$\begin{aligned} & a + b \longrightarrow c + d \\ \text{and} \quad & \bar{c} + b \longrightarrow \bar{a} + d \end{aligned} \qquad (1.6.3)$$

are said to be related by line reversal. The nomenclature is easily understood on drawing symbolic t-channel exchange graphs (Figure (1.6.1))

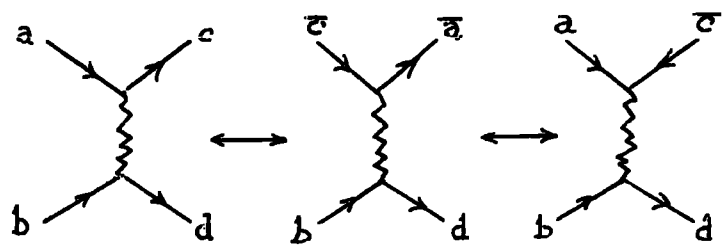

Fig.(1.6.1)

which are evidently related by "twisting" the top lines. In our case if

$$A(\bar{K}N \longrightarrow \pi Y) \approx \beta_V(1-e^{-i\pi\alpha_V})s^{\alpha_V} + \beta_T(1+e^{-i\pi\alpha_T})s^{\alpha_T} \qquad (1.6.4)$$

then

$$A(\pi N \longrightarrow KY) \approx -\beta_V(1-e^{-i\pi\alpha_V})s^{\alpha_V} + \beta_T(1+e^{-i\pi\alpha_T})s^{\alpha_T} \qquad (1.6.5)$$

where v denotes the vector (1^-) K*(890) and T denotes the tensor (2^+) K*(1420). The vector sign change comes from its negative signature ($\xi = -1$). For the measurables, relations (1.6.4) and (1.6.5) imply certain symmetries (e.g. $P\frac{d\sigma}{dt}(\bar{K}N) \approx -P\frac{d\sigma}{dt}(\pi N)$† for all s and t) which are readily subject to experimental text.

Finally if we apply the duality constraints of paragraph 1.2 simply summarised by the Harrari-Rosner duality diagram rules[34], we find the diagram for $\bar{K}N \longrightarrow \pi Y$ to be non-planar (Figure (1.6.2)),

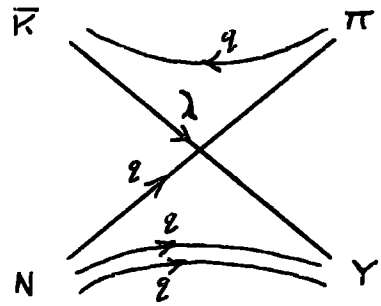

Fig.(1.6.2)

thus predicting $A(\bar{K}N \longrightarrow \pi Y)$ of equation (1.6.4) to be real at high energies and for all small $|t|$. Consequently we expect

$$\alpha_V(t) = \alpha_T(t) = \alpha(t)$$
$$\beta_V(t) = \beta_T(t) = \beta(t) \qquad (1.6.6)$$

† The measurables are defined in Appendix 2A.

in the small angle high energy scattering region, suggesting that

$$A(KN \longrightarrow \pi Y) \simeq 2\beta(t)s^{\alpha(t)} \qquad (1.6.7)(a)$$

and $$A(\pi N \longrightarrow KY) \simeq 2\beta(t)e^{-i\pi\alpha(t)}s^{\alpha(t)} \qquad (1.6.7)(b)$$

both very strong predictions. This is a specific example of the E.X.D. Regge poles referred to in Section 1.2.

These reactions, therefore, offer a possibility of investigating ideas (a), (b) and (c) of page 25 and perhaps shedding light on some general features already found in studies of the processes of Table (1.4.1). Such an analysis is recounted in Chapter 2.

Of the closely related processes

$$K^-p \longrightarrow \pi^-\Sigma^+ \qquad (1.6.8)(a)$$

$$K^-p \longrightarrow \pi^+\Sigma^- \qquad (1.6.8)(b)$$

only (a) falls into category (1.6.2) since (b) allows only t-channel exchange of isospin 3/2 (exotic) quantum numbers. This exchange can be achieved by the "double Regge" exchange of Section 1.5 - a Regge-Reggecut. In Chapter 3 we discuss an attempt to correlate the properties of such cuts as applied both to the allowed reactions (1.6.2) and to exotic exchange reactions typified by (1.6.8)(b).

In Chapter 4 we discuss an alternative approach to the problem of extracting from the data, information on strangeness exchange. Motivated by the lack of success of high energy models as discussed in Chapters 2 and 3, a method is proposed whereby the joint decays in strangeness

exchange processes of the type

$$\pi N \longrightarrow K_V^* Y_1$$

$$\bar{K}N \longrightarrow V \quad Y_1 \qquad (1.6.9)$$

are analysed in order to obtain directly the production amplitudes themselves. In (1.6.9) V is any non-strange vector meson and Y_1 a hyperon such as Λ or Σ^+ whose parity non-conserving decay enables 12 decay correlation parameters to be measured. From these 12 parameters we show how 10 of the 11 determinable amplitude parameters may be obtained. An efficient means of converting all the available decay data into information about the production process, is advocated. The results of an application to $\pi^- p \longrightarrow K^* \Lambda$ are compared to those of Chapter 2.

C H A P T E R T W O

STRANGENESS-EXCHANGE, LINE REVERSAL AND ABSORPTION

2. Strangeness-exchange, line reversal and absorption†

In this chapter the data on reactions (1.6.2) are analysed with regard to high energy models, in particular the weak cut model of Section 1.5.

2.1 Regge Poles in HCEX processes

We saw in Chapter 1 how high energy data are usefully analysed in terms of the crossed-channel angular momentum plane singularities of which Regge poles are the simplest, but that existing data have many finer details necessitating the inclusion of additional singularities. Among the more extended Regge models which have been considered are (a) complex poles[35], (b) strong cuts, and (c) EXD poles plus weak cuts. We shall show that of these only (c) easily predicts the observed hyperon polarisations in the line-reversed pairs of HCEX reactions. The shortcomings of model (c) in describing the non-asymptotic differential cross-sections, will be discussed as a prelude to Chapter 3.

As previously noted, the HCEX reactions are expected to be dominated by exchange degenerate (EXD) K^*_V and K^*_T Regge poles following application of the Harari-Rosner duality diagram rules. Thus we expect for both spin amplitudes (see equation (1.6.7)):-

$A(\bar{K}N \longrightarrow Y)$ real - denoted type R (real)

and $A(N \longrightarrow KY)$ $e^{-i\pi\alpha}K^*$ - denoted type C (complex)

Immediate consequences are that

$$P(R) = P(C) = 0$$

and

$$\frac{d\sigma}{dt}(R) = \frac{d\sigma}{dt}(C) \qquad (2.1.1)$$

†part of this work was done in collaboration with A.D.Martin and C. Michael and was published in Reference (42).

at any given s and t with $\frac{d\sigma}{dt}$ showing the Regge shrinkage of paragraph 1.3. None of these features is substantiated by the data in any sizeable region of s and t (see for example Figures (2.1.1) and (2.1.2)).

Allowing EXD breaking in residues and/or trajectories does not allow agreement with the data as can be seen by reference to equations (1.6.4) and (1.6.5).

(i) If $\beta_V \neq \beta_T$ but $\alpha_V = \alpha_T$, then

$$\frac{d\sigma}{dt}(R) = \frac{d\sigma}{dt}(C),$$

a prediction which is certainly wrong below 10 GeV , and

$$P(R) = -P(C) \neq 0$$

which is wrong for $|t| \lesssim .2$ GeV^2.

(ii) If $\beta_V \neq \beta_T$ and $\alpha_V \neq \alpha_T$ then

$$\frac{d\sigma}{dt}(R) = \frac{d\sigma}{dt}(C)$$

whenever $\alpha_T = 0$ or $\alpha_V = 0$. No such equality is seen in the data for any reasonable trajectory functions.

We are forced to conclude that a simple two-pole model (EXD or not) does not describe the data. A pole model which introduced daughter trajectories (one unit of spin lower than the parent K*) would not describe the energy independent polarisation features which are evident in Figure (2.1.2).

Before discussing possible models to remedy this we give a brief discussion of the data existing at the time of the analysis.

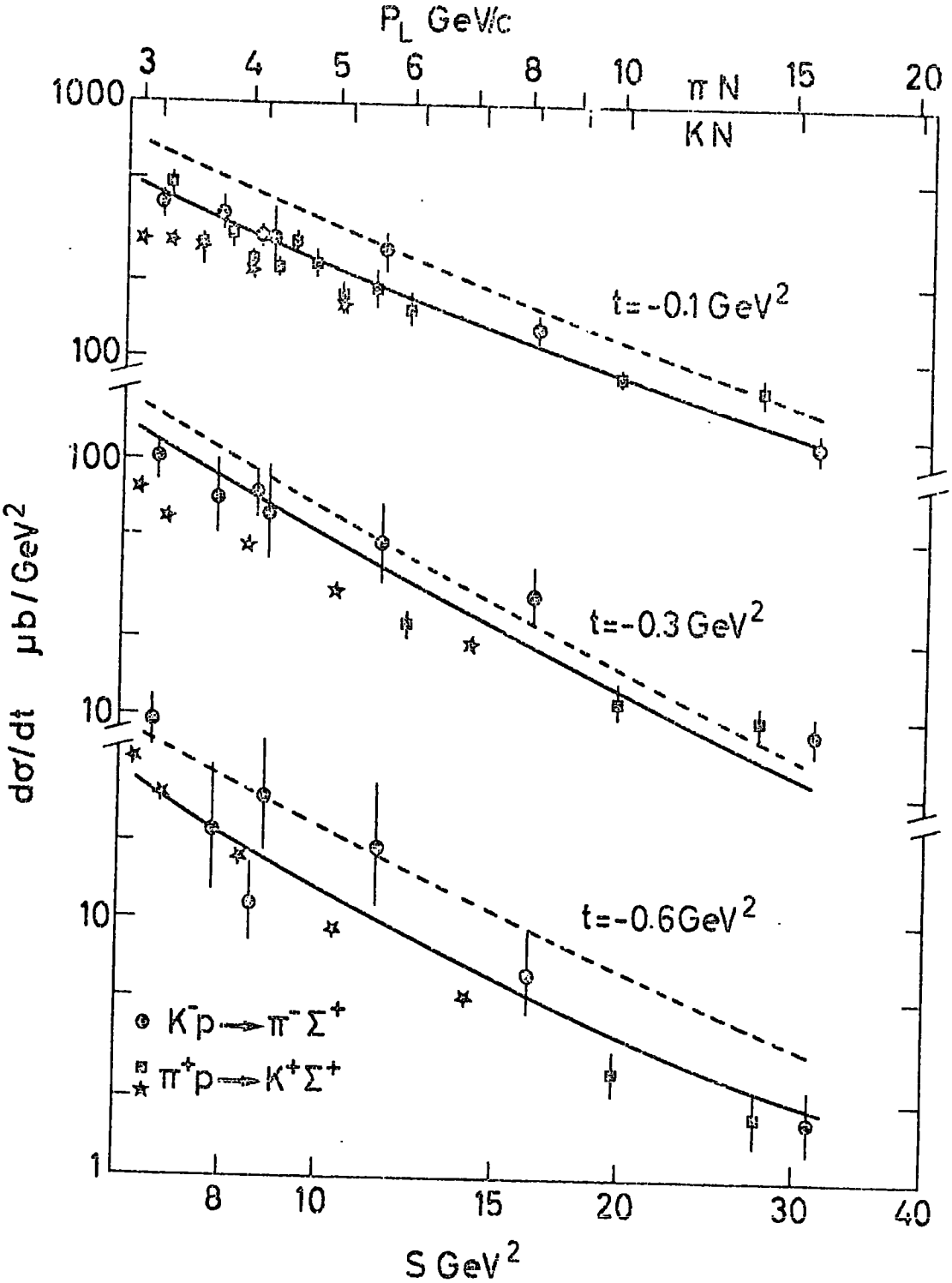

Fig. (2.1.1)

Data references are given in Section 2.2(ii)

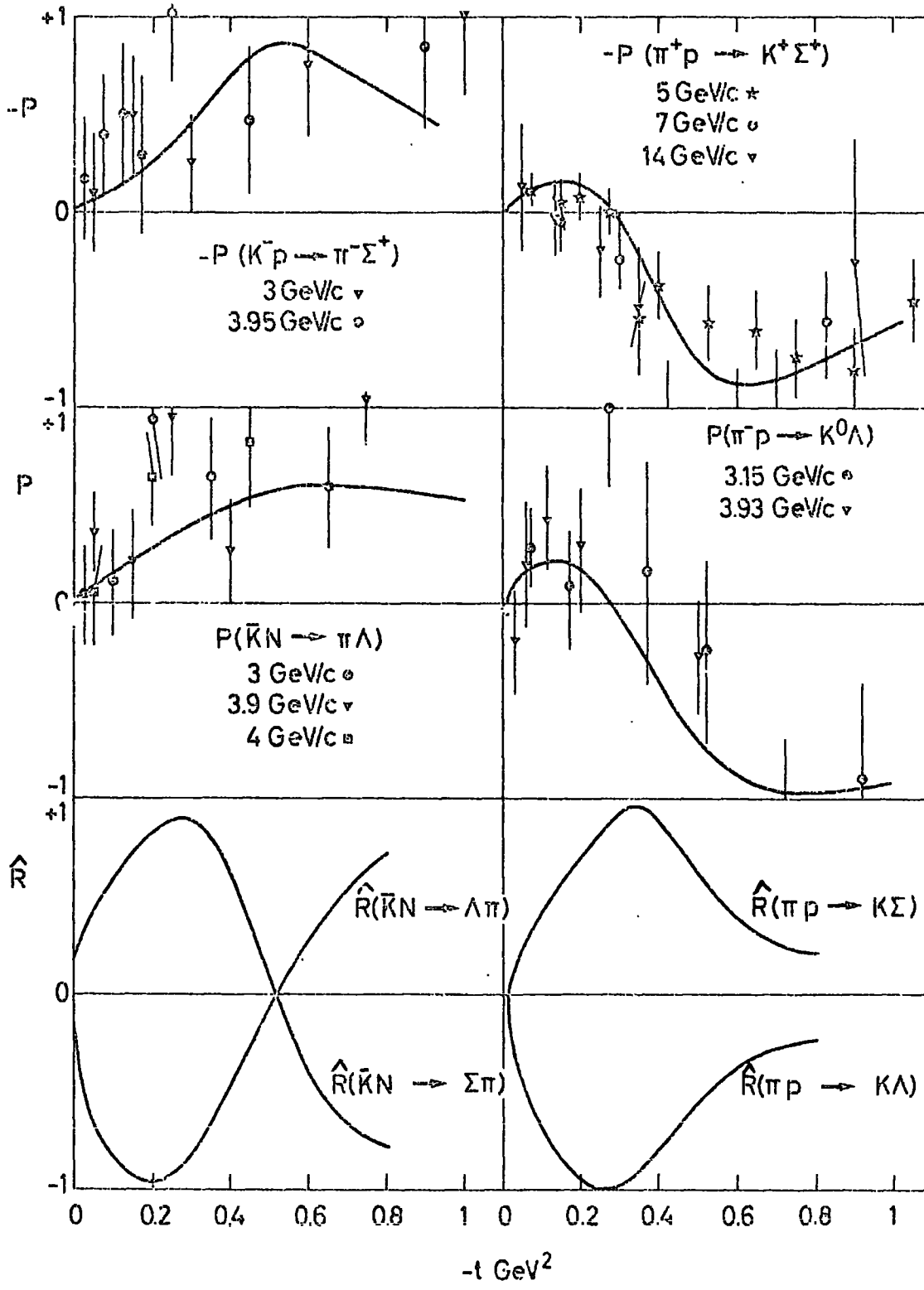

Fig. (2.1.2)

Data references are given in Section 2.2(iii)

2.2. The HCEX Data

In addition to the cross-section data there are sufficient polarisation data to illuminate the spin decomposition of the amplitudes although measurements of the R and A parameters[36,37], which describe the scattering from a polarised target, are necessary to complete this analysis (see Appendix 2A). Sufficiently accurate R and/or A data ($P^2 + R^2 + A^2 = 1$) would of course provide a definitive test for any high energy model, but in their absence there are many significant $\frac{d\sigma}{dt}$ and P features to challenge existing models. We discuss such features in the following subsections.

(i) The α_{eff} parameter

Before a detailed analysis of $\frac{d\sigma}{dt}$ is attempted, it is useful to assess the compatibility of the data with a Regge-type energy dependence and the mutual consistency of the various experiments themselves, in terms of the α_{eff} parameter[38,39]. Following convention we write[39]

$$\frac{d\sigma}{dt} = \frac{1}{p_L^2} \chi(s)\, A(t)\, \nu^{2\alpha_{eff}(t)} \qquad (2.2.1)$$

where $\nu = \frac{s - u}{4\bar{M}}$

For $s \gg 1$ and $t \ll 1$ ν behaves like $s/2\bar{M}$ where $\bar{M}$ is the mean mass of the target baryon and its recoil. The expression (2.2.1) may be fitted to the data (using least squares method) to obtain the effective trajectory $\alpha_{eff}(t)$ and effective residue $\sqrt{A(t)}$. The parameter $\chi(S_i)$ is

optional and allows a t-independent renormalisation factor for all energies s_i of a given experiment to be determined in the fit[40]. This latter facility is useful when the analysis includes $\frac{d\sigma}{dt}$ data from an experiment of uncertain normalisation. For example, analyses including the 8 and 16 GeV data of Birnbaum et al[43(e),48] have shown that in backward π-p elastic[41], $K^- p \longrightarrow \pi^- \Sigma^+$[42] and $\pi^- Y^*(1385)$ a common renormalisation factor of 0.66 is suggested. In subsequent work we assume the presence of this factor.

Plots of the α_{eff} parameter are shown in figures (2.2.1) and (2.2.2) where the following features are in evidence.

(a) $\pi N \longrightarrow K\Sigma$, $K\Lambda$ show high intercepts ($\alpha_{eff}(0) \simeq .6$) and steep slopes ($\alpha'_{eff} \simeq 1.1$) although the $K\Lambda$ data is not abundant (see (ii)).

(b) $\bar{K}N \longrightarrow \pi\Sigma$, $\pi\Lambda$ show lower intercepts (nearer the K* pole expectation of 0.4) but very little shrinkage - $\alpha'_{eff} \simeq 0.4$.

That (a) and (b) are incompatible with an EXD K* trajectory of

$$\alpha(t) = .35 + .8t \qquad (2.2.2)$$

is plain. It is also worth noting that within the errors the $\pi N \longrightarrow K\Sigma$ data are the most at odds with an EXD pole model energy dependence.

(ii) Differential cross-section structure

All $\frac{d\sigma}{dt}$ data[43-47] show a forward peak with no obvious turnover at $t = t_o$, indicating dominance of the

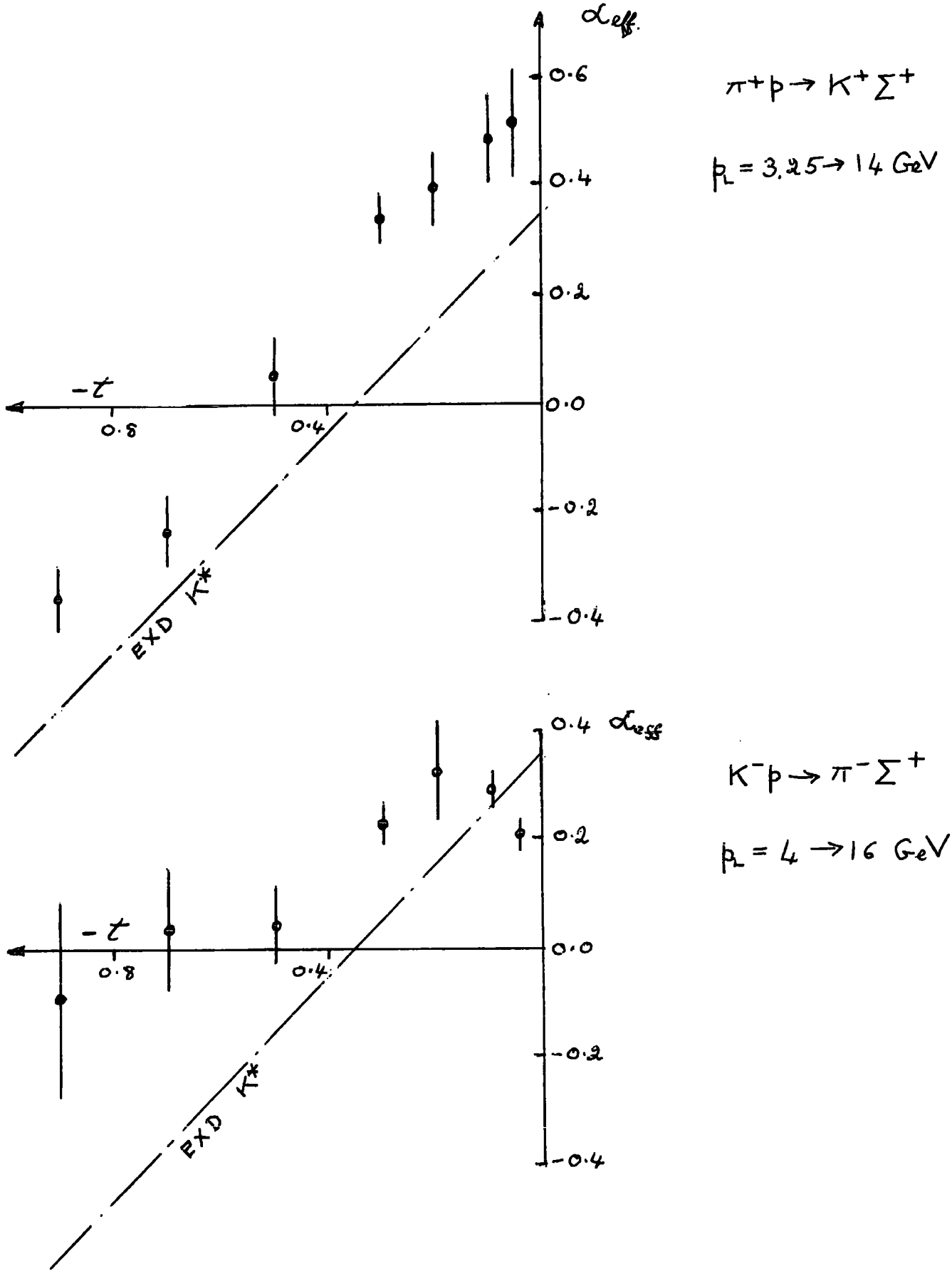

Fig. (2.2.1)

Effective trajectory plots.

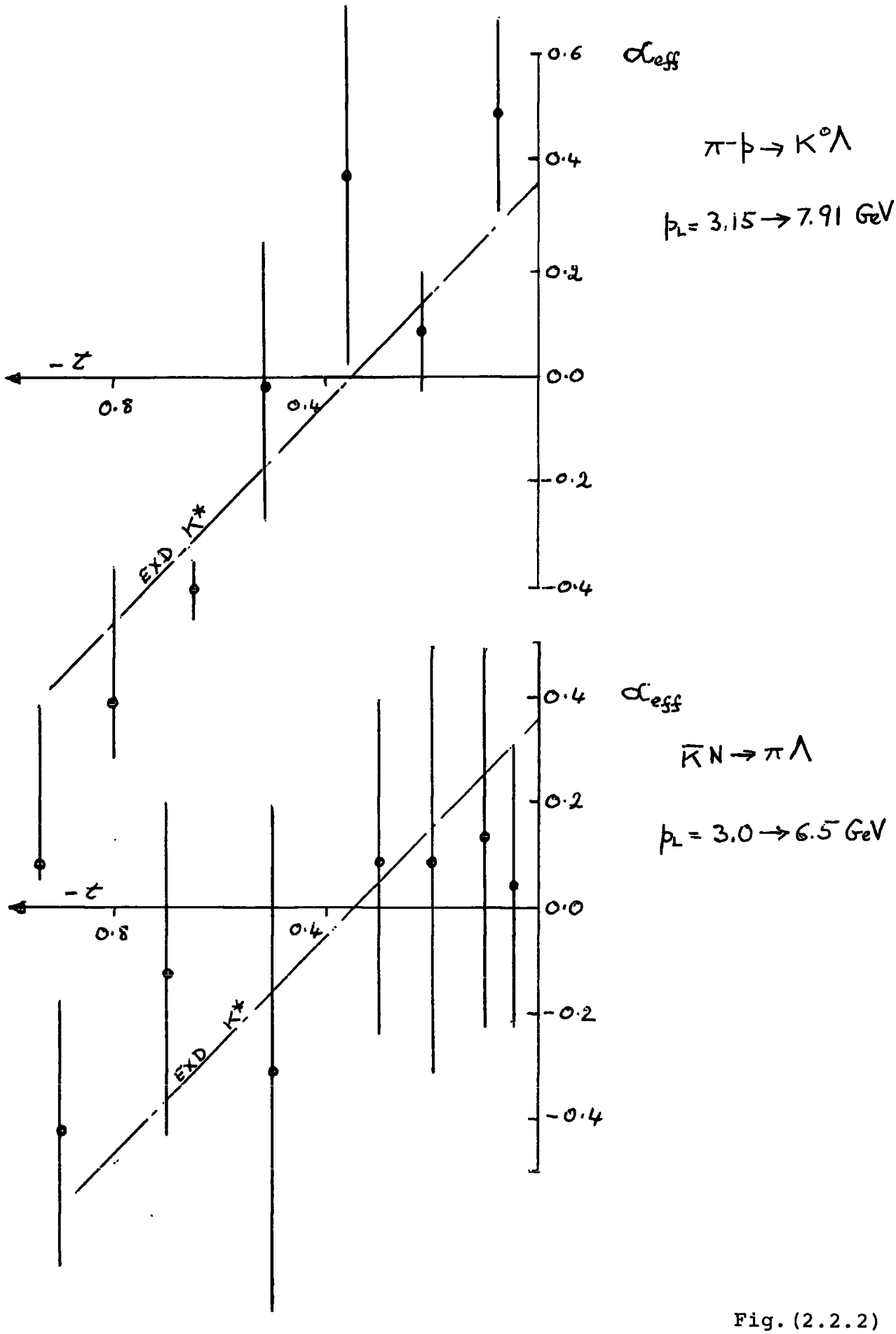

Fig. (2.2.2)

Effective trajectory plots.

cross-sections by the non-flip amplitudes. We define the cross-section slope b GeV^{-2} by

$$\frac{d\sigma}{dt} = Ae^{b(t-t_o)} \qquad (2.2.3)$$

at a given energy. All data for these HCEX reactions show a shoulder or break in slope at $t \simeq -0.4$ GeV^2 which is most pronounced in $\pi^+p \longrightarrow K^+\Sigma^+$ [46(e)] where it is seen to disappear rapidly with momentum from 3 to 14 GeV (shrinkage). In general at intermediate momenta the slope b of the forward peak for a C type reaction is greater than that for the corresponding R type, as can be seen by reference to Table (2.7.1). The cross-section of the R type is some two times larger than its C counterpart at lower momentum. This is clearly shown in Figure (2.1.1) where a sample plot of $\frac{d\sigma}{dt}$ for Σ final states is shown. The data is interpolated at fixed t to exhibit the relative shrinkages and the momentum dependence of the cross-sections inequality. As in the case of KN and $\bar{K}N$ CEX [49] a disappearance of the line-reversal symmetry violation is seen towards higher momenta - 5 GeV in the CEX case, but more like 10 GeV in our case.

We emphasise two features of this cross-section difference:-

(a) a decrease with increasing momenta

(b) a decrease with increasing t.

(iii) Polarisation structure

The available polarisation data [43-47] are shown in Figure (2.1.2). The $\pi^+p \rightarrow K^+\Sigma^+$ data show no

measurable energy dependence between 3 and 14 GeV and we make the plausible assumption that the other reaction polarisations have a similarly constant behaviour. From SU(3) considerations[50] the polarisation is expected to change sign under $\Lambda \longrightarrow \Sigma$ interchange and the data (Figure 2.1.2) clearly support this. $P(\pi N \longrightarrow K\Lambda)$ and $-P(\pi N \longrightarrow K\Sigma)$ are zero near $t \simeq -0.3$ GeV^2 and reach almost -1 for $-0.8 \lesssim t \lesssim -0.6$. A positive maximum of $P(KN \longrightarrow \pi\Lambda)$ and $-P(KN \longrightarrow \pi\Sigma)$ is reached and maintained by $-t = 0.4$ GeV^2. At such maxima we have the fullest possible spin decomposition since $R \simeq A \simeq 0$ necessarily.

2.3 High energy models

(a) Regge Poles

For the reasons set out in paragraph 2.1, simple pole models (e.g. ref. (51)) are not expected to describe the data. The complex pole model[35] can explain[52] the line reversal symmetry violation at a given energy but not the energy dependence of the cross-sections themselves and finds difficulty in reproducing the polarisations. The theoretical motivation for such a model is dubious[53] and its implications unpleasant (the symmetry properties of the residues for example).

(b) Strong cut model

This model[30], which uses a structureless Regge pole (with the phase expected of a Regge signature factor) as input to a convolution integral (see Appendix 2B), is only predictive when amplitude zero systematics are imposed as follows.

Schematically, a helicity amplitude A_n is constructed as

$$A_n(s,t) = R_n(s,t) + \lambda_n C_n(s,t) \qquad (2.3.1)$$

where n = net s-channel helicity flip

R_n = Regge pole amplitude

and C_n = corresponding cut amplitude.

We saw in section 1.5 that the convolution C_n involves a diffractive amplitude (Pomeron exchange) as well as the exchange amplitude R_n. The diffractive amplitude can connect to the initial state certain inelastic final states as well as the elastic one. The multiplicative factor λ_n is inserted in equation (2.3.1) to help reproduce the additional absorption due to these diffractive inelastic intermediate states and is expected to be about 1-2 in value[30]. With these canonical values of λ_n, a cancellation in $A_n(s,t)$ occurs at $t \simeq -0.2$ GeV^2 for n = 0 and at $t \simeq -0.6$ GeV^2 for n = 1. These cancellations are used for example to reproduce respectively the observed $\pi^{\pm}p$ cross-over effect[54] and dip in the $\pi^- p \longrightarrow \pi^o n$ cross-section[30] at the above t-values.

These systematics therefore predict small or zero polarisations in HCEX processes at around t = -0.2 and -0.6 GeV^2, since P is a bilinear of A_o and A_1. The data for $P(\pi N \longrightarrow KY)$ clearly contradicts the second zero and $P(\bar{K}N \longrightarrow \pi Y)$ both zeros (Figure (2.1.2)).

(c) EXD Poles with Weak Cuts Model

We briefly summarise the results of previous attempts using Models of this class to describe the HCEX data.

The model of reference (55) used a Regge pole input whose residues satisfied a solution[56] to a weaker set of duality constraints than is usually applied. A necessary ingredient of their good description of the cross-sections was an uncomfortably large violation of exchange degeneracy in one of their amplitudes. The accompanying polarisation description is poor. A very restrictive weak cut model which assumes U(6)⊗U(6)⊗O(3) symmetry for residues has been reported[57]. The resulting failure to describe the sign of the cross-sections difference is not surprising (see Section 2.5). The polarisation predictions are also wrong in sign.

A qualitative discussion of the polarisation predictions of EXD pole plus weak cut models was given by Krzywicki and Tran Thanh Van[119], and in the next section some quantitative calculations using this framework are presented.

2.4 A new HCEX analysis : the model

In the spirit of equation (1.4.1) we parametrised the K_V^* and K_T^* EXD pole contributions to s-channel helicity non-flip (n=0) and flip (n=1) amplitudes as,

$$R_n(s,t) = (t_o - t)^{n/2} \; \gamma_n^{\Lambda,\Sigma} \varepsilon_n t \; (se^{i\phi})^{\alpha(t)} \qquad (2.4.1)$$

in units of GeV. For R type reactions $\phi = 0$ and for

C type ones, $\phi = -\pi$ as predicted by duality diagrams. The overall amplitude normalisation is as given in Appendix 2A.

Following reference (30), the amplitude $R_n(s,t)$ was absorbed using the procedure of Appendix 2B. The absorption parameters which were the same for all reactions, were an effective diffraction cross-section of σ = 30 millibarns, a diffraction peak slope of A = 8 GeV^{-2} and a Pomeron slope of $\alpha'_p = 0.5$ as indicated in the pp scattering data of reference (58). For practical reasons a non-zero value of α'_p was found necessary to avoid (i) a deep dip in $\frac{d\sigma}{dt}$ ($\bar{K}N \longrightarrow \pi Y$) at $t \simeq -0.4$ GeV^2 from amplitude cancellation of R_o and C_o (c.f. equation (2.3.1.)) and (ii) zero polarisation in the same process since both amplitudes would then be real.

2.5 The fit

Since the polarisation comes from a phase difference between non-flip and flip amplitudes it was found easier to obtain larger polarisation with no absorption in the flip amplitude (λ_1=0). Such a conclusion is supported by the simple pole-dominated flip amplitude description of the mirror symmetry of the πN elastic polarisation data[59]. If we assume the non-flip amplitudes to be dominated by the largely imaginary Pomeron contribution the difference $P\sigma(\pi^+p) - P\sigma(\pi^-p)$ is seen to be the product of a smooth Pomeron amplitude and the real part of the ρ-pole flip amplitude which contains a double zero, in agreement with the data[59]. The pole-like shrinkage observed in

flip-dominated $\frac{d\sigma}{dt}$ $(\pi^- p \longrightarrow \pi^o n)$ is also evidence for little absorption in flip amplitudes.

The cut contribution to the R-type process is expected to be larger than to the C-type. This is simply understood as follows. In equation (2.3.1), which applies equally well to our model, C_n has the schematical form,

$$C_n(s,t) = \iint e^{-i\pi\alpha'_p t_1} e^{i\phi\alpha(t_2)} k_n(s,t,t_1,t_2)\,dt_1 dt_2 \qquad (2.5.1)$$

where k_n has a constant phase. Since α'_p is not large the contributions to the double integral add coherently giving a large result for $\phi = 0$, but cancel somewhat for $\phi = -\pi$ giving a smaller result. Destructive interference of R_n and C_n then forces the prediction of the model

$$\frac{d\sigma}{dt}\,(R) \lesssim \frac{d\sigma}{dt}\,(C) \qquad (2.5.2)$$

at non-asymptotic energies. Asymptotically of course the cut terms vanish and cross-section equality is regained. (2.5.2) is in complete disagreement with the data (Figure (2.1.1)) so that in this model a simultaneous description of R and C cross-sections is not feasible at intermediate energies. In view of the α_{eff} analysis of Section 2.1 we choose to fit the R type reactions and predict the C ones.

The $\frac{d\sigma}{dt}$ (R) fit is good, the break to a flatter slope at $t \simeq -0.4$ GeV^2 being accounted for by the flatter t-dependence of the cut contribution beginning to dominate. Figure (2.1.1) shows a sample of the $\frac{d\sigma}{dt}$ (R) fit at fixed t along with the $\frac{d\sigma}{dt}$ (C) prediction which is

obviously only reasonable asymptotically ($\gtrsim$ 10 GeV).

The large polarisation P(R) was readily described by the model and the prediction for P(C) astonishingly good (Figure (2.1.2)) and is in accord with SU(3) expectations (Section 2.2 (iii)). The origin of the polarisations is easily seen:-

$$P\frac{d\sigma}{dt} = 2\ \mathrm{Im}\ (A_o A_1^*)$$

$$= -2\lambda_o\ \mathrm{Im}\ (C_o R_1^*) \qquad (2.5.3)$$

In the R case ($\phi = 0$), R_1 is real so that the slowly varying cut phase is directly reflected in the smooth rise of $P\frac{d\sigma}{dt}$ (R). When $\phi = -\pi$ however C_o and R_1 both have varying phases. The phase of R_1 starts behind C_o at $t = t_o$ but varying more rapidly ($\alpha' = .8$) soon overtakes C_o at $t \simeq -0.3$ GeV^2 and begins to dominate. The equal phase situation at $t \simeq -0.3$ of course produces a zero in P(C) (see Figure (2.1.2)).

Also shown in Figure (2.1.2) are predictions from our fits to $\bar{K}N \longrightarrow \pi Y$ for the $\hat{R}$ parameter of Appendix 2A - $\hat{A}$ is not shown since $\hat{A}^2 = 1 - P^2 - \hat{R}^2$ and its sign is simply obtainable from the parameters listed in the next section (see also Table (4.5.1)). We claim, contrary to the suggestion of Reference (60), that the $\hat{R}$ and $\hat{A}$ predictions of weak cut and strong cut models can be qualitatively similar, as in this case (c.f. Reference (60)). An experimental measurement of the R and A parameters would need to be extremely accurate to separate them.

2.6 Parameters of the fit

The fits to all available $\bar{K}N \longrightarrow \pi\Lambda,\Sigma$ $\frac{d\sigma}{dt}$ and P data above 4 GeV, discussed in Section 2.5 yielded the parameter values

$$\begin{aligned} \gamma_o^{\Sigma^o} &= 42.1 & \gamma_o^{\Lambda} &= 47.3 & \varepsilon_o &= 1.07 \\ \gamma_1^{\Sigma^o} &= 17.0 & \gamma_1^{\Lambda} &= -33.0 & \varepsilon_1 &= 0.77 \\ \alpha(t) &= .4+.8t & \lambda_o &= 1.2 \end{aligned} \qquad (2.6.1)$$

The trajectory is very close to the straight line through the K_V^* and K_T^* poles on a Chew-Frautschi plot. The enhancement factor of $\lambda_o = 1.2$ is not unusual for meson baryon processes.

Assuming SU(3) for the constant residue factors $\gamma^{\Sigma,\Lambda}$ we may write

$$\frac{\gamma_n^{\Sigma^o}}{\gamma_n^{\Lambda}} = \frac{\sqrt{3}\,[(F/D)_n - 1]}{3(F/D)_n + 1} \qquad (2.6.2)$$

yielding

$$\begin{aligned} (F/D)_o &= -2.8 \\ (F/D)_1 &= 0.38 \end{aligned} \qquad (2.6.3)$$

in fair agreement with other estimates[50]. In terms of the f mixing parameter[61]

$$f = \frac{F}{F + D} \qquad (2.6.4)$$

our estimates are

$$\begin{aligned} f_o &= 1.6 \ (1.0) \\ f_1 &= 0.28 \ (.24) \end{aligned} \qquad (2.6.5)$$

The figures in brackets for comparison are those suggested by vector meson dominance[62]. We may compare the residues obtained in the fits with those of ρ exchange, using SU(3). We form the flip/non-flip ratio of the ρ couplings to a nucleon-nucleon vertex:-

$$\frac{(\gamma_{\rho N\bar{N}})_1}{(\gamma_{\rho N\bar{N}})_0} \approx -1.9 \qquad (2.6.6)$$

which is lower than most other estimates[62]. The magnitude of γ_1^{Λ} is not well determined in our fit, due to lack of precise data and the non-flip dominance of the processes, so that the result (2.6.6) is not expected to be very reliable in comparison with those using finite energy sum rule information.

In the above residue calculations the expediency of comparing couplings at $t = t_o$ was used. SU(3) symmetry is expected to apply to couplings at the particle poles (in this case, $t = 0.89$ or $t = 1.42$ GeV^2) but the constant factors γ_n and residue exponents ε_n are only determined in the scattering region $t < t_o$, and it would be unwise to extrapolate as far as the poles themselves.

The overall dominance of non-flip amplitudes in K^* exchange processes (especially Σ production) is to be contrasted with the SU(3) - analogous situation in πN and KN charge-exchange (CEX) reactions where the ρ and A_2 exchanges are dominantly flip. If we believe the suggestions (Section 2.5) that absorption effects are more important in non-flip than in flip amplitudes, then it is clear that HCEX reactions offer a better chance than CEX for studying absorption systematics. Indeed we

have already noted one feature of standard absorption prescriptions inconsistent with the HCEX data - the relative overabsorption of the real amplitude as compared to the complex one. We devote some attention to this in the next section.

2.7 Non-asymptotic contributions

The observed violation of line-reversal symmetry of HCEX cross-sections in a direction and to a degree not explained by our asymptotic model can be usefully analysed from two standpoints. Firstly in the t-channel exchange formalism, it is conceivable that at intermediate energies lower lying J-plane singularities may be important. Alternatively (or perhaps equivalently in a duality sense) we may feel that at such energies an s-channel discussion of resonance effects is more relevant. These are considered in turn.

(i) Regge-Regge cuts

These lower lying J-plane singularities have been suggested[63] as a possible duality violation mechanism. Chapter 3 is devoted to a discussion of their calculation and application.

(ii) Direct channel approach

We remarked in Section 1.6 that duality diagrams predict a real amplitude for $\bar{K}N \longrightarrow \pi Y$ at high energies. If we take seriously the duality assumption that the imaginary part of the amplitude can be saturated by

resonances[12] then we must conclude that those contributing to $ImA(\bar{K}N \longrightarrow \pi Y)$ must couple with alternating signs thus cancelling on the average, while those to $ImA(\pi N \longrightarrow KY)$ will not. This is shown schematically in Figure (2.7.1).

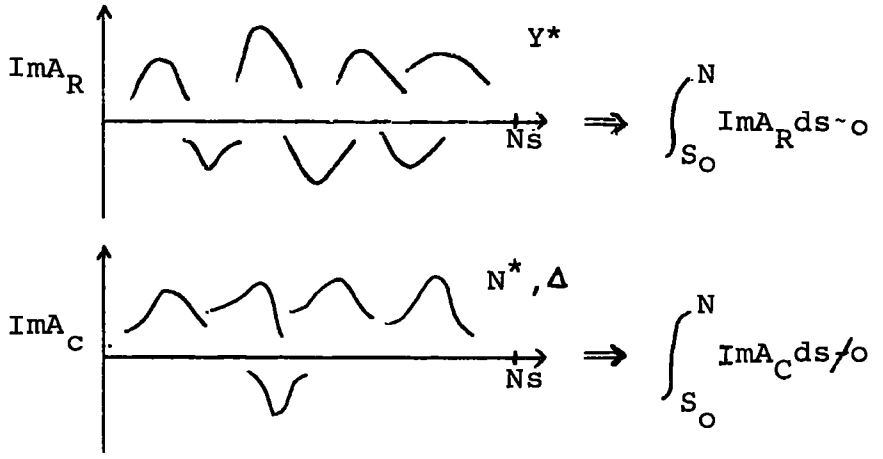

Fig. (2.7.1)

The first of these finite energy sum-rules (FESR) involving Y^* resonances and hyperon bound states has been checked at $t = m^2_{K^*_V}$ (where the K^*_V pole is expected to dominate) by Schmidt and Storrow[64] and found to be well satisfied. A scattering region FESR for $K^-n \longrightarrow \pi^-\Lambda$ and $\pi^+n \longrightarrow K^+\Lambda$ has been reported by Jackson and Field[65]. Despite several parametrisation problems (see Reference (65)), the following tentative conclusions were reached:-

(a) The EXD pole prediction was good for the t-channel helicity flip amplitudes only (and consequently the s-channel flip also).

(b) The $\frac{d\sigma}{dt}$ energy and momentum transfer dependence was well described only in $\bar{K}N \longrightarrow \pi\Lambda$.

(c) It was concluded that the natural duality of leading resonances and leading poles is broken in $\pi N \longrightarrow K\Lambda$ by the presence of strongly coupled resonances which lie lower in the Chew Frautschi Plot.

We show a direct link between dominant s-channel resonances and $\frac{d\sigma}{dt}$ slope at intermediate energies. Ignoring spin and using equal mass kinematics we partial-wave decompose the amplitude as

$$T = \sum_{\ell} (2\ell+1) P_{\ell} (\cos\theta) f_{\ell}(s) \qquad (2.7.1)$$

where

$$\frac{d\sigma}{dt} = |T|^2 \qquad (2.7.2)$$

If we define the slope b as in equation (2.2.3), then since

$$\cos\theta = 1 + \frac{t}{2q^2} \qquad (2.7.3)$$

we find

$$\frac{b}{2} \simeq \frac{1}{T} \frac{dT}{dt}\bigg|_{t=0} = \frac{\sum_{\ell} (2\ell+1) f_{\ell} \frac{\ell(\ell+1)}{4q^2}}{\sum_{\ell} (2\ell+1) f_{\ell}} = \frac{\langle \ell(\ell+1) \rangle}{4q^2} \qquad (2.7.4)$$

We thus expect processes dominated at low energies and small angles by the higher spin resonances to exhibit the greater forward peak slopes at momenta where FESR arguments can apply, say 2-4 GeV.

Mean values of b in the range 3-4 GeV were calculated and are compared in Table (2.7.1) reaction by reaction with the positions in the Chew-Frautschi plot of the relevant dominant baryon resonance trajectories. The integers in the third column qualitatively describe in

ascending order the highest to lowest trajectories.

Reaction	Dominant s-channel Resonances	J-plane Position	Mean b GeV^{-2}
$\pi^+ p \rightarrow K^+\Sigma^+$	Δ	1	10
$\pi^- p \rightarrow K^o\Sigma^o$	Δ,N*	2	10
$\pi^- p \rightarrow K^o\Lambda^o$	N*	3	9
$K^- p \rightarrow \pi^o\Sigma^o$	Y_o^*	4	-
$K^- p \rightarrow \pi^-\Sigma^+$	Y_o^*, Y_1^*	5	8
$K^- n \rightarrow \pi^-\Sigma^o$	Y_1^*	6	5
$K^- n \rightarrow \pi^-\Lambda^o$	Y_1^*	6	5
$K^- p \rightarrow \pi^o\Lambda^o$	Y_1^*	6	5
$K^o p \rightarrow \pi^+\Lambda^o$	Y_1^*	6	5

Table (2.7.1)

A high degree of correlation between the s-channel resonances and the cross-section slopes is evident, indicating the relevance of considering direct channel effects at momenta as high as 3 or 4 GeV.

Also by inspection of the Particle Data Group tables[66] of masses, spins and branching ratios, we note that empirically the Y* resonances are more strongly coupled to $\bar{K}N$ than the N*'s are to KY even allowing for threshold factors, so one would expect that $\frac{d\sigma}{dt}$ (R) > $\frac{d\sigma}{dt}$ (C) at intermediate energies as observed.

Finally, in this chapter we summarise our findings. We believe from the evidence of the high energy fits to the data presented in this chapter and from sundry FESR arguments, that HCEX reactions are reasonably well described by EXD poles with weak absorption only at high momenta and small $|t|$. At lower momenta the absorptive corrections to the predominantly real R-type amplitude appear too strong as compared to the C-type. In view of this the excellent polarisation description is surprising.

The necessary extra corrections can be appreciated as the persistent effects of direct channel resonances which are outside a classical dual scheme (non-peripheral)[65] Alternatively it may be (see Chapter 3) that a multiple t-channel exchange picture is relevant at intermediate energies.

C H A P T E R T H R E E

LINE REVERSAL, EXOTIC EXCHANGES AND REGGE-REGGE CUTS

3. Line reversal, exotic exchanges and Regge-Regge cuts

In this chapter we investigate a possible explanation of the observed line-reversal equality violation noted in Section 2.1 and of certain non-zero double charge (exotic) exchange reaction cross-sections[67]. The explanation is in terms of multiple Regge exchanges and the formalism used is the same "box-diagram" prescription of Section 2.4. Its interpretation in terms of J-plane singularities is briefly discussed.

3.1 Motivation for Regge-Regge cuts

The need for some J-plane cuts to shield fixed poles at wrong signature nonsense points[24] has already been noted. The assumption that simply Pomeron-Regge cuts are phenomenologically important is only obvious at very high energies assuming we know correctly how to calculate the branch points. In the absence of any well-defined method of calculating their strength, the possibility of Regge-Regge cuts cannot be discounted in any consistent picture of multiple t-channel exchanges.

A hierarchy of Reggeised exchanges has been considered by Harrari[68] and can be represented schematically by

$$T = R + P \otimes R + R \otimes R + R \otimes P \otimes R + R \otimes R \otimes R + \ldots\ldots \qquad (3.1.1)$$

(3.1.2)

where R are non-Pomeron Regge exchanges and P is the Pomeron. As is the case throughout this chapter, the

symbol ⊗ denotes a b or t-space convolution (see Appendix 2B and Section 3.3) so that the second, third etc. terms of equations (3.1.1) and (3.1.2) loosely represent absorbed Regge pole, Regge-Regge cut, absorbed Regge-Regge cut, and so on. The question of whether such box diagrams can approximate true J-plane Regge cuts is considered in Section 3.2,

When the R term in equation (3.1.1) is taken to be EXD Regge poles, it was shown in Chapter 2 that the first two terms of equation (3.1.1) together predict a Line-Reversal Symmetry Violation (LRSV) of the wrong sign and of too small magnitude at intermediate energies. It was suggested by Michael[63] that inclusion of the next term of series (3.1.1) might account for the observed energy dependence (Figure (2.1.1)) of the LRSV since the branch point of a Regge-Regge cut can be estimated to be typically about $\alpha_{cut}(0) = -.5$ compared with $\alpha_{pole}(0) = .4$.

Analogously to forward scattering, the presence or absence of a peak in backward meson-baryon scattering is usually correlated with the presence or absence of a non-exotic u-channel baryon exchange. The observation of a sizeable peak in backward K^-p scattering at 5 GeV[69] can then only be understood in terms of exotic u-channel quantum numbers. One realisation of this exotic exchange would be in terms of the simultaneous exchange of non-exotic meson and baryon Regge trajectories.

We have noted a LRSV in

$$K^-p \longrightarrow \pi^-\Sigma^+$$

and

$$\pi^+p \longrightarrow K^+\Sigma^+ \qquad (3.1.3)$$

These processes are intimately related to the processes

$$K^- p \longrightarrow \pi^+ \Sigma^-$$

and $$\pi^- p \longrightarrow K^+ \Sigma^- \qquad (3.1.4)$$

In terms of t-channel amplitudes, (3.1.3) involve isospin $I_t = \frac{1}{2}$ and exotic $I_t = 3/2$ (assumed zero in the arguments of Chapters 1 and 2), whereas (3.1.4) involve only $I_t = 3/2$. Thus at high energies where t-channel single exchange amplitudes are expected to be a good approximation, to the same extent we expect vanishing cross-sections for processes (3.1.4). This is not what is observed[67] (see Figure (3.1.1)). The possibility then exists that the LRSV in reactions (3.1.3) and the non-vanishing cross-sections for (3.1.4) have a common explanation - non-zero $I_t = 3/2$ amplitudes described by the simultaneous exchange of $I_t = 1$ and $I_t = \frac{1}{2}$ Regge trajectories.

Before proceeding to more theoretical considerations and a quantitative calculation, we give an estimate of the magnitudes of the above effects.

The relevant amplitudes are

$$A^t(K^- p \longrightarrow \pi^- \Sigma^+) = \frac{2}{3} I_{\frac{1}{2}} + \frac{1}{3} I_{3/2} \qquad (3.1.5)$$

$$A^t(\pi^+ p \longrightarrow K^+ \Sigma^+) = -\frac{2}{3} I^1_{\frac{1}{2}} + \frac{1}{3} I^1_{3/2} \qquad (3.1.6)$$

$$A^t(K^- p \longrightarrow \pi^+ \Sigma^-) = I_{3/2} \qquad (3.1.7)$$

$$A^t(\pi^- p \longrightarrow K^+ \Sigma^-) = I^1_{3/2} \qquad (3.1.8)$$

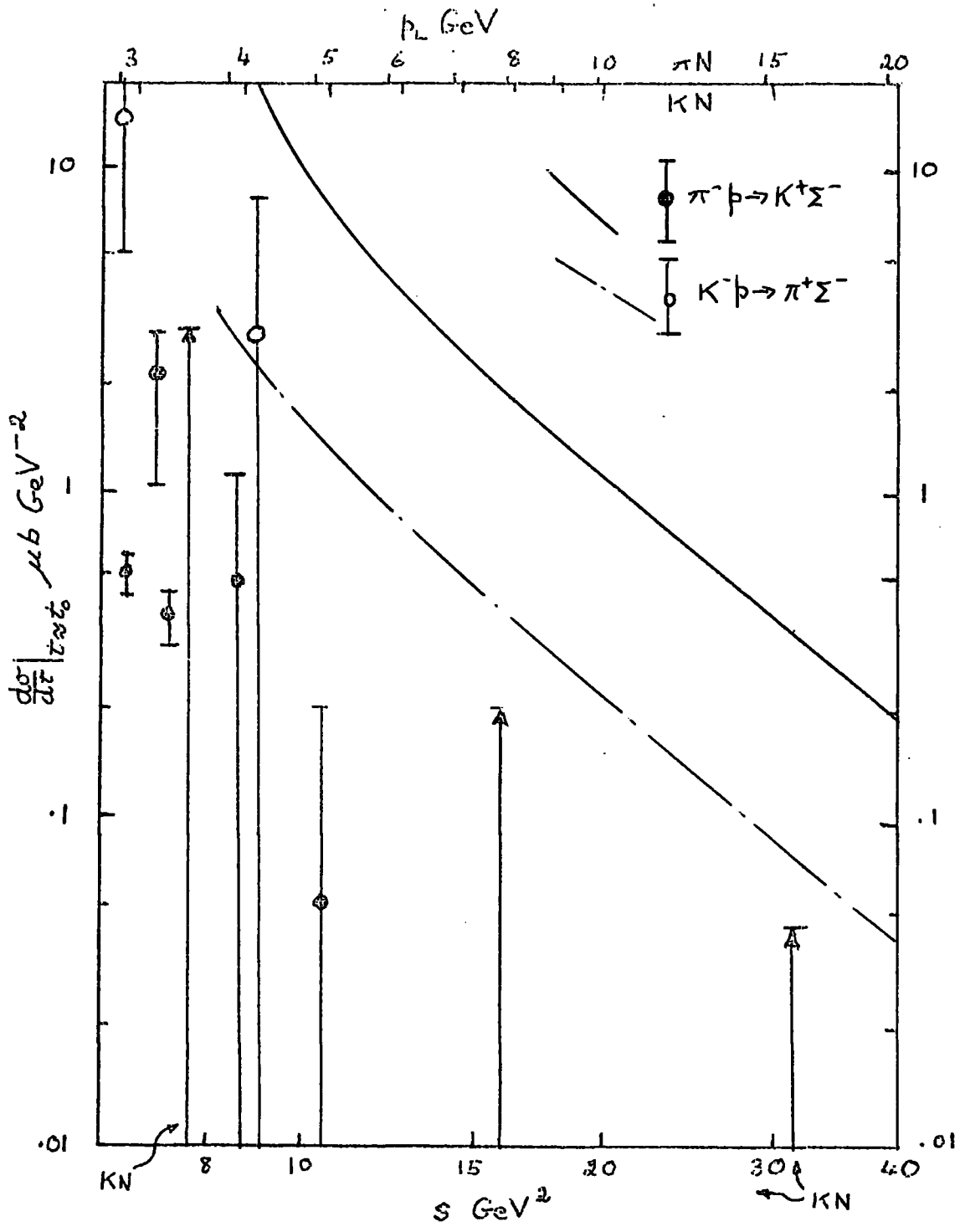

Fig. (3.1.1)

Exotic exchange data with predictions from lowest intermediate states, unsymmetrised, unabsorbed box diagram. The data is from reference (67).

Note that for line-reversal symmetry

$$|I^1_{\frac{1}{2}}| = |I_{\frac{1}{2}}|$$

and $$I^1_{3/2} = I_{3/2} = 0 \qquad (3.1.9)$$

At $t = t_o$, only the non-flip amplitudes are non-zero. We consider this situation:-

$$\text{Let } I_{n/2} = M_{n/2}\, e^{i\phi n/2} \qquad (3.1.10)$$

Then

$$\frac{\frac{d\sigma}{dt}(\pi^-\Sigma^+)}{\frac{d\sigma}{dt}(K^+\Sigma^+)} = \frac{\frac{4}{9}(M_{\frac{1}{2}})^2 + \frac{1}{9}(M_{3/2})^2 + \frac{4}{9}M_{\frac{1}{2}}M_{3/2}\cos(\phi_{\frac{1}{2}}-\phi_{3/2})}{\frac{4}{9}(M^1_{\frac{1}{2}})^2 + \frac{1}{9}(M^1_{3/2})^2 - \frac{4}{9}M^1_{\frac{1}{2}}M^1_{3/2}\cos(\phi^1_{\frac{1}{2}}-\phi^1_{3/2})}$$

$$\simeq \left(\frac{M_{\frac{1}{2}}}{M^1_{\frac{1}{2}}}\right)^2 \frac{1 + \frac{M_{3/2}}{M_{\frac{1}{2}}}\cos(\phi_{\frac{1}{2}} - \phi_{3/2})}{1 - \frac{M^1_{3/2}}{M^1_{\frac{1}{2}}}\cos(\phi^1_{\frac{1}{2}} - \phi^1_{3/2})} \qquad (3.1.11)$$

assuming $$\left(\frac{M_{3/2}}{M_{\frac{1}{2}}}\right)^2 << 1 \qquad (3.1.12)$$

Now suppose $M_{\frac{1}{2}}$ is given by abosrbed Regge exchange as in Chapter 2 (P is assumed to be an isosinglet) and that $M_{3/2}$ is given by

$$M_{3/2} = \sqrt{\frac{d\sigma}{dt}(\pi^+\Sigma^-)} \simeq \sqrt{3\mu b\,GeV^{-2}} \qquad (3.1.13)$$

$$M^1_{3/2} = \sqrt{\frac{d\sigma}{dt}(K^+\Sigma^-)} \simeq \sqrt{.5\mu b\,GeV^{-2}} \qquad (3.1.14)$$

using data from Figure (3.1.1) at 4 GeV. The largest possible cross-section ratio (3.1.11) occurs when both cosines are near unity.

i.e.

$$\frac{\frac{d\sigma}{dt}(\pi^- \Sigma^+)}{\frac{d\sigma}{dt}(K^+ \Sigma^+)} \lesssim \frac{300}{500} \times \frac{1 + .1}{1 - .03} \simeq .68 \qquad (3.1.15)$$

The LRSV due to pole plus Pomeron cut (in the wrong direction) completely outweighs any LRSV due to the $I_t = 3/2$ amplitudes. We conclude that if Regge-Regge cuts do provide a common explanation of the features of processes (3.1.3) and (3.1.4), then $I_t = 3/2$ cuts $[(I_t = \frac{1}{2}) \otimes (I_t = 1)]$ are responsible in the exotic exchange case, but $I_t = \frac{1}{2}$ [probably from $(I_t = \frac{1}{2}) \otimes (I_t = 0)$] are responsible for the cross-section inequalities in (3.1.3).

3.2 Theoretical aspects of Regge-Regge Cuts

It has been well known for some time that the angular momentum plane cuts represented by amplitudes such as (3.3.15) and diagrams such as in (3.1.2) and Figure (3.4.1) are cancelled by other graphs (whose presence is required by unitarity), when interpreted in terms of Feynman diagrams[70]. The essential feature lacking in diagrams like those of Figure (3.4.1) is the presence of a third double spectral function[71] which would ensure a non-zero angular momentum plane discontinuity in a Froissart-Gribov projection of the partial-wave amplitude. The simplest Feynman ladder diagram with this property, necessarily a non-planar one, is shown in Figure (3.2.1).

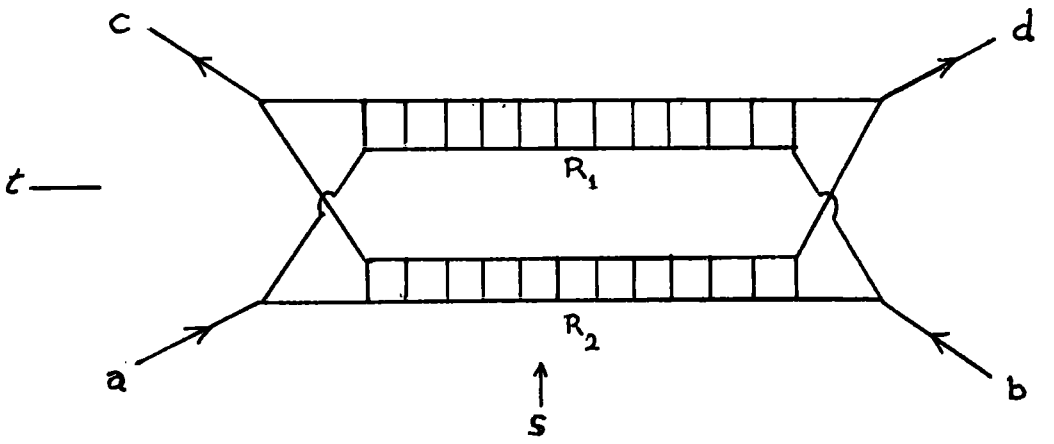

Fig. (3.2.1)

The "ladders" R_1 and R_2 are the Feynman diagram representations of Reggeons used in the Gribov Reggeon Calculus[72]. It is formally possible to calculate diagrams like that in Figure (3.2.1) together with its higher order analogues but as with other hadronic perturbative expansions, the convergence problems are insuperable at present.

In the course of the unitarisation program of the Veneziano amplitude[73] considerable progress[74] has been made in developing perturbative expansions of dual amplitudes each term of which corresponds in some way to an order of multiple Regge exchange. Two results from consideration of the dual aspects of double exchange concern the present analysis.

(i) <u>The Finkelstein Selection Rule[75]</u>

Suppose a double exchange diagram can be represented as two successive Reggeon-particle amplitudes each in principle constructed from a dual amplitude (e.g. Veneziano) as shown in Figure (3.2.2).

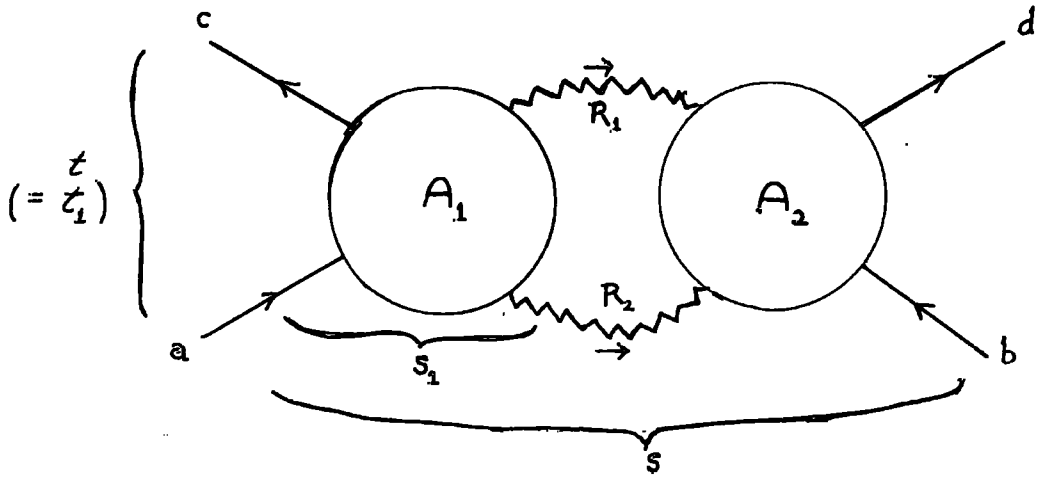

Fig. (3.2.2)

The kinematics for amplitude $A_1(s_1,t_1,u_1)$ are as shown. The third double spectral function requirement can be satisfied by demanding the existence of a planar su dùality diagram for each of the s-channel processes.

$$a\ \bar{R}_2 \longrightarrow c\ R_1 \tag{3.2.1}$$

and

$$R_2\ b \longrightarrow \bar{R}_1\ d \tag{3.2.2}$$

For example, if an s_1u_1 Veneziano term can be written for the amplitude A_1 of Figure (3.2.2) then the s_1 and u_1 channels will both contain resonances so that the double discontinuity (third double spectral function) will be non-zero.

This strong necessary condition derived from a reasonably weak set of assumptions has several implications for the existence properties of Regge-Regge cuts[75]. However no constraints are imposed on,

(a) Pomeron-Regge cuts, since the Pomeron lies outside single exchange dual schemes,

or (b) the R⊗R cuts in processes (3.1.3) and (3.1.4), which we shall consider.

(ii) Single loop diagrams and multiple scattering models

Lovelace[76] has compared the explicit cut amplitudes implied by the naive multiple scattering model (Appendix 2B and Section 3.4) and by the double scattering dual expansion analogue of Figure (3.2.1) that is a single loop non-planar diagram which has been shown[77] to contain a Regge-Regge cut. The comparison is made in terms of the Gribov Regge cut calculus[72] in which the third double spectral function is non-zero through the presence of fixed poles in the sub-amplitudes whose residues are crucial in determining the strength of the double-exchange cut. Thus

$$T_{Gribov} = \iint d^2\underset{\sim}{k}\,[N(\underset{\sim}{k},\underset{\sim}{\Delta}-\underset{\sim}{k})]^2 R(-\underset{\sim}{k}^2,s)R(-(\underset{\sim}{\Delta}-\underset{\sim}{k})^2,s) \qquad (3.2.3)$$

where R are Reggeon propagators

$\underset{\sim}{k}$ is a loop momentum

$\underset{\sim}{\Delta}^2 = -t$

Lovelace shows that N is a residue of a fixed pole (in the Veneziano subgraph in this instance, an (s,u) term in fact - see (i)). By comparison the multiple scattering (MS) model would give

$$T_{MS} = g^4 \iint d^2\underset{\sim}{k}\; R(-\underset{\sim}{k}^2,s)R(-(\underset{\sim}{\Delta}-\underset{\sim}{k})^2,s) \qquad (3.2.4)$$

where g is the coupling of a box diagram vertex.

Direct comparison yields

$$N^2 = g^4 \, 2^{-2(\alpha(s)+\alpha(u))} \tag{3.2.5}$$

when a zero'th order Veneziano graph is used. The extra factor amounts to

$$2^{-2\alpha'[\Sigma m_i^2 - t]} \tag{3.2.6}$$

where m_i is the mass on each Veneziano leg. Since the convolution (3.2.3) is dominated by $|t| << 1$ this does not represent any great departure from the amplitude structure predicted by the MS model. The application to reactions with spin (our case) is not clear since we cannot even describe realistically single exchanges with spin in a dual model, but the form of the results is encouraging. A more serious problem is the convergence properties of sums of terms like (3.2.4) each representing a particular pair of intermediate states. The approximation of the MS model can be summarised as being the assumption of saturation of the Schwarz[78] sum rule

$$N(t) = \int_{s_o}^{\infty} \mathrm{Im}\, A^{(s)}(s^1,t)\,ds^1 \tag{3.2.7}$$

by the first intermediate bound state possible in the Reggeon-particle scattering amplitude $A^{(s)}(s^1,t)$, the effect of higher states being accounted for by a multiplicative constant $\lambda>1$. Lovelace has shown[76] that in some cases, assuming saturation by all possible intermediate states,(3.2.7) may not converge and that in all cases any finite truncation (as in the MS model) will produce an incorrect result.

In the absence of any other prescription, we will assume that the coupling constants g are decreasing and that some renormalisation procedure exists such that the finite sum of the terms like (3.2.4) is approximately given by the lowest well-known strongly coupled states.

3.3 The multiple scattering model

The absorption prescription of Chapter 2 can be seen to be only the second term in a multiple scattering expansion which arises in an eikonalisation procedure. In this latter treatment[79] which has its origins in nuclear physics, a small angle scattering process is viewed as a plane wave (the projectile) passing through the scattering medium (the target) suffering a series of infinitessimally small deflections such that at each stage the wave gathers a small phase change, the momentum being unaltered (i.e. the partial waves have small non-zero phase shifts).

The helicity amplitudes† for the process may be partial-wave decomposed

$$A_n(s,t) = 16\pi \sum_{J=\min(\lambda,\mu)}^{\infty} (2J+1) d^J_{\lambda\mu}(\cos\theta) f^J_n(s) \qquad (3.3.1)$$

where λ and μ are baryon helicities and $n = |\lambda - \mu|$, the net helicity flip. We follow the treatment of Reference (71) and make the impact parameter approximation to equation (3.3.1)

†The normalisation of Chapter 2 is again used.

$$A_n(s,t) = 32\pi q^2 \int_0^\infty bdb\ f_n(b,s) J_n(b\sqrt{-t}) \tag{3.3.2}$$

where $$J = qb - \tfrac{1}{2} \tag{3.3.3}$$

defines b, the impact parameter and

$$f_n^J(s) \approx f_n(b,s) \tag{3.3.4}$$

The eikonal phase $\chi_n(b,s)$ is defined by

$$f_n^J(s) = \frac{e^{2i\delta_J^n(s)} - 1}{4iq/\sqrt{s}} \tag{3.3.5}$$

$$\approx f_n(b,s) = \frac{e^{i\chi_n(b,s)} - 1}{4iq/\sqrt{s}} \tag{3.3.6}$$

Substituting equation (3.3.6) in equation (3.3.2) leads, on expanding the exponential, to

$$A_n(s,t) \approx 8\pi q\sqrt{s} \int_0^\infty bdb\left[\chi_n(b,s) + i\frac{\chi_n^2}{2}(b,s) - \frac{\chi_n^3(b,s)}{3!} \ldots\right] \times J_n(b\sqrt{-t}) \tag{3.3.7}$$

which should be a rapidly convergent series if the small phase shift assumption is good. At this stage we replace the χ, χ^2, χ^3, ... terms by

$$\chi_n \longrightarrow \chi^R$$

$$\frac{\chi_n^2}{2} \longrightarrow \tfrac{1}{2}(\chi^R\chi^P + \chi^P\chi^R + \chi^R\chi^{R^1} + \chi^{R^1}\chi^R)$$

$$\frac{\chi_n^3}{3!} \longrightarrow \frac{1}{3!}(\chi_R\chi_{R^1}\chi_P + \ldots\ldots) \tag{3.3.8}$$

etc.

It will be seen that ignoring the R^1 term in the first two lines of (3.3.8) reproduces the absorption model result of Chapter 2. Of course the right side of (3.3.8) is summed over all possible helicity configurations giving net helicity flip n. The m! in the denominators of (3.3.8) corresponds to the number of ways of ordering the m exchanges in a box diagram.

The inverse of equations (3.3.2) and (3.3.6) is

$$\chi_n^R(b,s) = \frac{1}{8\pi q\sqrt{s}} \int_{-\infty}^{o} \frac{dt}{2} J_n(b\sqrt{-t})\ A_n^R(s,t) \qquad (3.3.9)$$

where $A_n^R(s,t)$ is some single exchange amplitude. Suppose we can express this amplitude in the simple parametric form

$$A_n^R(s,t) = (-t)^{\frac{n}{2}} \left(\sum_m a_n(s) t^m\right) e^{b_n(s)t} \qquad (3.3.10)$$

$$\text{then} \quad \chi_n^R(b,s) = \frac{1}{8\pi q\sqrt{s}} \sum_m (-)^m a_m I_{m,n} \qquad (3.3.11)$$

$$\text{where } I_{m,n} = \int_o^{\infty} \frac{dx}{2}\, x^{m+n/2} e^{-b_n x} J_n(b\sqrt{x}) \qquad (3.3.12)$$

$$\text{Now } I_{o,n} = \frac{b^n e^{-b^2/4b_n}}{(2b_n)^{n+1}} \qquad (3.3.13)$$

$$\text{and } I_{m,n} = (-)^m \frac{d^m}{db_n^m} I_{o,n} \qquad (3.3.14)$$

Consequently, using equation (3.3.7), a double exchange (1 and 2) gives a contribution to $A_n(s,t)$ of

$$A_n^{1,2}(s,t) = \frac{i}{8\pi q\sqrt{s}} \frac{a_{n_1} a_{n_2}}{(2b_{n_1})^{n_1+1} (2b_{n_2})^{n_2+1}} H_{n_1,n_2}(s,t) \qquad (3.3.15)$$

where

$$H_{n_1,n_2}(s,t) = \int_o^\infty bdbb^{n_1+n_2} e^{-\frac{b^2}{4}(\frac{1}{b_{n1}} + \frac{1}{b_{n2}})} J_n(b\sqrt{-t}) \qquad (3.3.16)$$

in the case where no summation is involved in equation (3.3.11). When higher terms are present, derivatives are taken as in equation (3.3.14). The n_i in equations (3.3.15) and (3.3.16) are the net helicity flips at the single exchange vertices. Thus we see that although $A_1(s,t)$ can receive contributions only from $\chi_o^{R_1}\chi_1^{R_2}$ and permutation, $A_o(s,t)$ includes terms both like $\chi_o^{R_1}\chi_o^{R_2}$ and like $\chi_1^{R_1}\chi_1^{R_2}$. We therefore use

$$H_{n_1,n_2}(s,t) = \frac{(-t)^{n/2} e^{t/(\frac{1}{b_{n1}} + \frac{1}{b_{n2}})}}{(\frac{1}{2})^{n/2} (\frac{1}{b_{n_1}} + \frac{1}{b_{n_2}})^{n+1}} \qquad (3.3.17)$$

for all n_1, n_2 such that $n_1 + n_2 = n$, and

$$H_{1,1}(s,t) = \frac{8\left[1 + \frac{t}{(\frac{1}{b_{n1}}+\frac{1}{b_{n2}})}\right] e^{t/(\frac{1}{b_{n1}} + \frac{1}{b_{n2}})}}{(\frac{1}{b_{n_1}} + \frac{1}{b_{n_2}})^2} \qquad (3.3.18)$$

when $n = 0$ and $n_1 = n_2 = 1$.

In our applications only the first three lines of series (3.3.8) are used. The possible inclusion of the third line follows the work of reference (80), which was received after most of the analysis to be described was completed. When an extra Pomeron exchange is included, the alteration to terms like (3.3.17) and (3.3.18) is

simple if the Pomeron is assumed to couple only to non-flip baryon vertices (as in Chapter 2). Equations (3.3.15) and (3.3.17) for example then acquire the additional term

$$A_n^{1,2,P}(s,t) = - \frac{a_{n_1}\, a_{n_2}\, a_P}{(8\pi q\sqrt{s})^2 (2b_{n_1})^{n_1+1} (2b_{n_2})^{n_2+1} (2b_P)} H_{n_1,n_2,P}(s,t) \qquad (3.3.19)$$

where

$$H_{n_1,n_2,P}(s,t) = \frac{(-t)^{n/2}\, e^{t/\left(\frac{1}{b_{n_1}} + \frac{1}{b_{n_2}} + \frac{1}{b_P}\right)}}{(\tfrac{1}{2})^{n/2} \left(\frac{1}{b_{n_1}} + \frac{1}{b_{n_2}} + \frac{1}{b_P}\right)^{n+1}} \qquad (3.3.20)$$

The $\frac{1}{3!}$ in equation (3.3.7) is cancelled since for each of the 2! configurations in double exchange there are three orderings of the extra Pomeron exchange. When (3.3.19) is added to (3.3.15) it is found that a very close cancellation occurs between them, especially in the n = o amplitude. This cancellation, which is made important at t near t_o by inclusion of an enhancement factor (λ), is much more complete than that between single exchange and its cut term where the cut is only some 20% of the pole in magnitude in the forward direction. This fact will be made use of in the next section.

3.4 Application to exotic exchange processes

Previous model calculations in the field of exotic hypercharge exchange processes such as (3.1.4) have been made. Those of Michael[63] and Dean[81] took little

account of the effects of spin which will be shown to be qualitatively as well as quantitatively important. A K-matrix calculation by Rivers[82] of the $t = t_o$ cross-section for these processes agrees well with one of our estimates under a similar set of assumptions (lowest intermediate states only, no s-u symmetrisation, and no additional absorption). Calculations taking into account the effects of spin were made contemporarily but independently of the present work, by Quigg[83] and by Henyey, Kane and Scanio[80]. The similarities and differences with our analysis will be noted.

The data ($\frac{d\sigma}{dt}$ near $t=t_o$) for the reactions

$$K^- p \rightarrow \pi^+ \Sigma^- \qquad (3.4.1)(a)$$

$$\pi^- p \rightarrow K^+ \Sigma^- \qquad (3.4.1)(b)$$

are shown in Figure (3.1.1). Note that little data (particularly for (3.4.1)(a)) are available above 3 GeV where a t-channel description might be thought relevant. The strong s-dependence (s^{-9}) of $\frac{d\sigma}{dt}$ between 2 and 4 GeV has already been noted[67]. The scarcity of data above 3 GeV prevents the possibility of a Regge-Regge cut description (energy dependence $\sim s^{-3}$) being discounted at the outset.

We make the assumption of lowest intermediate states only, leading to the diagrams in Figure (3.4.1) which may be broken down as indicated into the convolution of a charge exchange (CEX) and a hypercharge exchange (HCEX)

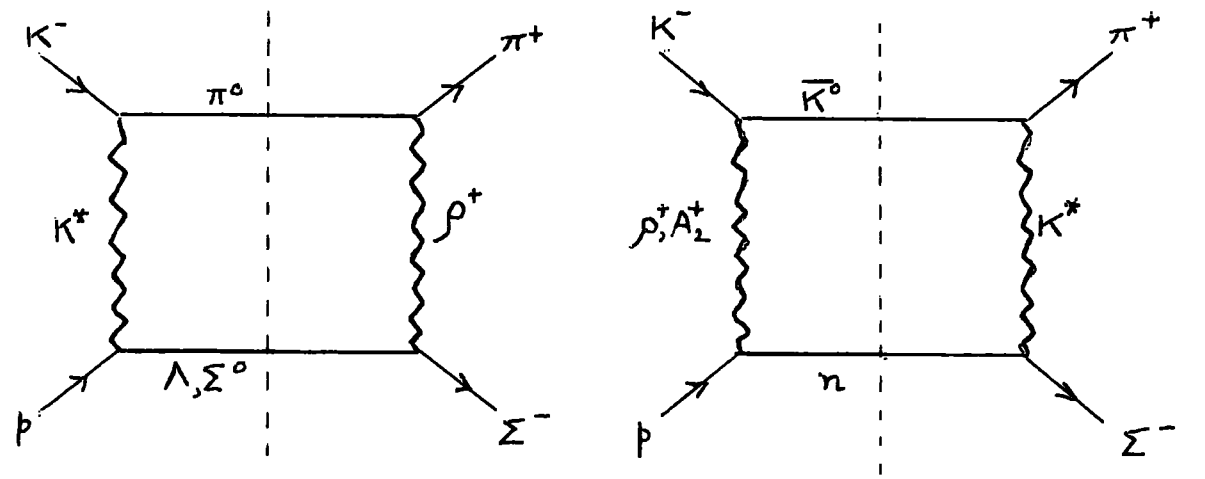

(a) $K^- p \to \pi^+ \Sigma^-$

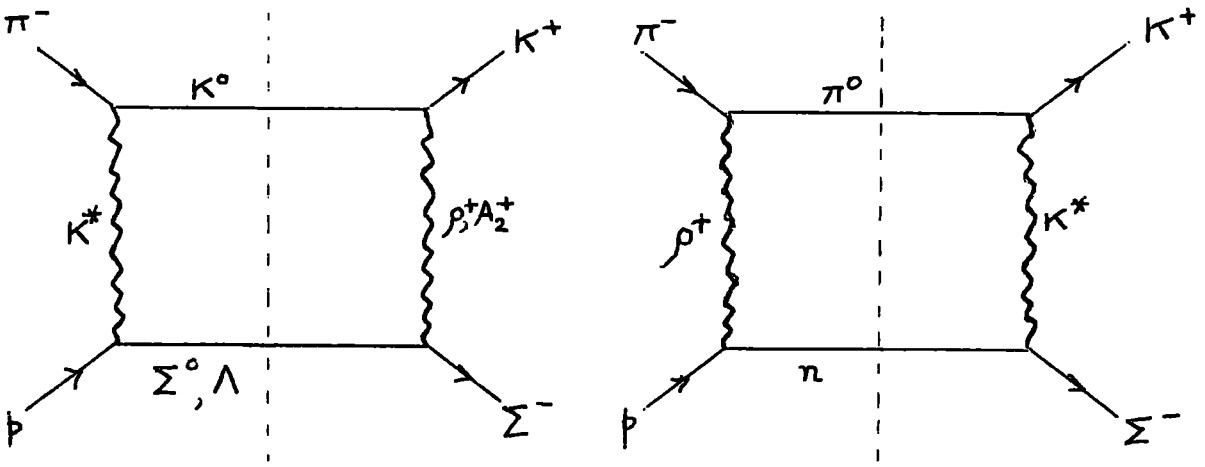

(b) $\pi^- p \to K^+ \Sigma^-$

Fig. (3.4.1)

Lowest intermediate state diagrams for exotic exchange.

graph. Where a single exchange graph does not correspond to a well-measured process for which phenomenological fits exist, SU(3) and/or isospin is used as necessary to relate it to one which does, as follows:-

$$2(K^- p \longrightarrow \pi^o \Sigma^o) = K^- p \longrightarrow \pi^- \Sigma^+ = \bar{K}^o n \longrightarrow \pi^+ \Sigma^- \qquad (3.4.2)$$

$$K^- p \longrightarrow \pi^o \Lambda = \frac{1+2f}{2\sqrt{3}(1-2f)} (K^- p \longrightarrow \pi^- \Sigma^+) \qquad (3.4.3)$$

$$\pi^o \Sigma^o \longrightarrow \pi^+ \Sigma^- = -\sqrt{2} f (\pi^- p \longrightarrow \pi^o n) \qquad (3.4.4)$$

$$\pi^o \Lambda^o \longrightarrow \pi^+ \Sigma^- = -\sqrt{\frac{2}{3}} (1-f) (\pi^- p \longrightarrow \pi^o n) \qquad (3.4.5)$$

$$K^o \Sigma^o \longrightarrow K^+ \Sigma^- = \sqrt{2} f (K^o p \longrightarrow K^+ n) \qquad (3.4.6)$$

$$K^o \Lambda^o \longrightarrow K^+ \Sigma^- = \sqrt{\frac{2}{3}} (1-f) (K^o p \longrightarrow K^+ n) \qquad (3.4.7)$$

$$\pi^o n \longrightarrow K^+ \; ^- = -\frac{1}{\sqrt{2}} (\pi + p \longrightarrow K^+ \Sigma^-) \qquad (3.4.8)$$

where f is given by equation (2.6.4).

The pole parameters for use in equation (3.3.10) were taken from the references of Table (3.4.2). For the EXD poles K_V^*, K_T^* and ρ, A_2 the parameters were expressed as

$$\begin{aligned} a_n &= \gamma_n e^{\alpha_o (i\phi + \log s)} \\ b_n &= \alpha^1 (i\phi + \log s) + \varepsilon_n \end{aligned} \qquad (3.4.9)(a)$$

and for the ρ pole we wrote

$$m a_n = i\gamma_n e^{\alpha_o(\log s - \frac{i\pi}{2})} \times \begin{cases} \alpha_o & m = 0 \\ \alpha^1 & m = 1 \\ \frac{\alpha_o}{2m_\rho^4} & m = 2 \\ \frac{\alpha^1}{2m_\rho^4} & m = 3 \end{cases} \qquad (3.4.9)(b)$$

$$b_n = \alpha^1(\log s - i\tfrac{\pi}{2}) + \varepsilon_n$$

$$\varepsilon_n = \frac{1}{m_\rho^2}$$

The values of α_o, α^1, γ_n, ε_n and ϕ used in the cases (a) and (b) are shown in Table (3.4.1) where the couplings refer to the processes of Table(3.4.2).

Exchange	$K^*_{V,T}$	ρ, A_2	ρ
α_o	0.4	0.5	0.5
α^1	0.8	1.0	1.0
γ_o	59.5	7.5	-17.0
γ_1	24.0	62.0	-139.0
ε_o	1.07	0.0	0.54
ε_1	0.77	0.0	0.54
ϕ	0	$-\pi$	—

Table (3.4.1)

Note that:

(i) Since the KN CEX fit was not absorbed we made a 20% increase in the non-flip residues for the sake of consistency.

(ii) Since the $K^- p \rightarrow \pi^o \Lambda$ data are inferior to those for $K^- p \rightarrow \pi^- \Sigma^+$, parameters for the latter were used in every case (see equation (3.4.2)).

Exchange	Process	Type of Fit	Reference
K^*	$K^- p \rightarrow \pi^- \Sigma^+$	EXD poles/weak cuts	(42) and Chapter 2.
ρ	$\pi^- p \rightarrow \pi^o n$	pole/weak cut	(84)
ρ, A_2	$K^- p \rightarrow \bar{K}^o n$	Veneziano	(85)

Table (3.4.2)

The approximate compatibility (via SU(3)) of the exchange parameters in πN and KN CEX graphs was checked. Currently acceptable[50,62] octet mixing parameters of

$$\left.\begin{aligned} (F/D)_{n=0} &= -5 \\ (F/D)_{n=1} &= \frac{2}{3} \end{aligned}\right\} \quad \text{or} \quad \left\{\begin{aligned} f_o &= \frac{5}{4} \\ f_1 &= \frac{2}{5} \end{aligned}\right. \tag{3.4.10}$$

were used to give the results presented, although other values such as those of Chapter 2 were tried. Cross-section predictions were essentially independent of these changes.

Under the assumptions outlined above and in the case of no extra absorption, we predict the cross-sections

shown in Figures (3.1.1) and (3.4.2). Note that (Figure (3.1.1)) the prediction for $K^-p \longrightarrow \pi^+\Sigma^-$ is compatible within the large error bars but that for $\pi^-p \longrightarrow K^+\Sigma^-$ is much too large being on the wrong side of the $K^-p \longrightarrow \bar{\pi}^+\Sigma^-$ prediction. The energy dependence of the calculated values corresponds to

$$\alpha_{eff}(t) \simeq -0.3 + 0.1t \qquad (3.4.11)$$

as compared to the simple asymptotic argument[71],

$$\alpha_c(t) = \alpha_1(0)+\alpha_2(0)-1+\frac{\alpha_1^1\alpha_2^1 t}{\alpha_1^1+\alpha_2^1} = -0.1 + 0.4t \qquad (3.4.12)$$

where $\alpha_1 = \alpha_{K^*}$ and $\alpha_2 = \alpha_\rho$

The outstand feature of the angular distribution (Figure (3.4.2)) is of course the overall helicity-flip dominated character of the predictions. The origin of the effect can be appreciated in Figure (3.4.3). Because of our EXD pole assumption we expect vector exchanges to contribute little to cut amplitudes since unlike the tensor components they contain nonsense factors, $\alpha(t)$, which induce cancellations in the convolution. The dominance of the non-flip K_T^*/flip A_2 contribution is thus anticipated. Our estimates contrast with the overall non-flip dominance predicted in Reference (83) where unreasonable quark model spin couplings are used. We are also at variance in this respect with Reference (80) where the non-flip dominance is claimed to come from the relative importance of the double flip cut (c.f. our estimate in Figure (3.4.3)). We shall return to this point.

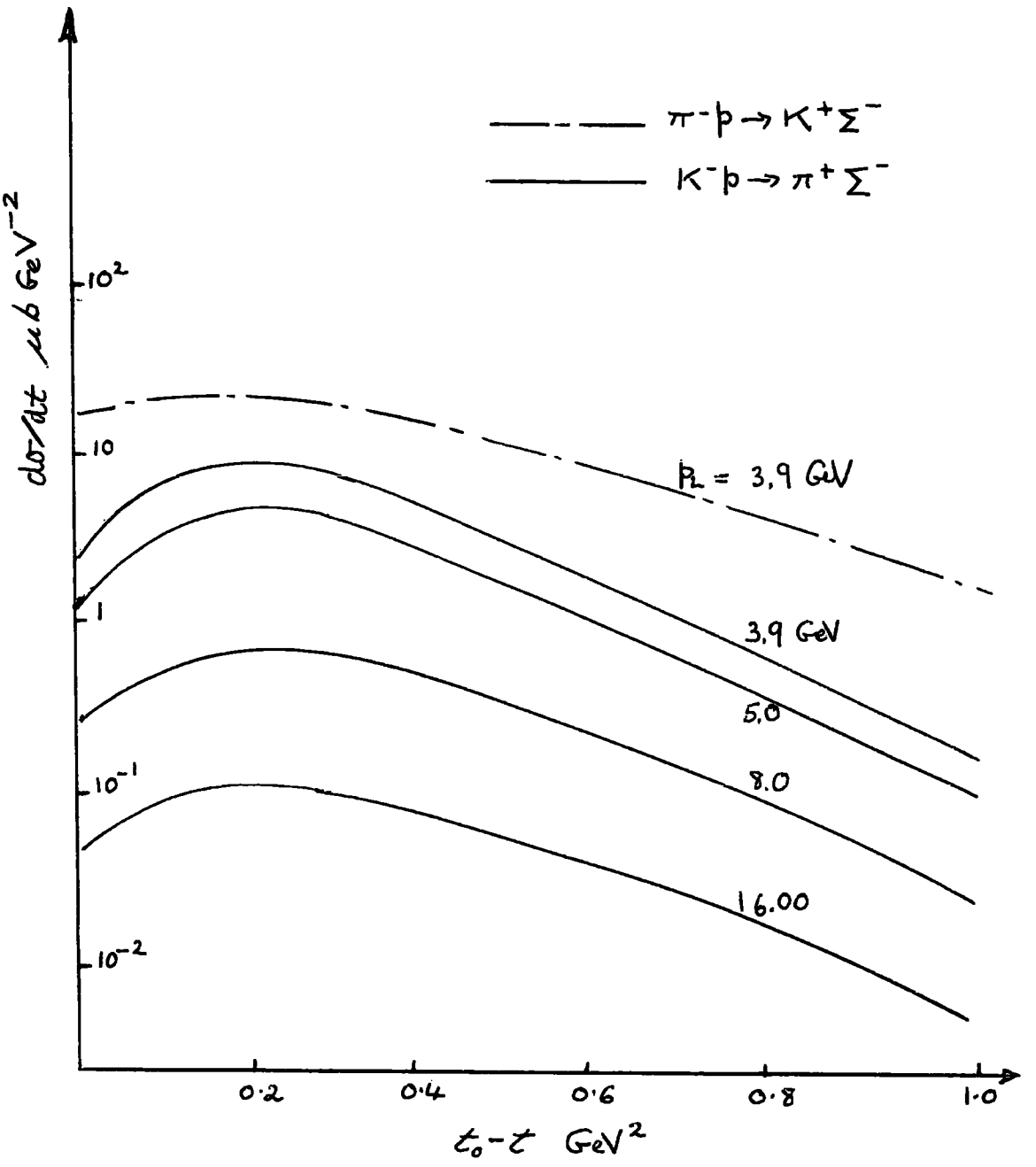

Fig. (3.4.2)

Regge-Regge cut prediction from unsymmetrised, unabsorbed box diagram.

$$\alpha_{eff}(t) = -0.26 + 0.1t$$

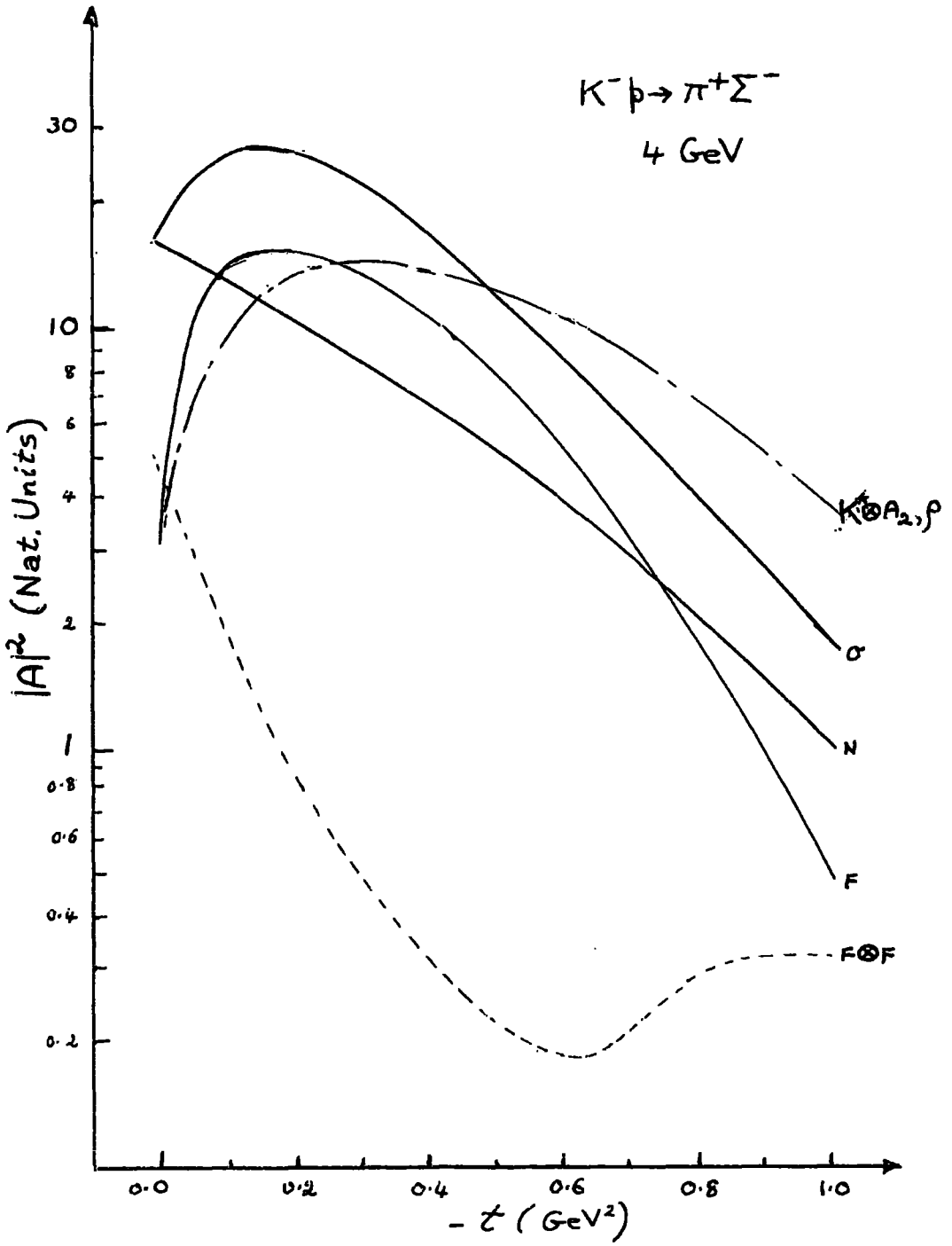

Fig. (3.4.3)

Amplitude contributions to the cut of Fig. (3.4.2)

--------- total double-flip
—— - —— K^*(non-flip) ⊗ ρ, A_2(flip)
————F total overall-flip
————N total overall-non-flip
————σ total (cross-section)

Quigg has observed[86] that amplitudes for processes like (3.4.1) constructed in this way are not s-u crossing-symmetric and suggests a simple ad hoc way of ensuring this symmetry. It amounts, in our model, to allowing the incoming particle to scatter off the outgoing baryon first so giving a box diagram as given in Figure (3.4.4)(a).

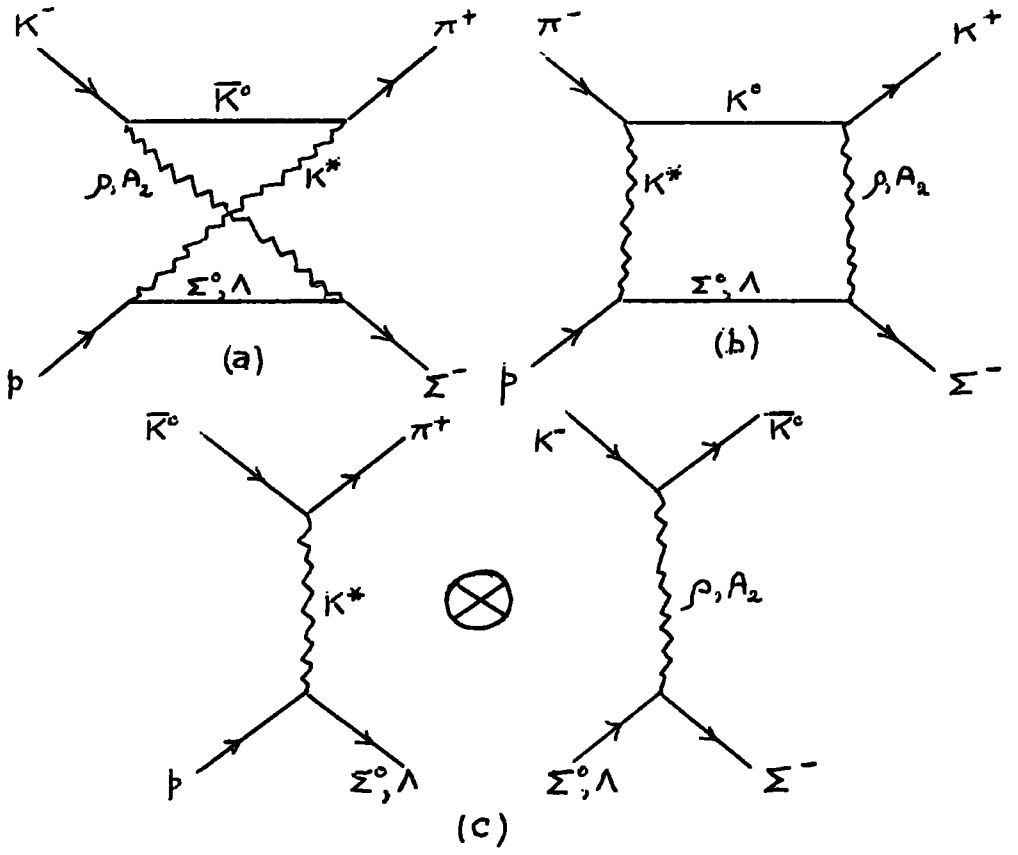

Fig. (3.4.4)

To calculate this diagram it is first untwisted giving[72,86] the product of the signatures times the graph of Figure (3.4.4)(b). In this example, to calculate the contributions of the single exchanges (K_V^*, K_T^*, ρ, A_2) we line-reverse the graphs of Figure (3.4.4)(c) picking up $(1)^{\xi}$ for each exchange. It is then noticed that the crossed box diagrams reduce to those uncrossed ones for

the u-channel process but with the phases of the poles corresponding to the s-channel one. As a consequence, in this s-u symmetric scheme processes (3.4.1)(a) and (b) have the same diagrams (c.f. Figure (3.4.1)), the only difference (apart from the obvious kinematic ones) being that of the phases of the individual exchanges.

This modification to our unabsorbed model yielded the following predictions for the near-forward differential cross-section at 4 GeV

$$\frac{d\sigma}{dt}\,(K^- p \longrightarrow \pi^+ \Sigma^-) \quad = \quad 4.7(2.3) \quad \mu b\ GeV^{-2} \qquad (3.4.13)$$

$$\frac{d\sigma}{dt}\,(\pi^- p \longrightarrow K^+ \Sigma^-) \quad = \quad 7 \quad (16) \quad \mu b\ GeV^{-2} \qquad (3.4.14)$$

showing a line-reversal splitting which is less marked (the figures in brackets are the corresponding unsymmetrised ones). The magnitudes are compatible with the estimates of references (81, 82, 63) but much larger than those of Quigg[83]. Our prediction of overall flip dominance remains.

During this analysis details of the work of Henyey, Kane and Scanio[80] were received. In this last work, absorption by P⊗R⊗R terms is included. As hinted in Section 3.3 this greatly suppresses the R⊗R amplitude, in fact by almost an order of magnitude in the cross-section.

By using $K^* N \bar{\Lambda}$ couplings with more flip character than indicated by the data (see Section 2.2(ii)) and by assuming the $\rho B \bar{B}$ coupling to be dominantly flip for all octet baryons, Henyey et al[80] claim the processes (3.4.1)

to be overall non-flip dominated by (flip) ⊗ (flip) cuts so taking advantage of their kinematic suppression due to the two $\sqrt{-t}$ factors in the convolution. We claim that the $A_2\Sigma\bar{\Sigma}$ coupling is sufficiently non-flip that, because of the above-mentioned kinematic suppression, even the A_2(non-flip) ⊗ K^* (flip) contribution is larger than the A_2 (flip) ⊗ K^* (flip) one. In the notation of Section 2.6 we have

$$\frac{(\gamma A_2 \Sigma\bar{\Sigma})_o}{(A_2\Sigma\bar{\Sigma})_1} \approx 0.3 \frac{(\gamma A_2 N\bar{N})_o}{(A_2 N\bar{N})_1} \qquad (3.4.15)$$

and

$$(\gamma A_2 \Sigma\bar{\Sigma})_o \approx 1.8\ (\gamma A_2 N\bar{N})_o \qquad (3.4.16)$$

using the mixing parameters of equations (3.4.10).

Finally with respect to the work of Reference (80), we comment on the importance of decuplet intermediate states. It is reasonable to assume following Stodolsky and Sakurai[87] that the most significant $\rho N\Delta$ couplings (Δ a member of the $J^P = 3/2^+$ decuplet) correspond to the $\lambda_N = \frac{1}{2} \rightarrow \lambda_\Delta = -\frac{1}{2}$ or $3/2$ transitions (i.e. n = 1). Using this assumption, the authors claim a cancellation between octet and decuplet intermediate states of the form,

$$\frac{d\sigma}{dt}\ (\text{octet})\ \left[1 - \frac{g^2_{\rho N\Delta}}{500}\right]^2 \qquad (3.4.17)$$

where $g^2_{\rho N\Delta} \approx 22^2$ and the cross-section is assumed to be dominantly flip ⊗ flip. In our view the ρ, A_2 exchange and ρ exchange cut contributions of Figures (3.4.1)(a) and (b) for the flip ⊗ flip diagrams become

$$\text{Cut}_{\rho} = \text{Cut}_{\Sigma}\left[1 - \frac{1}{3}\frac{1+2f_1}{1-2f_1}\ \frac{1-f_1}{f_1} + \frac{R}{6f_1(1-2f_1}\right] \tag{3.4.18}$$

and $$\text{Cut}_{\rho,A_2} = \text{Cut}_{n}\left[1 - \frac{4}{3}\frac{R}{1-2f_1}\right] \tag{3.4.19}$$

when the Δ contribution is included. Cut_{Σ} refers to the Σ intermediate state part of diagram (3.4.1)(a) and Cut_{ρ,A_2} refers to the diagram with ρ,A_2 exchange and including both octet and decuplet baryon states.

$$R = \frac{g^2_{\rho N\Delta}}{g^2_{\rho N\bar{N}}} \tag{3.4.20}$$

where $g_{\rho N\Delta}$ corresponds to the $\lambda = \frac{1}{2} \longrightarrow -\frac{1}{2}$ transition. A rough comparison of the 4 GeV differential cross-sections for

$$\pi^- p \longrightarrow \pi^o n \quad (30) \tag{3.4.21}$$

and

$$\pi^+ p \longrightarrow \pi^o \Delta^{++} \quad (88) \tag{3.4.22}$$

assuming n = 1 coupling dominance, suggests a rough value for R of

$$R \simeq .38 \tag{3.4.23}$$

With this value of R, the $\rho,A_2 \otimes K^*$ cut suffers an enhancement of about 100% in the cross-section. By inspection, it would appear impossible to obtain large cancellations simultaneously in equations (3.4.18) and (3.4.19) for <u>any</u> reasonable values of R and f_1. Even with the couplings of Reference (80) a cancellation of the form (3.4.17) is unrealistic since the (non-flip) $\otimes$ (flip) cuts for example would then be expected to be dominant. In this analysis we proceed no further with a speculative treatment of

decuplet states and return to our (perhaps unrealistic) "lowest states only" model.

We saw how in the lowest states approximation, the prediction for $\pi^- p \longrightarrow K^+ \Sigma^-$ was much too large (Figure (3.1.1)). For the sake of completeness we follow Reference (80) and absorb the box diagrams which we have so far considered (Figure (3.4.1)). As with absorption of simple poles we enhance the absorbing cross-section of 30 millibarns with a factor

$$\lambda = 1.5 \qquad (3.4.24)$$

in this case the same for all diagrams. Equations (3.3.10), (3.3.19) and (3.3.20) are used to calculate the additional terms. This time since the R⊗R and R⊗R⊗P cancellation is much more complete than that of R and R⊗P, the choice of λ is very sensitive. With the value given in equation (3.4.24) we reproduce the observed cross-sections within the very-considerable errors (see Figure (3.4.5)).

The overall flip character of the predicted angular distributions is enhanced by the absorption since the cancellation is more pronounced for the (non-flip)⊗(non-flip) cuts than for the (flip)⊗(non-flip) ones.

We conclude this section by emphasising the difficulty in reproducing the small size of the data using $I_t = 3/2$ cuts without some kind of absorption. However the freedom allowed by the absorptive mechanism which we have employed reduces the usefulness of the description. The problem of magnitude becomes even more accute at higher

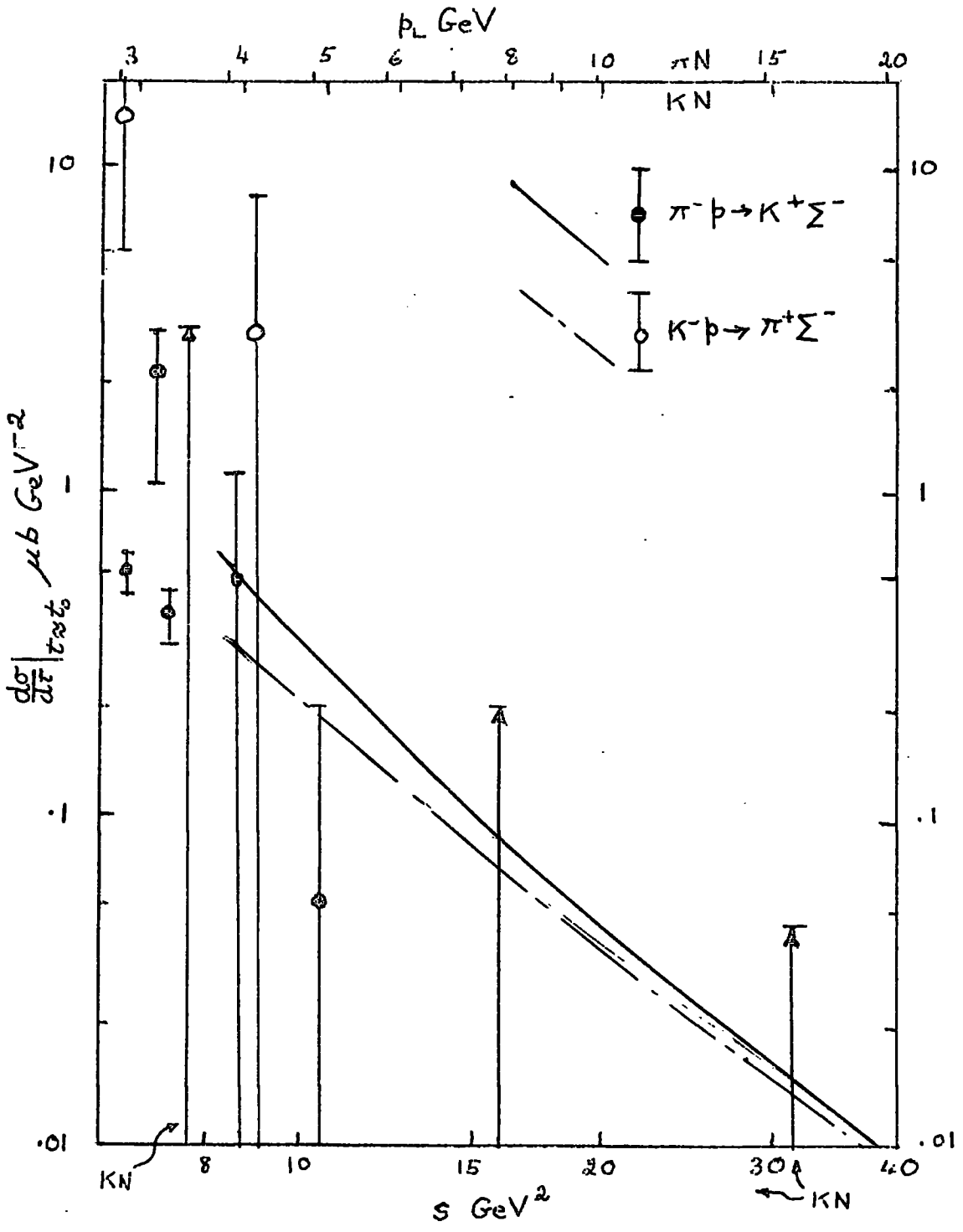

Fig.(3.4.5)

Predictions from (s-u)symmetric, absorbed, lowest intermediate states diagrams. Data as in Fig.(3.1.1)

momenta (see Figure (3.4.5)) since the $\alpha_{eff}(0)$ of even the absorbed cut is,

$$\alpha_{eff}(0) \approx -0.27 \qquad (3.4.25)$$

while the data represented by the upper limits shown suggest (although do not demand) a somewhat lower value.

3.5 Application to Line Reversal Symmetry Violation

We showed in Section 3.1 that the assumption that most of the Line-Reversal Symmetry Violation (LRSV) came from a non-zero $I_t = 3/2$ exotic amplitude[42] is untenable. Also we showed in Section 3.4 that Regge-Regge cuts in a multiple scattering formalism do not naturally describe the anomalously small observed $I_t = 3/2$ cross-section. In this section we investigate whether, on the other hand, $(I_t = 0) \otimes (I_t = \frac{1}{2})$ Regge-Regge cuts can explain the large difference in magnitude between the $I_{\frac{1}{2}}$ and $I'_{\frac{1}{2}}$ amplitudes of equations (3.1.5) to (3.1.8) which we have to conclude are mainly responsible for the LRSV.

The lowest order diagrams to be considered in a description of

$$K^- p \longrightarrow \pi^- \Sigma^+ \qquad (3.5.1)(a)$$

and

$$\pi^+ p \longrightarrow K^+ \Sigma^+ \qquad (3.5.1)(b)$$

are shown in Figure (3.5.1). In the s-u symmetric model which we considered, both sets of diagrams in Figure (3.5.1) would be shared by processes (3.5.1) in the manner described in Section 3.4. As well as the $I_t = 1$ exchanges

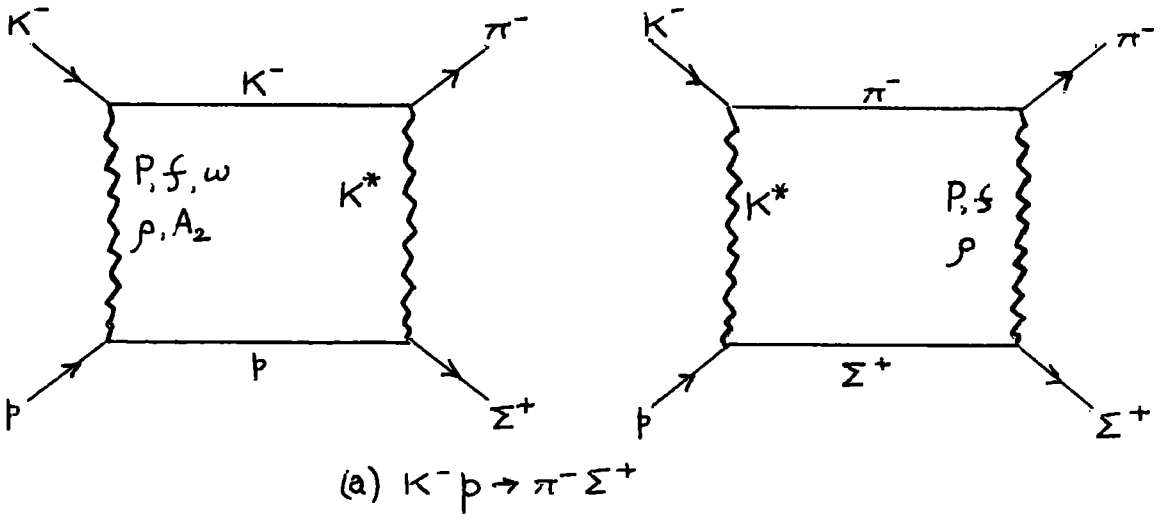

(a) $K^- p \to \pi^- \Sigma^+$

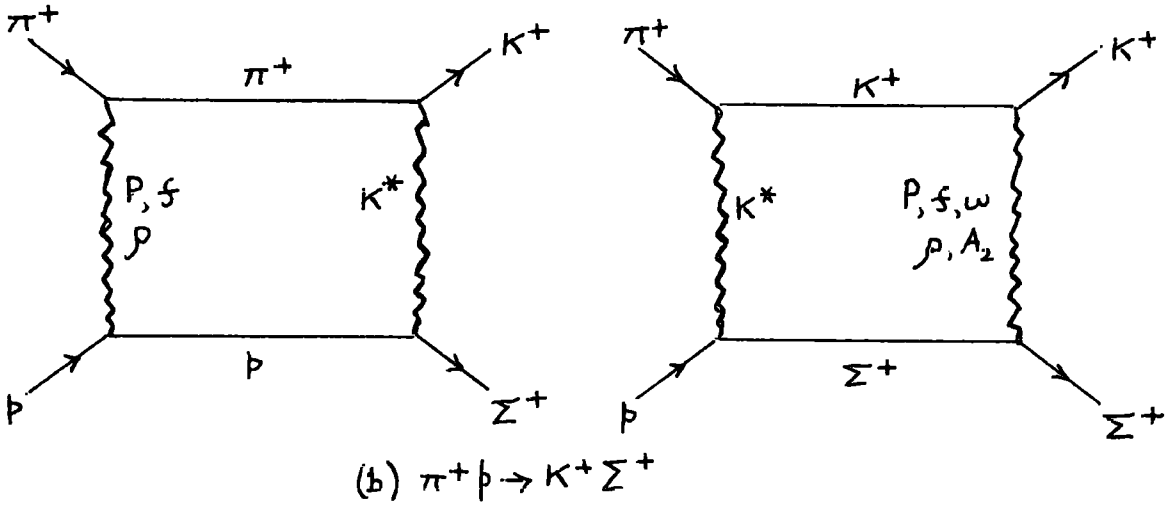

(b) $\pi^+ p \to K^+ \Sigma^+$

Fig. (3.5.1)

Lowest intermediate-states box diagrams for non-exotic HCEX reactions.

whose dominantly flip character we noted in the last section, we now have the $I_t = 0$ exchanges, P, f and w which in an EXD framework have dominantly non-flip couplings[62].

The contribution from the P⊗R cuts has already been estimated in Chapter 2. As regards the non-Pomeron cuts we expect the dominantly non-flip w, f and K^* exchanges to ensure the overall dominance of (non-flip) ⊗ (non-flip) diagrams, remembering the natural kinematic pre-eminence of such diagrams. We can go further in selecting from Figure (3.5.1) the dominant diagram in a rough calculation. We have already noted that (tensor) ⊗ (tensor) cuts are by far the most important in an EXD framework because of the lack of nonsense zeroes in the convolution, i.e. we expect $f \otimes K_T^*$ to be dominant. Assuming SU(3), ideal mixing[61] and EXD

$$\frac{g_{fN\bar{N}}}{g_{f\Sigma\bar{\Sigma}}} = \frac{4f_o - 1}{2f_o} \approx 1.6 \qquad (3.5.2)$$

for non-flip couplings. The diagrams of Figure (3.5.2) are then selected for calculation as the most significant contributions from Regge-Regge cuts towards LRSV in the $I_t = \frac{1}{2}$ amplitudes.

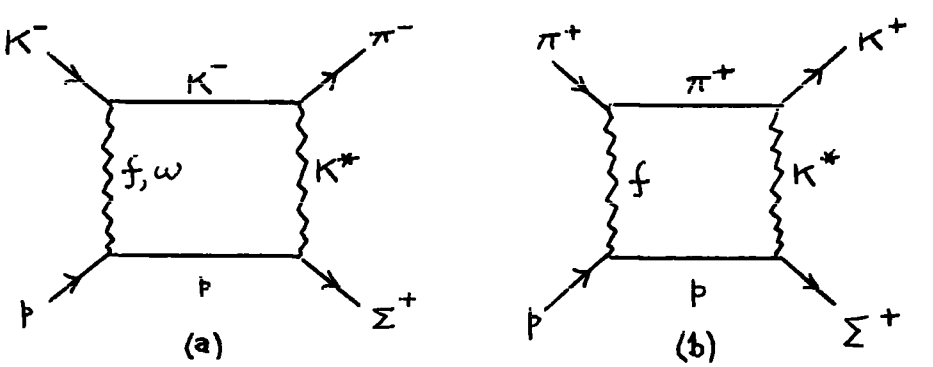

Fig. (3.5.2)

In order to calculate the largest possible effects due to these diagrams, we do not consider an s-u symmetric model, i.e. Figure (3.5.2)(a) is the dominant non-Pomeron contribution to $K^- p \longrightarrow \pi^- \Sigma^+$ and Figure (3.5.2)(b) contributes to $\pi^+ p \longrightarrow K^+ \Sigma^+$.

The contribution of Figure (3.5.2)(a) was calculated via SU(3) and EXD from the analogous diagram of Figure (3.4.1), taking care to estimate correctly, within our EXD scheme, the relation sign of w,f and P couplings (see Appendix 3A). The non-flip amplitudes at 4 GeV from $P \otimes K^*$ (Chapter 2) and from $P \otimes K^* + (w+f) \otimes K^*$ are shown in Figure (3.5.3).

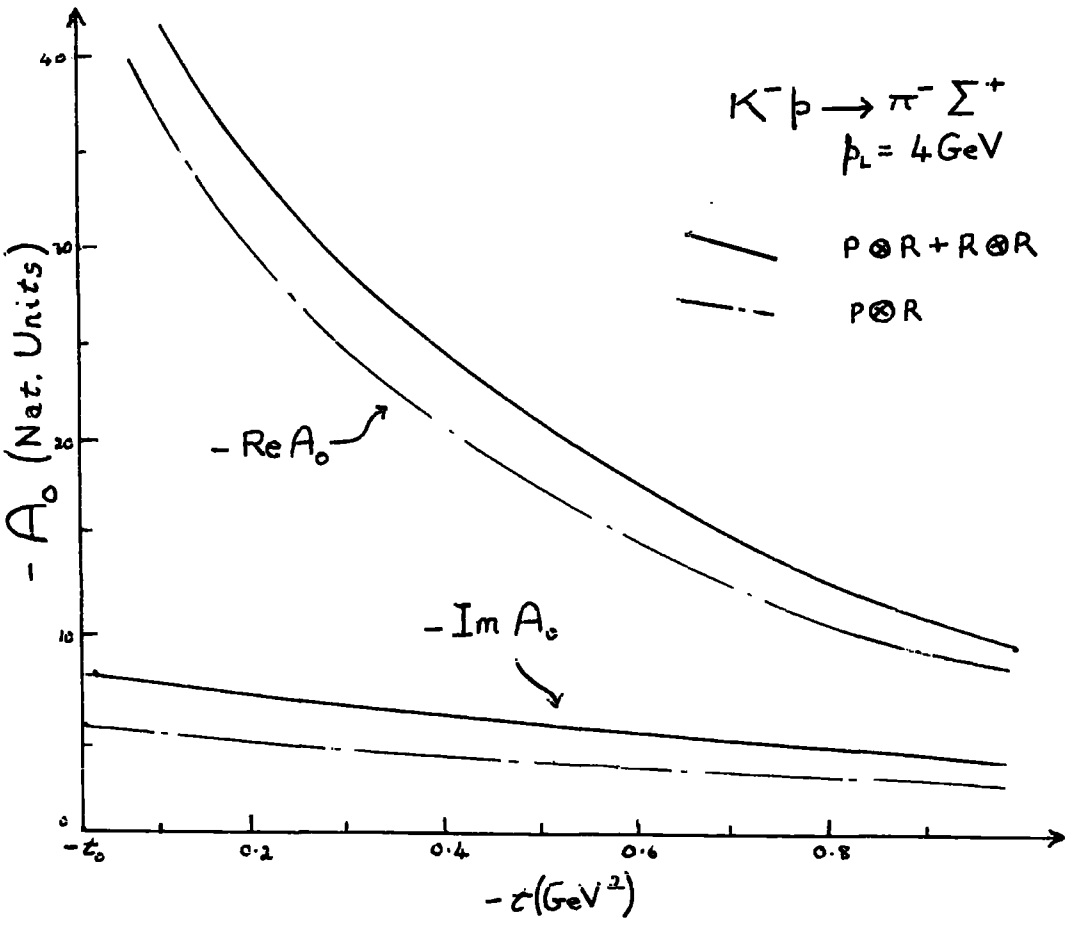

Fig. (3.5.3)

At best the non-Pomeron cuts are only some 10% in modulus of the leading cut and are only comparable (in the present case of a dominantly real amplitude) in the imaginary part (see Figure (3.5.3)). More significant, however, is the prediction that these secondary cuts add in both the real and imaginary parts. A similar effect is found in $\pi^+p \longrightarrow K^+\Sigma^+$ since the f and P couplings have the same sign in π^+p elastic scattering (see Appendix 3A). We therefore claim that inclusion of Regge-Regge cuts makes the prediction of the leading cut model worse, and that their effect may be summarised by replacing

$$\lambda \longrightarrow 1.1\lambda \qquad (3.5.6)$$

in the estimates of Chapter 2. This result is in accord with the calculation of Michael[63].

Finally in this section we estimate the effect of the inclusion of non-leading cuts in the polarisation description put forward in Chapter 2.

We have demonstrated that the overall flip Regge-Regge cuts in processes (3.5.1) are expected to be small compared with the non-flip ones. Indeed the flip cuts will be comparable in magnitude with those calculated in Section 3.4 which were typically one tenth or less in magnitude of the flip pole amplitudes. If we therefore neglect them, the polarisation model of Chapter 2 is only altered in that we now include Regge-Regge terms in the non-flip amplitudes as shown in Figure (3.5.3). For simplicity we consider the origin of the hyperon polarisation in $K^-p \longrightarrow \pi^-\Sigma^+$ but the argument applies analogously

to $\pi^+p \longrightarrow K^+\Sigma^+$. We have

$$P\frac{d\sigma}{dt} \approx 2\,\mathrm{Im}(A_o A_1^*) \qquad (3.5.7)$$

$$= 2A_1^R\,(\mathrm{Im}A_o^{P\otimes R} + \mathrm{Im}A_o^{R\otimes R}) \qquad (3.5.8)$$

since A_1^R (in an obvious notation) is purely real within our assumptions. From Figure (3.5.3) and Equation (3.5.8) we deduce that $\left|P\frac{d\sigma}{dt}\right|$ will have the same shape as in simple absorption, but larger since the two terms in (3.5.8) add. In a fit to the data $\frac{d\sigma}{dt}$ will remain constant so that we predict the polarisation to be similar to that in Chapter 2 but larger if anything.

The above arguments allay the naive suspicion of Chapter 2 that if Regge-Regge cuts are required to reproduce the LRSV at intermediate energies, an immediate consequence might be to ruin the simple polarisation description which in some sense is a rather delicate (second order) phase effect. Similar conclusions were arrived at independently by O'Donovan in Reference (89).

3.6 Conclusions on the Role of Regge-Regge Cuts

The theoretical justification of saturation of the Schwarz sum-rule for the Reggeon-particle scattering amplitude, by lowest intermediate states only, is very weak although given this saturation, the multiple scattering formalism is thought (Section 3.2) to give a reasonable approximation (Section 3.3) to a more correct but impracticable calculation of a Regge-Regge cut.

Great difficulty is experiencedin explaining the small size of exotic exchange cross-sections (Section 3.4), some kind of additional absorption being found necessary.

The LRSV observed in reactions (3.5.1) is found to originate almost entirely in the $I_t = \frac{1}{2}$ amplitudes. The observed size of the violation cannot be explained (Section 3.5) by Regge-Regge cuts whose effects on the cross-sections and polarisations are almost negligible.

C H A P T E R F O U R

STRANGENESS-EXCHANGE AMPLITUDES FROM DECAY CORRELATIONS

4. Strangeness-exchange amplitudes from decay correlations†

Since the analyses described in Chapter 2 and Chapter 3 were performed it has become clear that no exchange model with any predictive power can describe in detail all the $0^-\frac{1}{2}^+ \longrightarrow 0^-\frac{1}{2}^+$ scattering data. In the case of strangeness-exchange (HCEX) reactions we showed in Chapter 2 how the weak absorption model implies that the $K^-p \longrightarrow \pi^-\Sigma^+$ pole amplitude which is expected to be predominantly real is reduced by absorption more than that of $\pi^+p \longrightarrow K^+\Sigma^+$ which has a large imaginary part at small angles. This predicts a line-reversal symmetry violation (LRSV) opposite to that shown by the data. There has been presented, other evidence[90] that it should be the predominantly imaginary non-flip amplitude which should be heavily absorbed rather than the real.

In $0^-\frac{1}{2}^+ \longrightarrow 0^-\frac{1}{2}^+$ scattering there are two spin amplitudes (Section 1.4) and, since there is an overall phase which is not in general directly determinable, we can describe a process having one t-channel isospin component by three real numbers. Such numbers could be taken to be $\frac{d\sigma}{dt}$, P and R (see Appendix 2A) but in order to compare the underlying structure of high energy exchange models it is more useful to use as the three numbers, the moduli and relative phase of the amplitudes. When R and A

†Part of the work described in this chapter was done in collaboration with M. Abramovich, A.D. Martin and C. Michael, and was published in Reference (105).

measurements were made[91] for $\pi^{\pm}p$ elastic scattering, the processes $\pi^{\pm}p$ elastic and $\pi^{-}p$ charge exchange scattering which as a set involve 2 isospin times 2 spin amplitudes (7 real numbers) were analysed in this way by Halzen and Michael[92]. As a result, the suspected absorption systematics outlined in the first paragraph were confirmed in πN scattering. Significantly perhaps, the five Regge pole fit of Reference (93) was shown to provide an excellent interpolation of the amplitudes derived in the analysis. Making the assumption that this model provides a good extrapolation of the amplitudes to larger momentum transfers, an impact parameter decomposition can then be made[95], so elucidating the partial wave structure (see e.g. Figure (1.5.1)) which is relevant to a discussion of absorption effects.

In this chapter we will propose analogous techniques for extracting exchange amplitudes from the data for resonance production processes.

4.1 Decay correlation parameters

The measurement of P in $\pi N \longrightarrow \pi N$ scattering illuminates the spin state of the final nucleon while R and/or A measurements correlate this with the spin state of the target nucleon in a scatter. In HCEX reactions a measurement of P, the recoil polarisation, is simply given by observation of the parity non-conserving hyperon decay. However for technological reasons, R and A measurements have not yet been possible in this case so that the

complete "amplitude analysis" described above is not a current possibility for strangeness-exchange amplitudes. We now explore a different but related line of approach.

Reactions of the kind

$$\begin{aligned} \pi^- p &\longrightarrow K^{*o}\Lambda \\ \pi^+ p &\longrightarrow K^{*+}\Sigma^+ \\ K^- p &\longrightarrow \rho^o\Lambda \\ K^- p &\longrightarrow \omega\Lambda \\ K^- p &\longrightarrow \phi\Lambda \end{aligned} \qquad (4.1.1)$$

are expected to be mediated by strange meson exchange. Because of the extra unit of spin in the final state, unnatural parity poles such as K may be exchanged in addition to the natural parity K_V^* and K_T^* trajectories. In all, some six independent production amplitudes are involved in each process. These may be taken as, for example, the helicity amplitudes of equation (1.3.7).

$$T^s_{0++} \quad T^s_{0+-} \quad T^s_{1++} \quad T^s_{1--} \quad T^s_{1+-} \quad T^s_{1-+} \qquad (4.1.2)$$

where +(-) refer to $\lambda = +\frac{1}{2}(-\frac{1}{2})$ and we have used the parity relation[20]

$$T^s_{\lambda_c\lambda_d\lambda_a\lambda_b} = \eta(-)^{\lambda_c+\lambda_b-\lambda_d-\lambda_a} T^s_{-\lambda_c-\lambda_d-\lambda_a-\lambda_b} \qquad (4.1.3)$$

to identify the independent amplitudes. In equation (4.1.3) η is the product of the intrinsic parities and $(-)^{S_c+S_d-S_a-S_b}$ which in our case of

$$0^-\tfrac{1}{2}^+ \longrightarrow 1^-\tfrac{1}{2}^+ \qquad (4.1.4)$$

gives $\eta = -1$.

Although in the absence of polarised target experiments we can never measure the scattering dependence on the target nucleon spin, we can come very near to a complete amplitude analysis. Of the 11 real numbers describing the production amplitudes it turns out (Section 4.3) that we can determine unambiguously 10 by using the vector meson and hyperon decay correlations to give information about the spin states produced in the collision.

Besides learning about the role of natural parity exchanges in the vector meson production processes (4.1.1) and its implications for $0^-\tfrac{1}{2}^+ \longrightarrow 0^-\tfrac{1}{2}^+$ scattering through factorisation, we might also hope to investigate unnatural parity K exchange which, although important, has so far been difficult to isolate. SU(3) of course relates K exchange in reactions (4.1.1) to π exchange in $\pi N \longrightarrow \rho N$ - a mechanism of great theoretical importance[96] due to the proximity of the π pole to the scattering region ($-1 \leqslant \cos\theta \leqslant 1$). Measurement of the above-mentioned 10 real numbers for this process however involves the use of a polarised target, and the possibility of acquiring, without this effort, the same degree of information for the SU(3) related processes (4.1.1) is certainly an attractive one.

A convenient link between the production amplitudes for a final state resonance and the angular

distribution of its decay products is provided by the spin density matrix. An expression for the angular distribution in terms of the density matrix elements was given by Gottfried and Jackson[97]. For example for the K^* vector meson decay in

$$\pi^- p \longrightarrow K^{*o}\Lambda \qquad (4.1.5)$$

the angular distribution is

$$W_v(\theta_1,\phi_1) = \rho_{11}\sin^2\theta_1 + (1-2\rho_{11})\cos^2\theta_1 - \rho_{1-1}\sin^2\theta_1\cos 2\phi_1$$

$$- \sqrt{2}\ \mathrm{Re}\ \rho_{10}\ \sin 2\theta_1\ \cos\phi_1 \qquad (4.1.6)$$

in the case where the polar axis and the resonance spin quantisation are along the direction of flight of the resonance (helicity quantisation). The angular distribution $W_v(\theta_1,\phi_1)$ is the probability per unit solid angle of observing one of the decay products (in a two-body decay) in the direction (θ_1,ϕ_1). An analogous distribution $W_Y(\theta_2,\phi_2)$ for the parity non-conserving decay of the spin-½ Λ can be expanded[98] in terms of one parameter e.g. the polarisation parameter, P.

The 3 independent measurables from the K^* decay $(\rho_{11},\rho_{1-1},\mathrm{Re}\rho_{10})$ together with the one measurable from the Λ decay (P) constitute only 5 pieces of information. If the decays are simultaneously observed, however, (i.e. $W(\theta_1,\phi_1,\theta_2,\phi_2)$) 10 independent pieces of information are measurable since in general the K^* and Λ decays are correlated. An expression for $W(\theta_1,\phi_1,\theta_2,\phi_2)$ in terms of double density matrix elements, $\rho_{nn'}^{mm'}$, was given in reference (99), and in terms of statistical tensors in

Reference (100). For the case of processes (4.1.4) where the baryon decay does not conserve parity (e.g. process (4.1.5)) the angular distribution is

$$W(\theta_1,\phi_1,\theta_2,\phi_2) = \sum_{\substack{J_1J_2\\M_1M_2}} F_1(J_1)F_2(J_2)T^{J_1J_2}_{M_1M_2}\, Y^{M_1}_{J_1}(\theta_1,\phi_1)Y^{M_2}_{J_2}(\theta_2,\phi_2) \tag{4.1.7}$$

where

$$J_1 \leqslant 2S_1 = 2, \qquad J_2 \leqslant 2S_2 = 1 \tag{4.1.8}$$

and the $F_i(J_i)$ are known[100] constants of the decays. This expression is in terms of statistical tensors but the relation between them and density matrix elements is linear[100]

$$\rho^{m_1m_1^1}_{m_2m_2^1} = \sum_{\substack{J_1J_2\\M_1M_2}} (-)^{1+m_1-J_1+\frac{1}{2}+m_2-J_2} C(1,-m_1;1,m_1^1|J_1,M_1)C(\tfrac{1}{2},-m_2;\tfrac{1}{2},m_2^1|J_2,M_2) \times T^{J_1J_2}_{M_1M_2} \tag{4.1.9}$$

Pilkuhn and Svenson[99] have given the relation between the double density matrices and helicity production amplitudes. For processes (4.1.4) it is

$$\rho^{m_1m_1^1}_{m_2m_2^1} = \sum_{\mu} H^{m_1}_{m_2\mu} H^{m_1^1*}_{m_2^1\mu} \tag{4.1.10}$$

where (as throughout this chapter) we choose to normalise† so that in the reactions being considered

† i.e. the cross-section, the 10th measureable, is taken as 1 for the time being.

$$\frac{d\sigma}{dt} = \sum_{\lambda_\mu \nu} | H^{\lambda}_{\mu \nu} |^2 = 1 \qquad (4.1.11)$$

In equations (4.1.10) and (4.1.11) the $H^{\lambda}_{\mu\nu}$ are either s- or t- channel helicity amplitudes where λ, μ and ν are the vector meson, final baryon and initial baryon helicities, respectively.

Using the orthogonality properties of the Y^M_J in equation (4.1.7) it is possible to project out from the experimental angular distribution, certain combinations of the $T^{J_1 J_2}_{M_1 M_2}$ or $\rho^{m_1 m_1'}_{m_2 m_2'}$ (see Appendix 4A for example). This extraction procedure is termed "the moment method." Having extracted various combinations of the ρ elements it is then possible to use them to gain insight via equation (4.1.10) into the production process. Certain limitations on the amount of information gained in this way are worth noting. Although stated in terms of density matrices, similar remarks apply to the use of statistical tensors.

(i) Given (as we shall see) only 10 real numbers by the method of moments, it is impossible to invert equation (4.1.10) uniquely.

(ii) Since only 10 of the 12 measureable ρ's (Appendix 4A) are independent there exist among them relations (linear or quadratic). The moment method does not guarantee that these constraints be satisfied.

(iii) In view of (ii), one may ask what is the physically allowable range of a given element? Is the measured value significant in terms of the estimated error and the

physical range? For example it is shown in references (101, 102) that in the case of a vector meson single density matrix the allowed ranges of the 3 independent elements can be represented by a 3-dimensional cone. The naive supposition that the physical domain be the cube superscribing this cone would be misleading. It is not practicable to extend this geometrical argument, however, to joint decays described by 10 independent parameters.

(iv) In view of (iii) it is useful to attempt to identify which elements should be well-determined experimentally. It turns out that many of the observed elements are ill-determined in that they have large (although correlated) errors. We may form combinations of these having small errors. For example we know that

$$\rho_{11} = \sum_{m_2 m_2'} \rho^{1\,1}_{m_2 m_2'} \qquad (4.1.12)$$

being the coefficient of $\sin^2\theta_1$ in the expansion (4.1.6), is in some sense a "low moment," and consequently well-determined by the data.

(v) Although we have stated that 10 of the 12 measurable elements are independent, this is not obvious from consideration of equations (4.1.7) and (4.1.9) alone. No general algorithm for calculating the maximum number of independent measureables, for arbitrary spin and parity, is known.

We will, however, introduce an expansion of $W(\theta_1,\phi_2,\theta_2,\phi_2)$, involving directly a set of six production

amplitudes, which in some measure will answer the questions and criticisms raised in points (i) to (v) regarding the use of density matrices and statistical tensors as representations of the decay data.

Following Byers and Yang[103] we expand W in terms of the 6 direction cosines

$$(x_i, y_i, z_i) \qquad i = 1,2 \tag{4.1.13}$$

where

$$z_i = \cos\theta_i \tag{4.1.14}$$

$$x_i + iy_i = \sin\theta_i e^{i\phi_i} \tag{4.1.15}$$

That is, we use a cartesian basis (x, y, z) for the expansion rather than a spherical one, $Y_J^M(\theta,\phi)$. The choice of rectangular axes will be described in the next section. By noting that the K^* decay is parity conserving and the Λ decay not so, or simply by expanding the Y_J^M in terms of the (x_i, y_i, z_i) it is seen[103] that W is quadratic in (x_1, y_1, z_1) and linear in (x_2, y_2, z_2). It turns out (Section 4.3) that the coefficients of these terms are bilinear combinations of transversity amplitudes[104]. Transversity amplitudes differ from helicity amplitudes in that the particle spins are quantised along the normal to the reaction plane.

In a later section we will discuss the advantages of this expansion and demonstrate why an expansion directly in terms of helicity amplitudes is not practicable.

4.2 Transversity and helicity axes

Let us return, for demonstration purposes, to the well-known expansion (4.1.7). To completely specify it, we must first of all choose 2 sets of axes to which we may refer (θ_i,ϕ_i) and along which we may quantise the angular momenta. Our discussion will be in terms of

$$\pi^- p \longrightarrow K^* \quad \Lambda \qquad \Lambda \hookrightarrow p\pi^- \qquad K^* \hookrightarrow K^+\pi^- \tag{4.2.1}$$

where (θ_1,ϕ_1) specify the direction of the K^+ from the K^* decay and (θ_2,ϕ_2) refer to the Λ-decay proton direction. By convention, in helicity-type frames we quantize (choose Z_i) along the particle momenta (K^* and Λ), define Y_i as the production normal (Basle convention†) and introduce X_i to complete right-handed sets of axes (X_i,Y_i,Z_i). For transversity-type axes the Z_i are taken along the production normal, the X_i along the particle momenta and Y_i completing the right-handed sets. Relabelling axes

$$(X^T,\ Y^T,\ Z^T) \quad = \quad (Z^H,\ X^H,\ Y^H) \tag{4.2.2}$$

relates the two choices.

The complete definition of axes involves specifying the Lorentz frames in which the particle momenta are measured. Useful and conventional choices are

(i) s-channel frames: X_i^T are along the particle momenta in the s-channel centre of mass.

†the normal in meson baryon scattering is taken to lie along $\underset{\sim}{k}_i \times \underset{\sim}{k}_f$ where $\underset{\sim}{k}_i$ ($\underset{\sim}{k}_f$) is the ingoing (outgoing) meson momentum.

(ii) t-channel or Gottfried-Jackson[97] frames: X_i^T is taken along the incoming meson (baryon) in the rest frame of the decaying meson (baryon). The choices (i) and (ii) for the K^* axes are shown in Figure (4.2.1).

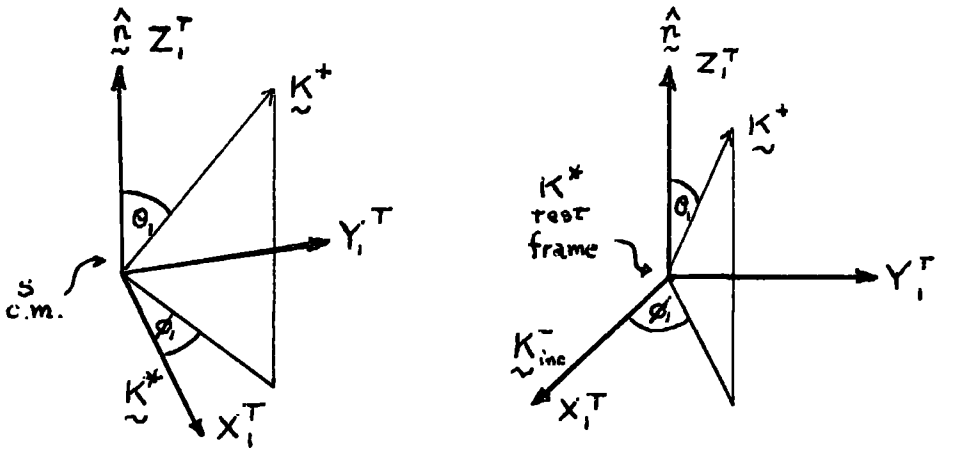

(i) s-channel (ii) t-channel

Fig. (4.2.1)

They are related by a rotation (in the sense of crossing angle), $\chi_1^{st}(s,t)$ about the production normal $\hat{n}$.

Under any rotations $\chi_1(s,t)$ and $\chi_2(s,t)$ about $\hat{n}$, statistical tensors transform as[100]

$$\left(T^{J_1J_2}_{M_1M_2} \right)' = e^{-iM_1\chi_1 - iM_2\chi_2} T^{J_1J_2}_{M_1M_2} \qquad (4.2.3)$$

The parity relations[100] and the hermiticity relations

$$T^{J_1J_2}_{M_1M_2} = (-)^{M_1+M_2} \left(T^{J_1J_2}_{-M_1-M_2} \right)^* \qquad (4.2.4)$$

leave the following set of measureable tensors

$$T^{00}_{00}\ ,\quad T^{10}_{00}\ ,\quad T^{02}_{00} \quad \text{and} \quad T^{12}_{00} \qquad (4.2.5)$$

which are real, and

$$T^{12}_{11}\ ,\quad T^{02}_{02}\ ,\quad T^{12}_{02} \quad \text{and} \quad T^{12}_{-1\ 1} \qquad (4.2.6)$$

which are in general complex - a total of 12 measureable real quantitites. From equation (4.2.3) we see immediately that tensors (4.2.5) and the moduli of tensors (4.2.6) are invariant under rotations about the production normal. We denote such quantities "frame invariants." Their uses will be discussed in Section 4.4.

We now define 3 sets of production amplitudes.

(i) Helicity amplitudes

We denote the helicity amplitudes of Jacob and Wick[18]† for this process by

$$H^1_{++}\ ,\quad H^1_{--},\quad H^1_{+-},\ H^1_{-+},\ H^0_{++}\quad \text{and}\quad H^0_{+-} \tag{4.2.7}$$

where the indices are those of equation (4.1.11).

(ii) Transversity amplitudes

We denote the transversity amplitudes of Kotanski[104] by

$$T^0_{++}\ ,\quad T^0_{--},\quad T^1_{-+},\quad T^1_{+-},\quad T^{-1}_{-+}\quad \text{and}\quad T^{-1}_{+-} \tag{4.2.8}$$

where in $T^{m_{K^*}}_{m_\Lambda m_p}$, m_{K^*}, m_Λ and m_p are respectively the K^*, Λ and p transversities (spin projections along the production normal).

(iii) Byers and Yang amplitudes

We define amplitudes $a_\pm$, $b_\pm$ and $c_\pm$, similar to those of reference (104), by the transitions shown in Table (4.2.1).

† Unlike references (18, 105) we do not include a factor $(-)^{s_2-\lambda_2}$ in our two-particle states.

	A_{K^*}	m_Λ	m_p
a_+	Z_1^T	$\frac{1}{2}$	$\frac{1}{2}$
b_+	X_1^T	$-\frac{1}{2}$	$\frac{1}{2}$
c_+	Y_1^T	$-\frac{1}{2}$	$\frac{1}{2}$
a_-	Z_1^T	$-\frac{1}{2}$	$-\frac{1}{2}$
b_-	X_1^T	$\frac{1}{2}$	$-\frac{1}{2}$
c_-	Y_1^T	$\frac{1}{2}$	$-\frac{1}{2}$

Table (4.2.1)

In the table A_{K^*} is the axis (X, Y or Z) along which the K^* has zero spin component.

Relation between (ii) and (iii)

We use particle spin states

$$|V\,1,\ m_V\rangle_u\ ,\quad |Y\ \tfrac{1}{2},\ m_Y\rangle_u\ m\quad |N\ \tfrac{1}{2},\ m_N\rangle_u \tag{4.2.9}$$

in which u is the (transversity) axis along which particles V (vector meson), Y (hyperon) and N (nucleon) have spin components m_V, m_Y and m_N. We may write for example,

$$a_+ = \langle V1,0|_z \langle Y\tfrac{1}{2},\tfrac{1}{2}|_z\ T|N\tfrac{1}{2},\ \tfrac{1}{2}\rangle_z = T^0_{++} \tag{4.2.10}$$

Similarly,

$$a_- = T^0_{--} \tag{4.2.11}$$

We also have

$$b_+ = \langle V1,0|_x \langle Y\tfrac{1}{2},\tfrac{1}{2}|_z\ T|N\tfrac{1}{2},\ \tfrac{1}{2}\rangle_z \tag{4.2.12}$$

and

$$c_+ = \langle V1,0|_Y \langle Y\tfrac{1}{2},\tfrac{1}{2}|_z\ T|N\tfrac{1}{2},\tfrac{1}{2}\rangle_z \tag{4.2.13}$$

Now

$$|1,0\rangle_x = e^{-\frac{i\pi}{2}J_Y}|1,0\rangle_z = \Sigma_m |1,m\rangle_z \underbrace{\langle 1,m|_z e^{-\frac{i\pi}{2}J_Y}|1,0\rangle_z}_{= d^1_{m,0}(\frac{\pi}{2})} \tag{4.2.14}$$

$$= \frac{1}{\sqrt{2}}\left[|1,-1\rangle_z - |1,1\rangle_z\right] \tag{4.2.15}$$

and

$$|1,0\rangle_Y = e^{-\frac{i\pi}{2}J_Z}|1,0\rangle_x \tag{4.2.16}$$

$$= \frac{1}{\sqrt{2}}\left[e^{\frac{i\pi}{2}}|1,-1\rangle_z - e^{-\frac{i\pi}{2}}|1,1\rangle_z\right]$$

$$= \frac{i}{\sqrt{2}}\left[|1,-1\rangle_z + |1,1\rangle_z\right] \tag{4.2.17}$$

Therefore from equations (4.2.12), (4.2.13), (4.2.15) and (4.2.17) we find

$$T^1_{-+} = \langle V1,1|_z \langle Y\tfrac{1}{2},-\tfrac{1}{2}|_z \; T \; |N\tfrac{1}{2},\tfrac{1}{2}\rangle_z$$

$$= -\frac{b_+ - ic_+}{\sqrt{2}} \tag{4.2.18}$$

and

$$T^{-1}_{-+} = \langle V1,-1|_z \langle Y\tfrac{1}{2},-\tfrac{1}{2}|_z T |N\tfrac{1}{2},\tfrac{1}{2}\rangle_z$$

$$= \frac{b_+ + ic_+}{\sqrt{2}} \tag{4.2.19}$$

An identical argument gives $T^{\pm 1}_{+-}$ and in summary we find

$$a_{\pm} = T^{0}_{\pm\pm}$$

$$-\frac{b_{\pm} - ic_{\pm}}{\sqrt{2}} = T^{1}_{\substack{-+\\+-}} \qquad (4.2.20)$$

$$\frac{b_{\pm} + ic_{\pm}}{\sqrt{2}} = T^{-1}_{\substack{-+\\+-}}$$

Relation between (i) and (ii)

We consider, for example, s-channel helicity amplitudes and relate these by axis rotation to the transversity amplitudes, (ii). The unique sequence of rectangular rotations about Z, Y and Z axes is shown in Figure (4.2.2) and is accomplished by the operation of D^{J} matrices,

$$D^{J}_{m^{1}m}(R) \equiv D^{J}_{m^{1}m}(-\tfrac{\pi}{2}, -\tfrac{\pi}{2}, 0) = e^{\frac{i\pi m^{1}}{2}}\, d^{J}_{m^{1}m}(-\tfrac{\pi}{2}) \qquad (4.2.21)$$

acting to the right.

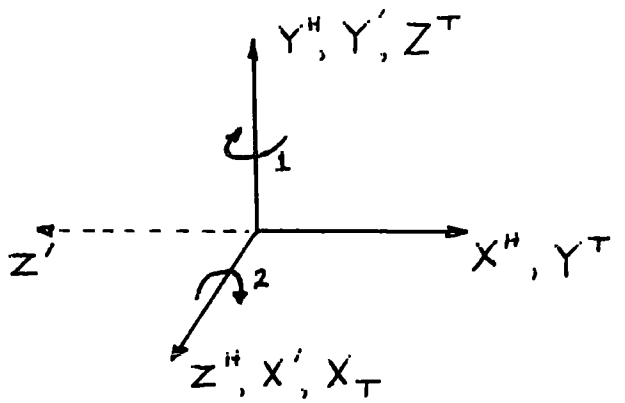

Fig.(4.2.2)

We therefore have[104]

$$T^{\lambda}_{\mu\nu} = \sum_{\lambda^1\mu^1\nu^1} D^{1*}_{\lambda^1\lambda}(R)\; D^{\frac{1}{2}*}_{\mu^1\mu}(R)\; D^{\frac{1}{2}}_{\nu^1\nu}(R)\; H^{\lambda^1}_{\mu^1\nu^1} \tag{4.2.22}$$

$$= \sum_{\lambda^1\mu^1\nu^1} e^{-\frac{i\pi}{2}(\lambda^1+\mu^1-\nu^1)} d^{1}_{\lambda^1\lambda}(-\tfrac{\pi}{2}) d^{\frac{1}{2}}_{\mu^1\mu}(-\tfrac{\pi}{2}) d^{\frac{1}{2}}_{\nu^1\nu}(-\tfrac{\pi}{2}) H^{\lambda^1}_{\mu^1\nu^1} \tag{4.2.23}$$

The $d^{1}_{m^1m}(\theta)$ and $d^{\frac{1}{2}}_{m^1m}(\theta)$ matrices are given in Appendix 4B. Evaluating equations (4.2.23), using the parity relations (equation (4.1.3))

$$H^{\lambda}_{\mu\nu} = -(-)^{\lambda-\mu+\nu} H^{-\lambda}_{-\mu-\nu}, \tag{4.2.24}$$

we find

$$T^{o}_{++} = \frac{-i}{2\sqrt{2}}(H^{1}_{++} + H^{1}_{--} + iH^{1}_{+-} - iH^{1}_{-+})$$

$$\frac{-i}{2\sqrt{2}}(H^{1}_{--} + H^{1}_{++} - iH^{1}_{-+} + iH^{1}_{+-})$$

$$= \frac{-i}{\sqrt{2}}\left[(H^{1}_{++} + H^{1}_{--}) + i(H^{1}_{+-} - H^{1}_{-+})\right], \tag{4.2.25}$$

$$T^{o}_{--} = \frac{-i}{\sqrt{2}}\left[(H^{1}_{++} + H^{1}_{--}) - i(H^{1}_{+-} - H^{1}_{-+})\right], \tag{4.2.26}$$

$$T^1_{-+} = \frac{-i}{4}\left[(H^1_{++}-H^1_{--})+i(H^1_{+-}+H^1_{-+})\right]-\frac{1}{2\sqrt{2}}\left[(H^0_{++}-H^0_{+-})+i(H^0_{+-}+H^0_{-+})\right]$$

$$\frac{+i}{4}\left[(H^1_{--}-H^1_{++})-i(H^1_{-+}+H^1_{+-})\right].$$

$$= \frac{-i}{2}\left[(H^1_{++}-H^1_{--})+i(H^1_{+-}+H^1_{-+})\right]-\frac{1}{\sqrt{2}}\left[H^0_{++}+iH^0_{+-}\right], \qquad (4.2.27)$$

$$T^{-1}_{-+} = \frac{-i}{2}\left[(H^1_{++}-H^1_{--})+i(H^1_{+-}+H^1_{-+})\right]+\frac{1}{\sqrt{2}}\left[H^0_{++}+iH^0_{+-}\right], \qquad (4.2.28)$$

$$T^1_{+-} = \frac{-i}{4}\left[(H^1_{++}-H^1_{--})-i(H^1_{+-}+H^1_{-+})\right]-\frac{1}{2\sqrt{2}}\left[(H^0_{++}-H^0_{--})-i(H^0_{+-}+H^0_{-+})\right]$$

$$\frac{+i}{4}\left[(H^1_{--}-H^1_{++})+i(H^1_{-+}+H^1_{+-})\right]$$

$$= \frac{-i}{2}\left[(H^1_{++}-H^1_{--})-i(H^1_{+-}+H^1_{-+})\right]-\frac{1}{\sqrt{2}}\left[H^0_{++}-iH^0_{+-}\right], \qquad (4.2.29)$$

and

$$T^{-1}_{+-} = \frac{-i}{2}\left[(H^1_{++}-H^1_{--})-i(H^1_{+-}+H^1_{-+})\right]+\frac{1}{\sqrt{2}}\left[H^0_{++}-iH^0_{+-})\right]. \qquad (4.2.30)$$

We introduce the notation

$$U^0_{++} = H^0_{++} \quad U^1_{++} = \frac{1}{\sqrt{2}}(H^1_{++}-H^1_{--}) \quad N^1_{++} = \frac{1}{\sqrt{2}}(H^1_{++}+H^1_{--})$$

$$U^0_{+-} = H^0_{+-} \quad U^1_{+-} = \frac{1}{\sqrt{2}}(H^1_{+-}+H^1_{-+}) \quad N^1_{+-} = \frac{1}{\sqrt{2}}(H^1_{+-}-H^1_{-+}) \qquad (4.2.31)$$

since we know[20] that to leading order, the combinations denoted N and U represent respectively natural and unnatural parity exchange in the t-channel. In terms of these, we have shown

$$T^{o}_{++} = -i\left[N^{1}_{++}+iN^{1}_{+-}\right] \qquad T^{o}_{--} = -i\left[N^{1}_{++}-iN^{1}_{+-}\right]$$

$$T^{1}_{+-} = \frac{-i}{\sqrt{2}}\left[U^{1}_{++}-iU^{1}_{+-}\right] - \frac{1}{\sqrt{2}}\left[U^{o}_{++}-iU^{o}_{+-}\right]$$

$$T^{1}_{-+} = \frac{-i}{\sqrt{2}}\left[U^{1}_{++}+iU^{1}_{+-}\right] - \frac{1}{\sqrt{2}}\left[U^{o}_{++}+iU^{o}_{+-}\right] \qquad (4.2.32)$$

$$T^{-1}_{+-} = \frac{-i}{\sqrt{2}}\left[U^{1}_{++}-iU^{1}_{+-}\right] + \frac{1}{\sqrt{2}}\left[U^{o}_{++}-iU^{o}_{+-}\right]$$

$$T^{-1}_{-+} = \frac{-i}{\sqrt{2}}\left[U^{1}_{++}+iU^{1}_{+-}\right] + \frac{1}{\sqrt{2}}\left[U^{o}_{++}+iU^{o}_{+-}\right]$$

Relation between (i) and (iii)

From equations (4.2.20),(4.2.31) and (4.2.32) we deduce[†]

$$H^{1}_{++} + H^{1}_{--} = \sqrt{2}N^{1}_{++} = \frac{i}{\sqrt{2}}(a_{+}+a_{-})$$

$$H^{1}_{+-} - H^{1}_{-+} = \sqrt{2}N^{1}_{+-} = \frac{1}{\sqrt{2}}(a_{+}-a_{-})$$

$$H^{1}_{++} - H^{1}_{--} = \sqrt{2}U^{1}_{++} = -\frac{1}{\sqrt{2}}(c_{+}+c_{-}) \qquad (4.2.33)$$

$$H^{1}_{+-} + H^{1}_{-+} = \sqrt{2}U^{1}_{+-} = \frac{i}{\sqrt{2}}(c_{+}-c_{-})$$

$$H^{o}_{++} = U^{o}_{++} = \frac{1}{2}(b_{+}+b_{-})$$

$$H^{o}_{+-} = U^{o}_{+-} = -\frac{i}{2}(b_{+}-b_{-})$$

[†]Our helicity amplitudes differ from those of reference (105) in not including the Jacob and Wick phase convention, and in being $\sqrt{2}$ smaller in normalisation.

Relations (4.2.33) apply equally well to both s- and t-channel amplitudes except that the notation N and U only has the interpretation described above, for s-channel helicity.

4.3 Derivation of a Byers and Yang-like distribution

The explicit expansion of equation (4.1.7) in terms of double density matrix elements has been written down† in reference (106) and is shown in Appendix 4A. Here we expand in terms of (x_i, y_i, z_i) as given by equations (4.1.14) and (4.1.15), and achieve a form

$$W = F_o + \alpha_\Lambda (x_2 F_1 + y_2 F_2 + {}_2F_3) \qquad (4.3.1)$$

where

$$F_i = F_{i1} x_1^2 + F_{i2} y_1^2 + F_{i3} z_1^2 + F_{i4} x_1 y_1 + F_{i5} x_1 z_1 + F_{i6} y_1 z_1 \qquad (4.3.2)$$

and

$$\begin{aligned}
3F_{O1} &= 1-2F_1 & F_{O4} &= -2\sqrt{2}F_2 \\
3F_{O2} &= 1+F_1-3F_3 & F_{34} &= 2\sqrt{2}F_9 \\
3F_{O3} &= 1+F_1+3F_3 & F_{15} &= 2\sqrt{2}F_5 \\
3F_{31} &= 2F_7-2F_4 & F_{25} &= 2\sqrt{2}F_8 \\
3F_{32} &= 3F_{11}-F_7-2F_4 & F_{16} &= 2F_6 \\
3F_{33} &= -3F_{11}-F_7-2F_4 & F_{26} &= 2F_{10} ,
\end{aligned} \qquad (4.3.3)$$

The other F_{ij} being zero.

†Note that in reference (106), the factor ½ in the expressions for F_8, F_9, F_{10} and F_{11} should not be present.

In equations (4.3.3) the F_i are the correlation parameters of Appendix 4A. Using the relations between the F_i and density matrix elements (given in Appendix 4A) along with equation (4.3.3) we relate the coefficients F_{ij} to helicity amplitudes.

$$F_{01} = \rho_{00} = 2\left|H^0_{++}\right|^2 + 2\left|H^0_{+1}\right|^2 \tag{4.3.4}$$

$$F_{02} = \rho_{11}-\rho_{1-1} = \left|H^1_{++} - H^1_{--}\right|^2 + \left|H^1_{+-} + H^1_{-+}\right|^2 \tag{4.3.5}$$

$$F_{03} = \rho_{11}+\rho_{1-1} = \left|H^1_{++} + H^1_{--}\right|^2 + \left|H^1_{+-} - H^1_{-+}\right|^2 \tag{4.3.6}$$

$$F_{04} = -2\sqrt{2}\,\mathrm{Re}\,\rho_{10} = -2\sqrt{2}\,\mathrm{Re}\left[H^{0*}_{++}(H^1_{++}-H^1_{--})+H^{0*}_{+-}(H^1_{+-}+H^1_{-+})\right] \tag{4.3.7}$$

$$F_{34} = 2\sqrt{2}\,\mathrm{Im}(\rho^{10}_{+-}-\rho^{10}_{-+}) = 2\sqrt{2}\,\mathrm{Im}\left[H^{0*}_{+-}(H^1_{++}-H^1_{--})-H^{0*}_{++}(H^1_{+-}+H^1_{-+})\right] \tag{4.3.8}$$

$$F_{31} = -2\,\mathrm{Im}\rho^{00}_{+-} = -4\,\mathrm{Im}\left[H^0_{++}\,H^{0*}_{+-}\right] \tag{4.3.9}$$

$$F_{32} = \mathrm{Im}(\rho^{1-1}_{+-}-\rho^{1-1}_{-+}-\rho^{11}_{+-}+\rho^{11}_{-+}) = -2\,\mathrm{Im}\left[(H^1_{++}-H^1_{--})(H^1_{+-}+H^1_{-+})^*\right] \tag{4.3.10}$$

$$F_{33} = \mathrm{Im}(-\rho^{1-1}_{+-}+\rho^{1-1}_{-+}-\rho^{11}_{+-}+\rho^{11}_{-+} = 2\,\mathrm{Im}\left[(H^1_{++}+H^1_{--})(H^1_{+-}-H^1_{-+})^*\right] \tag{4.3.11}$$

$$F_{15} = 2\sqrt{2}\,\mathrm{Im}(\rho^{10}_{++}-\rho^{10}_{--}) = 2\sqrt{2}\,\mathrm{Im}\left[H^{0*}_{++}(H^1_{++}+H^1_{--})+H^{0*}_{+-}(H^1_{+-}-H^1_{-+})\right] \tag{4.3.12}$$

$$F_{25} = 2\sqrt{2}\,\mathrm{Im}(\rho^{10}_{+-}+\rho^{10}_{-+}) = 2\sqrt{2}\,\mathrm{Im}\left[H^{0*}_{++}(H^1_{-+}-H^1_{+-})+H^0_{+-}(H^1_{--}+H^1_{++})\right] \tag{4.3.13}$$

$$F_{16} = 2\,\mathrm{Im}(\rho^{1-1}_{++}-\rho^{1-1}_{--}) = 4\,\mathrm{Im}(H^1_{++}H^{1*}_{--} - H^1_{+-}H^{1*}_{-+}) \tag{4.3.14}$$

$$F_{26} = 2\,\mathrm{Im}(\rho^{1-1}_{+-}+\rho^{1-1}_{-+}) = -4\,\mathrm{Im}(H^1_{++}H^{1*}_{+-} + H^1_{--}H^{1*}_{-+}) \tag{4.3.15}$$

With the aid of equations (4.2.33) we may finally express the F_{ij} of expansion (4.3.2) in terms of the Byers and Yang amplitudes of Section 4.2(iii). Thus

$$
\begin{aligned}
F_{01} &= |b_+|^2 + |b_-|^2 & F_{04} &= 2\mathrm{Re}(b_+ c_+^* + b_- c_-^*) \\
F_{02} &= |c_+|^2 + |c_-|^2 & F_{34} &= -2\mathrm{Re}(b_+ c_+^* - b_- c_-^*) \\
F_{03} &= |a_+|^2 + |a_-|^2 & F_{15} &= 2\mathrm{Re}(a_+ b_+^* + a_-^* b_-) \\
F_{31} &= -|b_+|^2 + |b_-|^2 & F_{25} &= -2\mathrm{Im}(a_+ b_+^* + a_-^* b_-) \\
F_{32} &= -|c_+|^2 + |c_-|^2 & F_{16} &= 2\mathrm{Re}(a_+ c_+^* + a_-^* c_-) \\
F_{33} &= |a_+|^2 - |a_-|^2 & F_{26} &= -2\mathrm{Im}(a_+ c_+^* + a_-^* c_-)
\end{aligned}
\qquad (4.3.16)
$$

An alternative derivation of the angular distribution (4.3.1), (4.3.2) and (4.3.16) was given by Byers and Yang[103] who advocated solving the 6 equations on the left side of (4.3.16) for the 6 amplitude moduli, using the last 4 of the right side to determine the relative phases within the sets (a_+, b_+, c_+), (a_-, b_-, c_-) and then resolving the discrete ambiguities in this solution with the measured values of F_{04} and F_{34}. Assuming the F_{ij} have been extracted from the decay data by the usual method of moments, this solution procedure is inefficient for the following reasons:

(a) There is no guarantee that the moduli, so determined, and the cross product measurements (last four in equation (4.3.16)) are compatible. This problem is partially analogous to (ii) of Section 4.1.

(b) Even if, in view of (a), a solution is possible, the use of the last two measurements as mere checks constitutes a waste of information.

(c) The sequential method of solution does not allow the last 6 moments of equation (4.3.16) to be treated with equal weights. Elimination of these problems will be discussed in the next section.

Already, with the introduction of these amplitudes, we note that some of the criticisms (i) to (v) of Section 4.1 have been answered.

(i) The amplitudes, a, describe t-channel natural parity exchange while b(c) describe unnatural parity production of helicity 0(1) vector mesons (see equation (4.2.33)).

(ii) The 6 moduli and 4 relative phases are independent, subject to compatibility of the measurements. A method of ensuring this is described in the next section.

(iii) The ranges of the 10 parameters are given simply by

$$|a_+|^2 + |b_+|^2 + |c_+|^2 + |a_-|^2 + |b_-|^2 + |c_-|^2 = \frac{d\sigma}{dt} \qquad (4.3.17)$$

and

$$-\pi \leq \text{phase } (a_+) < \pi \quad \text{etc.} \qquad (4.3.18)$$

(iv) Equations (4.3.1) and (4.3.2) indicate that the F_{oi}, then the F_{3i} are the "lowest" moments so that we expect the moduli to be better determined than the phases which depend in an intricate way on the higher moments.

(v) It is immediately obvious from the right sides of equation (4.3.16) that only 10 of the 12 measureable (F_{ij} in this case) can be independent since none of the moments relates the relative phases of '+' amplitudes to '-' ones.

From the last remark in (v) it is now clear that to solve equation (4.2.33) for helicity amplitudes one requires this extra relative phase between amplitudes for target nucleons of opposite transversity. Such information is obtainable only from polarised target experiments.

4.4 Maximum likelihood method

Some disadvantages ((a), (b), (c) of Section 4.3) of the moment method are avoided by using the moduli and 4 relative phases of the Byers and Yang amplitudes in a maximum likelihood[107] search. That is, we form the log-likelihood function

$$w(P) = -\mathrm{Log}\left[L(P)\right] \tag{4.4.1}$$

$$\text{where } L(P) = \prod_{i=1}^{N} W(P;\, x_1^i\, y_1^i\, z_1^i\, x_2^i\, y_2^i\, z_2^i)^{\omega_g^i} \tag{4.4.2}$$

In equation (4.4.2) W is given by equation (4.3.1), P is the set of 10 parameters

$$\begin{aligned} A_\pm &= |a_\pm| \\ B_\pm &= |b_\pm| \\ C_\pm &= |c_\pm| \end{aligned} \qquad \begin{aligned} \phi_{ab}^\pm &= \text{phase } (b_\pm) - \text{phase } (a_\pm) \\ \phi_{ac}^\pm &= \text{phase } (c_\pm) - \text{phase } (a_\pm) \end{aligned} \tag{4.4.3}$$

where

$$-\pi \leqslant \phi < \pi \tag{4.4.4}$$

$(x_j^i,\, y_j^i,\, z_j^i)$ are the two sets of direction cosines for each event (i) of the N events. ω_g^i is the geometrical weight assigned to event i (see Appendix 4C).

$$w(P) = -\sum_{i=1}^{N} \log\left[W(P;\ x_1^i\ y_1^i\ z_1^i,\ x_2^i\ y_2^i\ z_2^i)\right]\omega_g^i \qquad (4.4.5)$$

is then minimised to give the set of parameters P_o with "maximum likelihood". Calculation of the parameter variances and covariances is described in Appendix 4C.

Since the method involves minimisation, uniqueness is difficult to ensure (unlike the moment method). This is alleviated by using a set of frame invariant measureables (see Section 4.2) as consistency checks on independent t- and s-channel solutions. We introduce a set of 9 such quantities which are not, of course, all independent but which possess physical significance. They are

$$\sigma_N = |a_+|^2 + |a_-|^2 = F_{03} \qquad (4.4.6)$$

$$\sigma_U = |b_+|^2 + |b_-|^2 + |c_+|^2 + |c_-|^2 = F_{01} + F_{02} \qquad (4.4.7)$$

$$P_N\sigma_N = |a_+|^2 - |a_-|^2 = F_{33} \qquad (4.4.8)$$

$$P_U\sigma_U = |b_-|^2 - |b_+|^2 + |c_-|^2 - |c_+|^2 = F_{31} + F_{32} \qquad (4.4.9)$$

$$\Delta_\pm^2 n_\pm^2 = 4\,\mathrm{Im}^2(b_\pm c_\pm^*) = 4f_1^\pm f_2^\pm - (f_4^\pm)^2 \qquad (4.4.10)$$

$$\begin{aligned}\Delta_O^2\sigma_U^2 &= 4(|b_+|^2+|b_-|^2)(|c_+|^2+|c_-|^2) - 4\mathrm{Re}^2(b_+c_+^*+b_-c_-^*) \\ &= 4F_{01}F_{02} - F_{04}^2\end{aligned} \qquad (4.4.11)$$

$$\begin{aligned}I_\pm^2 p_\pm^2 &= 4\left|a_+(b_+\pm ic_+)^* + a_-^*(b_-\mp ic_-)\right|^2 \\ &= (F_{15}\mp F_{26})^2 + (F_{25}\pm F_{16})^2\end{aligned} \qquad (4.4.12)$$

where

$$n_{\pm} = \tfrac{1}{2}(1\mp P_U)\sigma_U \qquad (4.4.13)$$

$$p_{\pm} = \sigma_N+\sigma_U\pm(\Delta_+n_+-\Delta_-n_-) \qquad (4.4.14)$$

$$f_i^{\pm} = \tfrac{1}{2}(F_{0i} \mp F_{3i}) \qquad (4.4.15)$$

They are identified as being invariant with respect to rotations about the production normal, by noting the rotation properties of transversity amplitudes[104]

$$(T^{\lambda}_{\mu\nu})' = e^{i\lambda\chi_1+i(\mu-\nu)\chi_2}\, T^{\lambda}_{\mu\nu} \qquad (4.4.16)$$

The quantities in equations (4.4.6) to (4.4.12) are suitable combinations of the $|T^{\lambda}_{\mu\nu}|$ and moduli of bilinear combinations of the $T^{\lambda}_{\mu\nu}$ having the same $\lambda\chi_1 + (\mu-\nu)\chi_2$. They are expressed in terms of Byers and Yang amplitudes using equation (4.2.20).

$\sigma_N(\sigma_U)$ represents that part of the cross-section due to natural (unnatural) parity exchange. The polarisation $P_N(P_U)$ has a similar interpretation. The decomposition of σ_U, P_U into

$$\sigma_U^{\,0} = |b_+|^2 + |b_-|^2 = F_{01} = \rho_{00} \qquad (4.4.17)$$

$$\sigma_U^{\,1} = |c_+|^2 + |c_-|^2 = F_{02} = \rho_{11} - \rho_{1-1} \qquad (4.4.18)$$

$$P_U^{\,0}\sigma_U^{\,0} = -|b_+|^2 + |b_-|^2 = F_{31} \qquad (4.4.19)$$

$$P_U^{\,1}\sigma_U^{\,1} = -|c_+|^2 + |c_-|^2 = F_{32} \qquad (4.4.20)$$

is obviously not frame independent (the 0 and 1 refer to either s- or t-channel vector meson helicity). The quantities $\Delta_{\pm}$ which directly measure the phases $-\phi^{\pm}_{bc}$ whose sign they share, have the form of vector meson

polarisation parameters for unnatural parity exchange and lie in the range

$$0 \leq \Delta_{\pm} \leq 1. \qquad (4.4.21)$$

$I_{\pm}$, which are similarly normalised, measure the interference between natural and unnatural parity amplitudes. The above-mentioned 8 invariants are independent. The ninth invariant Δ_o, normalised as in (4.2.21), measures (like $\Delta_{\pm}$) the spin and phase coherence of the meson helicity 0 and 1 unnatural parity amplitudes, but is much better determined experimentally since it depends only on the meson decay,

$$\Delta_o\sigma_u = 2\left[\rho_{oo}(\rho_{11}-\rho_{1-1}) - 2(\mathrm{Re}\rho_{10})^2\right]^{\frac{1}{2}} \qquad (4.4.22)$$

It is a measure of to what extent the relation[108]

$$\rho_{oo}(\rho_{11}-\rho_{1-1}) \geq 2\,(\mathrm{Re}\rho_{10})^2 \qquad (4.4.23)$$

(sometimes known as the Kaidalov relation) is saturated.

Shown in Table (4.4.1) are the amplitude moduli and relative phases together with a selection of measureables resulting from independent maximum likelihood determinations carried out in the s- and t-channels for the process

$$\pi^- p \longrightarrow K^* \Lambda \qquad (4.4.24)$$

at 3.9 GeV. The data used were those of Abramovich et al[102] using a K^* effective mass cut[102] of

$$0.868 < M(K^+\pi^-) < 0.920 \text{ GeV} \qquad (4.4.25)$$

	$0 < -t' < 0.2$		$0.2 < -t' < 0.4$		$0.4 < -t' < 0.9$	
	t channel	s channel	t channel	s channel	t channel	s channel
$\|a_+\|^2$	0.09±0.13	0.05±0.14	0.17±0.19	0.17±0.18	0.09±0.22	0.07±0.22
	(0.11±0.17)	(0.11±0.17)	(0.10±0.17)	(0.10±0.17)	(0.04±0.17)	(0.04±0.17)
$\|b_+\|^2$	0.11±0.12	0.15±0.16	0.03±0.09	0.20±0.15	0.16±0.20	0.03±0.14
	(0.03±0.16)	(0.14±0.17)	(-0.03±0.13)	(0.24±0.15)	(0.16±0.15)	(0.03±0.16)
$\|c_+\|^2$	0.17±0.14	0.05±0.09	0.17±0.15	0.00±0.31	0.05±0.13	0.17±0.21
	(0.21±0.14)	(0.11±0.15)	(0.23±0.14)	(-0.04±0.12)	(0.06±0.16)	(0.19±0.15)
$\|a_-\|^2$	0.26±0.15	0.33±0.17	0.32±0.16	0.32±0.17	0.47±0.23	0.48±0.22
	(0.29±0.16)	(0.20±0.16)	(0.38±0.16)	(0.37±0.18)	(0.53±0.19)	(0.53±0.19)
$\|b_-\|^2$	0.32±0.13	0.31±0.15	0.28±0.12	0.07±0.14	0.17±0.19	0.07±0.12
	(0.36±0.19	(0.29±0.18)	(0.32±0.16)	(0.08±0.14)	(0.22±0.16)	(0.02±0.16)
$\|c_-\|^2$	0.05±0.12	0.11±0.10	0.03±0.15	0.23±0.09	0.07±0.11	0.17±0.21
	(-0.01±0.14)	(0.05±0.15)	(0.01±0.12)	(0.25±0.15)	(-0.01±0.15)	(0.19±0.16)
ϕ^+_{bc}	-0.7 ±1.1	-3.0 ±6.8	-0.2 ±5.3	2.5 ±78.6	-1.2 ±2.0	-2.4 ±4.2
ϕ^+_{ca}	-0.8 ±2.1	0.3 ±6.7	-1.4 ±2.0	-2.9 ±79.6	-2.9 ±5.2	1.0 ±7.1
ϕ^+_{ab}	1.5 ±2.0	2.6 ±2.5	1.6 ±5.8	0.3 ± 2.1	-2.3 ±5.5	1.5 ±5.9
ϕ^-_{bc}	1.5 ±1.0	1.7 ±0.7	1.4 ±1.4	2.3 ± 1.6	1.9 ±1.2	1.2 ±1.5
ϕ^-_{ca}	1.3 ±1.2	-0.7 ±1.3	0.7 ±1.8	-1.8 ± 1.1	1.9 ±2.5	-0.5 ±2.7
ϕ^-_{ab}	-2.7 ±0.8	-1.0 ±1.0	-2.2 ±1.3	-0.4 ± 1.8	2.5 ±2.8	-0.7 ±2.2
$\sigma^-_U(=1-\sigma^-_N)$	0.65	0.62	0.50	0.51	0.44	0.45
P_N	-0.50	-0.72	-0.30	-0.31	-0.66	-0.74
P_U	0.12	0.33	0.23	0.22	0.07	0.10
Δ_+	0.63	0.17	0.15	-0.02	0.72	0.48
Δ_-	-0.66	-0.87	-0.61	-0.65	-0.86	-0.84
Δ_o	0.87	0.81	0.92	0.94	0.87	0.85
σ^0_U	0.44	0.46	0.30	0.27	0.33	0.11
σ^1_U	0.22	0.16	0.20	0.23	0.11	0.34
P^0_U	0.47	0.33	0.81	-0.47	0.03	0.30
P^1_U	-0.57	0.33	-0.66	1.00	0.18	0.01

Table (4.4.1)

Moduli and relative phases of s- and t-channel amplitudes determined by maximum likelihood method.

The resonance is treated as pure p-wave since the narrow width renders negligible any s-wave contribution. In Table (4.4.1) the three event bins are

$$\begin{aligned} 0 \;\; &< -t' < 0.2 \quad , \quad 59 \text{ events} \\ 0.2 &< -t' < 0.4 \quad , \quad 58 \text{ events} \\ 0.4 &< -t' < 0.8 \quad , \quad 47 \text{ events} \end{aligned} \tag{4.4.26}$$

where

$$t' \;\; = \;\; t - t_o \; . \tag{4.4.27}$$

The figures in brackets are the equivalent quantities obtained from a conventional moment analysis[105].

4.5 Interpretation of results

The presented sample analysis of $\pi^- p \longrightarrow K^* \Lambda$ involved a total of 164 events with roughly 50 in each of 3 t-bins. These statistics are not sufficient to reliably determine 10 real numbers per bin, but the consistency of the method outlined in Section 4.4 is nevertheless evident. From Table (4.4.1) we note that

(i) the moduli are much better determined than the phases.

(ii) the phases of amplitudes with negative transversity are better determined than those with positive.

(iii) the invariant quantities (particularly those depending only on moduli) provide a consistency check on s- and t-channel solutions.

It is tempting to compare the natural parity exchange in $\pi^- p \longrightarrow K^* \Lambda$ with that in $\pi^- p \longrightarrow K^o \Lambda$. For example, the polarisation in the latter (see Chapter 2) is slightly positive for $-t < 0.3$ GeV^2 and large and negative at larger $-t$, whereas we see from Table (4.4.1) a consistently negative trend for P_N throughout these t ranges. With saturation of $a_\pm$ by absorbed K^* exchange we would expect identical polarisation behaviours so that the discrepancy indicates a different mechanism altogether and/or the presence of large absorption corrections to the unnatural parity pole exchange in $\pi^- p \longrightarrow K^* \Lambda$ — absorption is known to mix t-channel parities.

Δ_o has a significantly non-zero value implying the presence of more than one unnatural parity pole exchange since a single pole would give a phase coherence to all 4 amplitudes as indeed would an EXD pair (K, K_B) with their identical spin structure and correlated phases. This has independently been noted by Field[109].

An identical analysis of $K^- p \longrightarrow \phi \Lambda$ which is, by duality diagram and quark model arguments, expected to have the same amplitude structure, would provide a very interesting comparison with this work. The similarity of the two processes, at the more superficial level of density matrix elements, has already been noted[110], so giving further credence to the duality diagram/quark model scheme.

More detailed analysis of the implications of our results, in terms of helicity amplitudes requires a

knowledge of, or guess at, the relative phase between amplitudes of opposite nucleon transversity. We suggest 3 ways of obtaining this.

(i) A polarised target experiment[103]. This represents a lot of effort for one extra piece of information (the 11th observable).

(ii) Using theoretical prejudice gained from some exchange model to predict the vanishing of one of the N or U helicity amplitudes. For example if K alone couples to s-channel U^{o}_{++} one might anticipate this coupling to be small, in an SU(3) limit (c.f. $\pi N\bar{N}$ [111]).

Then $|U^{o}_{++}| = 0$ implies

$$\cos\phi^{b}_{-+} = -\frac{B_+^2 + B_-^2}{2B_+B_-} \qquad (4.5.1)$$

where ϕ^{b}_{-+} is the relative phase between b_+ and b_-.

(iii) Using an exchange model which successfully predicts some measureable combination(s) of the a, b, c amplitudes to predict the relative phase. For example, suppose the observed values of P_N in $\pi^- p \longrightarrow K^*\Lambda$ had more closely resembled the $\pi^- p \longrightarrow K^o\Lambda$ polarisation predicted in Chapter 2, then we might have assumed that model to give a good account of the natural parity $a_\pm$ amplitudes, in particular their relative phase. For pedagogical reasons we shall make this assumption.

We <u>identify</u>

$$a_+ \equiv \langle \Lambda\uparrow | T | p\uparrow \rangle \equiv f + ig \qquad (4.5.2)$$

$$a_- \equiv \langle \Lambda\downarrow | T | p\downarrow \rangle \equiv f - ig \qquad (4.5.3)$$

in an obvious notation, where f(g) is the pseudoscalar meson baryon spin non-flip (flip) scattering amplitude[1](a). Their connection with the equivalent helicity amplitudes is

$$\begin{pmatrix} f \\ g \end{pmatrix} = \frac{1}{\sin\theta} \begin{pmatrix} 1 & \cos\theta \\ 0 & -\sin\theta \end{pmatrix} \begin{pmatrix} \sin\frac{\theta}{2} & \cos\frac{\theta}{2} \\ \sin\frac{\theta}{2} & -\cos\frac{\theta}{2} \end{pmatrix} \begin{pmatrix} f_{++} \\ f_{+-} \end{pmatrix} \tag{4.5.4}$$

so that

$$a_{\pm} = e^{\mp \frac{i\theta}{2}} (f_{++} \pm i f_{+-}) \tag{4.5.5}$$

where θ is, as usual, the s-channel c.m. scattering angle. The polarisations are then connected by

$$P_N \sigma_N = |a_+|^2 - |a_-|^2 = 2\mathrm{Im}(f_{++} f_{+-}^*) = P \tag{4.5.6}$$

Similarly we notice that if (Appendix 2A)

$$\hat{R} = \frac{2\mathrm{Re}\ (f_{++} f_{+-}^*)}{|f_{++}|^2 + |f_{+-}|^2} \tag{4.5.7}$$

$$\hat{A} = \frac{|f_{++}|^2 - |f_{+-}|^2}{|f_{++}|^2 + |f_{+-}|^2} \tag{4.5.8}$$

then

$$\hat{A} + i\hat{R} \qquad \frac{2e^{i\theta} a_+ a_-^*}{|a_+|^2 + |a_-|^2} \tag{4.5.9}$$

To make a complete determination of all amplitudes (including the overall phase) we assume a phase for N^1_{+-} which, having baryon helicity flip, we expect to have a pure pole behaviour (Section 2.5):-

$$\frac{N^1_{+-}}{|N^1_{+-}|} = \frac{a_+ - a_-}{|a_+ - a_-|} = e^{-i\pi\alpha} \qquad (4.5.10)$$

where $\alpha = \alpha_{K^*}$

We then may write

$$N^1_{+-}a^*_- = \frac{1}{2}\left[-|a_-|^2 + \frac{(\hat{A}+i\hat{R})(|a_+|^2+|a_-|^2)}{2e^{i\theta}}\right] \qquad (4.5.11)$$

Then, up to 2π, we get

$$\text{phase}\,(N^1_{+-}a^*_-) = -\pi\alpha - \alpha_- = \text{phase}\left[\frac{\hat{A}+i\hat{R}}{\hat{A}^2+\hat{R}^2} \times \frac{|a_+|}{|a_-|e^{i\theta}} - 1\right] \qquad (4.5.12)$$

from which we may calculate α_- the phase of a_-. From equation (4.5.9) we then find

$$\alpha_+ = \text{phase}\,(\hat{A} + i\hat{R}) + \alpha_- - \theta \qquad (4.5.13)$$

and consequently

$$\beta_\pm = \alpha_\pm + \phi^\pm_{ab} \qquad (4.5.14)$$

$$\gamma_\pm = \alpha_\pm + \phi^\pm_{ac} \qquad (4.5.15)$$

where $\beta_\pm$ and $\gamma_\pm$ are respectively the phases of $b_\pm$ and $c_\pm$.

The results of such a calculation using the $\hat{R}$ and $\hat{A}$ predictions of Chapter 2 are shown in Table (4.5.1) along with the input $\hat{R}$ and $\hat{A}$. The entry marked $\frac{d\sigma}{dt}$ gives roughly the correspondingly binned cross-section of reference (102) to which the output

t'range GeV^2	0 ——— .2		.2 ——— .4		.4 ——— .8	
Amp.	Mod.	Phs.	Mod.	Phs.	Mod.	Phs.
N^1_{++}	.36	3.0	.33	3.0	.21	-1.4
N^1_{+-}	.25	-1.0	.37	-.5	.48	.25
U^1_{++}	.15	-1.5	.25	.73	.27	1.6
U^1_{+-}	.24	1.3	.25	2.3	.32	1.6
U^0_{++}	.16	1.5	.33	1.0	.21	2.3
U^0_{+-}	.45	2.1	.18	-1.5	.11	-1.3
$\frac{d\sigma}{dt}$	.16mb GeV^{-2}		.09mb GeV^{-2}		.04mb GeV^{-2}	
$\hat{R}$	-.7		-.95		-.4	
$\hat{A}$	.7		.3		-.45	

Table (4.5.1)

amplitudes must be normalised to give absolute values.

The results are exhibited graphically in Figure (4.5.1) and are merely indicative of a possible treatment given better statistics. The input EXD K^* phase for N^1_{+-} is shown along with the duality diagram expectation for an EXD (K,K_B) pair. It is perhaps fortuitous that the phase of U^1_{+-} is

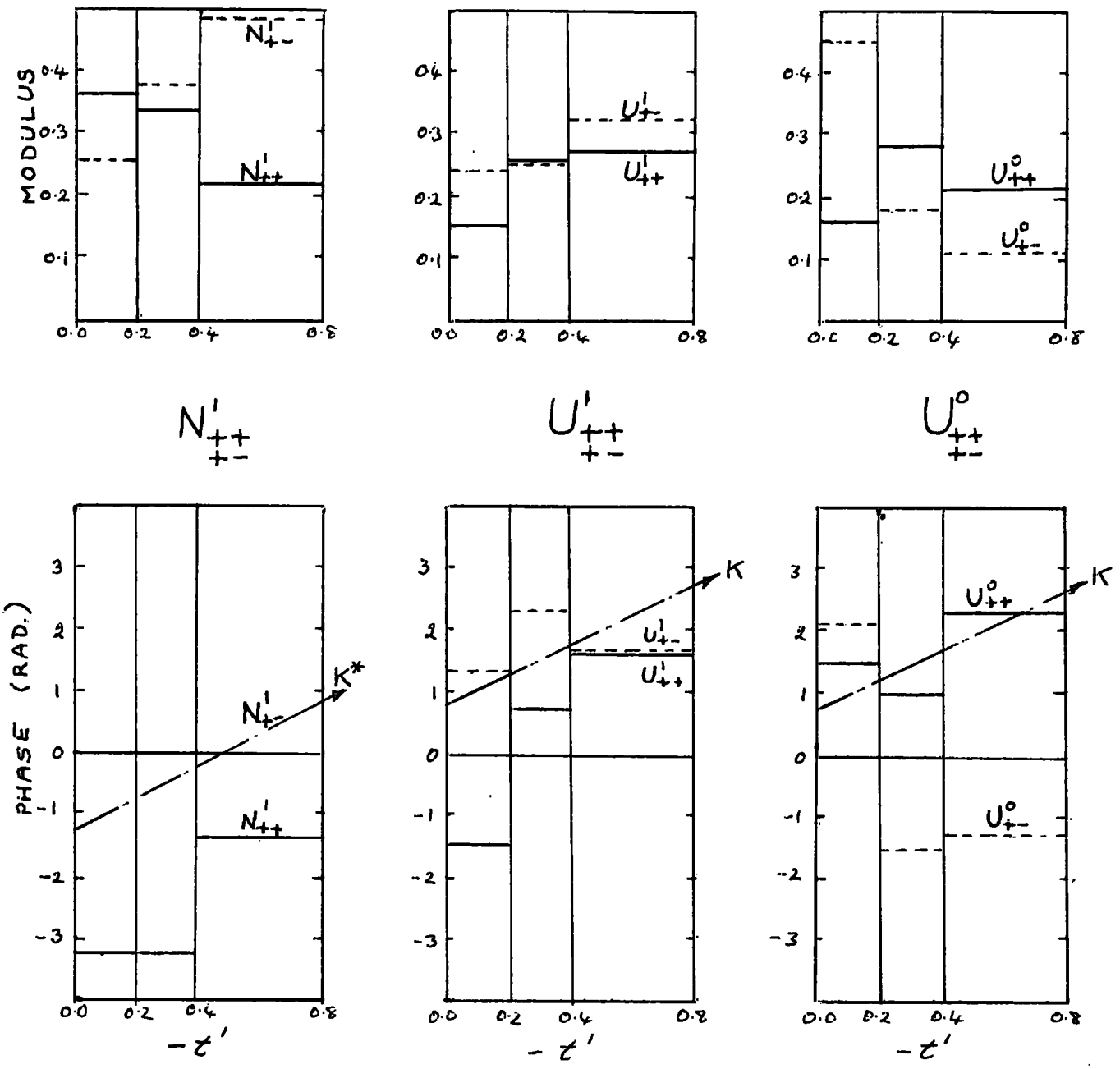

N^1_{++} U^1_{++} U^0_{++}
$+-$ $+-$ $+-$

Fig. (4.5.1)

Modulus and phase of natural and unnatural parity exchange s-channel helicity amplitudes under the assumption of Section 4.5(iii).

like that expected when pure EXD (K,K_B) poles unaffected by absorption are coupled to a baryon helicity-flip vertex. The N and U amplitudes have a small-t' behaviour of (see equation (1.3.7))

$$\begin{aligned} N^1_{++} &\sim \sqrt{-t'} \\ N^1_{+-} &\sim 1 \\ U^1_{++} &\sim \sqrt{-t'} \\ U^1_{+-} &\sim t \\ U^0_{++} &\sim 1 \\ U^0_{+-} &\sim \sqrt{-t'} \end{aligned} \qquad (4.5.16)$$

so that the very large value of U^0_{+-} compared to U^0_{++} at small -t confirms the expectation of a K exchange which couples predominantly to baryon s-channel helicity flip (c.f. π). This effect is not nearly so marked in U^1_{+-} and U^1_{++} possibly due to the importance of the EXD (K_A,K_Z) which are expected to couple predominantly to baryon helicity non-flip[111] (K_A is the SU(3) analogue of the A_1 trajectory).

The considerations following equation (4.5.1) are completely speculative and merely indicate a possible line of approach whereby a consistent set of assumptions may be arrived at, given better joint decay statistics.

The method of analysis advanced in this Chapter will be of most benefit when applied to pairs of reactions such as

$$\pi^- p \longrightarrow K^* \Lambda$$

and $$K^- p \longrightarrow \phi \Lambda \qquad (4.5.17)$$

using counter data of high statistics rather than, as here, bubble chamber data. Data over a spread of incident momenta would assist in identifying unambiguously whether the unnatural parity contributions present are due to some type of absorption effect acting on natural parity poles (a high $\alpha_{eff}(t)$ for the amplitude) or due to unnatural parity pole exchange itself (much lower lying effective trajectories).

C H A P T E R F I V E

C O N C L U S I O N S

5 : CONCLUSIONS

In this final chapter we summarise what has been achieved by the work reported in this thesis and point out some lessons for future analyses.

We have presented a model independent discussion of the cross-section and polarisation data which exists for meson-baryon strangeness-exchange reactions. We attempted to describe these data with a simple high-energy model which used the precise predictions of exchange-degeneracy for octet Regge pole exchange. These poles were absorbed with the weak cuts associated with a Pomeron moving pole so yielding, for the first time, a natural and unified description of all polarisations observed in HCEX reactions. The cross-section line reversal symmetry violation at intermediate energies was not successfully explained since the predicted real amplitude was too heavily reduced in our absorption prescription.

We demonstrated how anomalies in the intermediate energy cross-section data could be related semi-quantitatively (without performing FESR) to anomalies in the low energy resonance parameters of the direct channel process. It was suggested that the pressing problem of the cross-section inequality be attacked from two approaches - in terms of either s-channel effects as above or further crossed channel singularities which might be important at non-asymptotic energies.

This last possibility was thoroughly investigated within the rather dubious assumptions of the multiple

scattering model of Reggeised exchanges. Using knowledge of the spin properties of the octet meson-baryon couplings gained in the foregoing analysis, an attempt was made to give, for the first time, an honest treatment of the spin effects in double exchange diagrams. Critical comparisons with later and with contemporary but independent analyses were given. We presented explicit calculations of exotic HCEX reaction cross-sections ($K^- p \rightarrow \pi^+ \Sigma^-$ and $\pi^- p \rightarrow K^+ \Sigma^-$). It was shown how the direction of the cross-section inequality in these reactions was not correctly predicted (as in the non-exotic case) and that some degree of absorption of the Regge-Regge "cut" diagram was necessary to explain the observed smallness of the overall magnitude of these reaction rates. A unique prediction, of what we believe was a consistent treatment of spin couplings, was a forward dip present at all energies in both reaction cross-sections. This feature and the predicted cross-section energy dependence of s^{-3} are open to experimental test in the foreseeable future. In view of the artificial and imperfect cross-section descriptions, however, we were forced to conclude that the exotic amplitudes are not naturally or usefully described by the multiple scattering formalism of Regge-Regge cuts.

We put forward the hypothesis that although exotic cuts had to be very small, spin effects were such that the related non-exotic Regge-Regge cuts could, in contrast, be much larger. Explicit calculation in a typical case

showed this to be the case but none-the-less too small to significantly affect the incorrect cross-section description given by the leading Pomeron cuts. In fact we confirmed the statement of Michael[63] that these cuts made the situation worse. It was shown that the simple polarisation description by leading cuts was unaffected by the inclusion of non-leading terms.

Before leaving the topic of line reversal symmetry violation we now make a few further comments. Instead of attributing the cross-section suppression of C-type $\pi N \rightarrow KY$ relative to R-type $\bar{K}N \rightarrow \pi Y$, to their exchange degeneracy phase properties, we could point to another significant difference in their duality diagrams[115]. Only in the first case is a $\lambda\bar{\lambda}$ quark final state involved:-

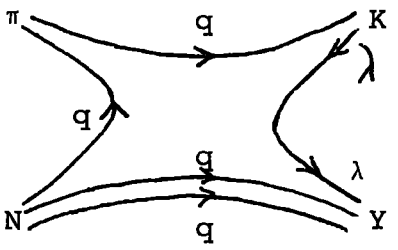

We also notice the relatively high mass of the final state in this type of reaction. In common with $\pi N \rightarrow KY$ it is found[116] that $\pi^- p \rightarrow \eta n$ at low energies has large contributions from non-peripheral resonances (see Section 2.7) in comparison with $\pi^- p \rightarrow \pi^o n$ for example. We note the high mass and $\lambda\bar{\lambda}$ content of η relative to π^o. The deviation of $\pi^- p \rightarrow \eta n$ from an exchange degenerate pole high energy behaviour has been well noted[38]. Other examples of reactions which have

$\lambda\bar{\lambda}$ high mass final states and which show anomalous behaviour at high and/or low energies are not difficult to find. The suppression of ϕ photoproduction relative to the standard quark model expectation via vector dominance from ρ and ω photoproduction has been noted in the literature[117]. The data for $\pi^- p \rightarrow K^* \Lambda$ and $K^- p \rightarrow \phi \Lambda$ (both with $\lambda\bar{\lambda}$ final states) show a similar suppression relative to $K^- p \rightarrow \rho \Lambda$ and $K^- p \rightarrow \omega \Lambda$. Note that KN and $\bar{K}N$ charge exchange cross-sections with their line reversal equality at intermediate energies and the pole-like behaviour prove no exception to these rules since both have equal mass kinematics and involve no $\lambda\bar{\lambda}$ production. A modified form of these cross-section systematics has recently been commented upon by Lo[118].

We submit that the cross-section suppression observed in certain strangeness-exchange reactions is not unique and that a unifying examination of all similar effects at high and low energies will be more fruitful than a model-dependent analysis of each of the separate reactions. The common element in the "abnormal" processes (e.g. $\pi^- p \rightarrow K^o \Lambda^o$, $\pi^+ p \rightarrow K^+ Y^*(1385)$ and $\pi^- p \rightarrow \eta n$) seems to be the production of $\lambda\bar{\lambda}$ pairs and consequent high mass final states. Some analysis in terms of quark dynamics thus seems appropriate.

In the fourth chapter of this thesis we proposed an alternative method of obtaining information on strangeness-exchange amplitudes. Rather than parametrise data with a high-energy model which was known to be wrong,

we chose to attempt to calculate directly from data, the scattering amplitudes themselves. By studying the correlations observed in joint decay angular distributions it was shown how, but for one piece of information, all production amplitudes for processes like $\pi^- p \rightarrow K^* \Lambda$ could be disentangled in a completely unambiguous and model-independent manner. Having described the disadvantages of using conventional density matrices and statistical tensors to represent the decay information, we introduced a set of transversity-like amplitudes in terms of which we presented a complete analysis of $\pi^- p \rightarrow K^* \Lambda$ at 4 GeV. The simple relation between these new amplitudes and conventional helicity amplitudes was derived. The implications of the numerical results for $\pi^- p \rightarrow K^* \Lambda$ were discussed and, in particular, it was concluded that K exchange alone was insufficient to account for the measured unnatural parity exchange amplitudes. Since high statistics counter experiments on vector meson production processes are now a very real prospect, it is to be hoped that the methods proposed in the latter part of this thesis will, in the near future, be used to gain much needed insight into both natural and unnatural parity strangeness-exchange amplitudes.

APPENDIX 1

A. Kinematics

We consider the 2-body scattering process shown in Fig.(1A.1)

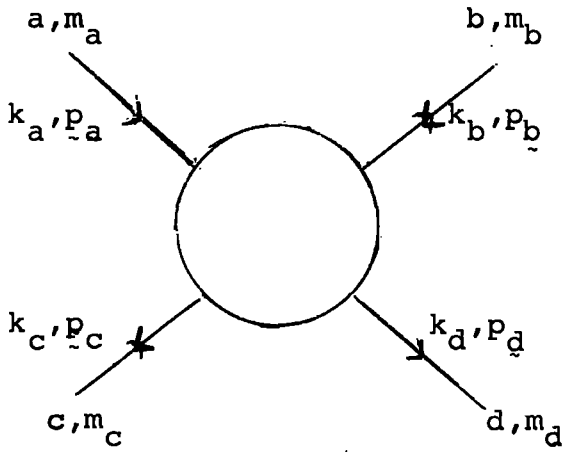

(1A.1)

Fig.(1A.1)

m_i are the particle masses and $k_i(p_i)$ are particle 4(3) - momenta in an arbitrary reference frame. We use a metric such that

$$k^2 = (-E, \underset{\sim}{p})^2 = \underset{\sim}{p}^2 - E^2 \qquad (1A.2)$$

where E is the total energy.

Conventionally we define

$$\begin{aligned} s &= -(k_a + k_b)^2 \\ t &= -(k_a - k_c)^2 \\ u &= -(k_a - k_d)^2 \end{aligned} \qquad (1A.3)$$

By s (t or u) - channel process we mean the process for which s (t or u) represents the total c.m. energy squared, viz.

$$\begin{aligned} &\text{s-channel:} \quad a + b \longrightarrow c + d \\ &\text{t-channel:} \quad a + \bar{c} \longrightarrow \bar{b} + d \\ &\text{u-channel:} \quad a + \bar{d} \longrightarrow c + \bar{b} \end{aligned} \tag{1A.4}$$

We use the following notation for kinematical quantities, standard throughout this thesis

q,q' — s-channel c.m. 3-momentum magnitudes of particles a and c.

p_L — beam particle laboratory momentum.

θ — s-channel c.m. scattering angle.

θ_t — t-channel c.m. scattering angle.

ψ_L — laboratory frame baryon recoil angle for near-forward scattering.

t_o — the value of t corresponding to $\theta = 0$.

Some useful relations involving these are collected together:-

$$s + t + u = m_a^2 + m_b^2 + m_c^2 + m_d^2 \tag{1A.5}$$

$$s = m_a^2 + m_b^2 + 2m_b\sqrt{p_L^2 + m_a^2} \tag{1A.6}$$

$$q = m_b p_L/\sqrt{s} \tag{1A.7}$$

$$q^2 = [s-(m_a + m_b)^2][s-(m_a - m_b)^2]/4s \tag{1A.8}$$

$$q'^2 = [s-(m_c + m_d)^2][s-(m_c - m_d)^2]/4s \tag{1A.9}$$

$$\cos\theta = \frac{s(t - u) + (m_a^2 - m_b^2)(m_c^2 - m_d^2)}{4sqq'} \tag{1A.10}$$

$$= 1 + \frac{t - t_o}{2qq'} \tag{1A.11}$$

$\cos\theta_t$ is found by replacing (s,t,m_b,m_c) by (t,s,m_c,m_d) in equations (1A.8) to (1A.10)

$$\tan\psi_L = \frac{m_b \sin\theta}{\frac{q}{q'}\sqrt{q'^2 + m_d^2} - \sqrt{q^2 + m_b^2}\cos\theta} \qquad (1A.12)$$

where ψ_L is in the first quadrant for near-forward scattering. In fact

$$\psi_L \longrightarrow \tfrac{\pi}{2}_-, \text{ as } s \longrightarrow \infty,\ t \longrightarrow 0_-. \qquad (1A.13)$$

$$t_o = m_a^2 + m_c^2 - 2\sqrt{(q^2 + m_a^2)(q'^2 + m_c^2)} + 2qq' \qquad (1A.14)$$

B. Helicity amplitude factorisation

We write the contribution of a single t-channel Regge pole (n) to s- and t-channel helicity amplitudes for the process $ab \longrightarrow cd$ as $H^{s(n)}_{cdab}$ and $H^{t(n)}_{\bar{b}da\bar{c}}$. Then [19]

$$H^{s(n)}_{cdab} = \sum_{\substack{a'\bar{c}' \\ \bar{b}'d'}} X^{\bar{b}'d'a'\bar{c}'}_{bdac}\ H^{t(n)}_{\bar{b}'d'a'\bar{c}'} \qquad (1B.1)$$

where $X^{\bar{b}'d'a'\bar{c}'}_{bdac} = d^{s_b}_{\bar{b}'b}(\chi_b)\ d^{s_d}_{d'd}(\chi_d)\ d^{s_a}_{a'a}(\chi_a)\ d^{s_c}_{\bar{c}'c}(\chi_c)$ (1B.2)

and s_i, χ_i is the spin and crossing angle [19] of particle i whose helicity is also represented by i. Note that X is exactly factorisable into four parts (one for each particle) at all energies.

We consider the four processes

$$\begin{aligned} a + b &\longrightarrow c + d \\ e + f &\longrightarrow g + h \\ e + b &\longrightarrow g + d \\ a + f &\longrightarrow c + h \end{aligned} \qquad (1B.3)$$

Then

$$H^{s(n)}_{gdeb}\ H^{s(n)}_{chaf} = \sum_{\substack{e^{l}\bar{g}^{l} \\ \bar{b}^{l}d^{l}}} \sum_{\substack{a^{l}\bar{c}^{l} \\ \bar{f}^{l}h^{l}}} X^{\bar{b}^{l}d^{l}e^{l}\bar{g}^{l}}_{bdeg}\ X^{\bar{f}^{l}h^{l}a^{l}\bar{c}^{l}}_{fhac}$$

$$\times\ H^{t(n)}_{\bar{b}^{l}d^{l}e^{l}\bar{g}^{l}}\ H^{t(n)}_{\bar{f}^{l}h^{l}a^{l}\bar{c}^{l}} \qquad (1B.4)$$

Following the Fox and Leader[113] we assume the asymptotic factorisation of t-channel Regge pole amplitudes,

$$H^{t(n)}_{\bar{b}^{l}d^{l}e^{l}\bar{g}^{l}}\ H^{t(n)}_{\bar{f}^{l}h^{l}a^{l}\bar{c}^{l}} \approx H^{t(n)}_{\bar{b}^{l}d^{l}a^{l}\bar{c}^{l}}\ H^{t(n)}_{\bar{f}^{l}h^{l}e^{l}\bar{g}^{l}} \qquad (1B.5)$$

so that equation (1B.4) becomes on substituting,

$$H^{s(n)}_{gdeb}\ H^{s(n)}_{chaf} \approx \sum_{\substack{e^{l}\bar{g}^{l} \\ \bar{b}^{l}d^{l}}} \sum_{\substack{a^{l}\bar{c}^{l} \\ \bar{f}^{l}h^{l}}} X^{\bar{f}^{l}h^{l}e^{l}\bar{g}^{l}}_{fheg}\ H^{t(n)}_{\bar{f}^{l}h^{l}e^{l}\bar{g}^{l}}$$

$$\times\ X^{\bar{b}^{l}d^{l}a^{l}\bar{c}^{l}}_{bdac}\ H^{t(n)}_{\bar{b}^{l}d^{l}a^{l}\bar{c}^{l}} \qquad (1B.6)$$

where we have regrouped the d^{s}- functions to form the new crossing matrix elements. Equation (1B.6) is now seen to contain the product of two s-channel amplitudes, thus

$$H^{s(n)}_{gdeb}\ H^{s(n)}_{chaf} \approx H^{s(n)}_{cdab}\ H^{s(n)}_{ghef} \qquad (1B.7)$$

i.e. for a given exchange, s-channel helicity amplitudes factorise as shown in Figure (1B.1)

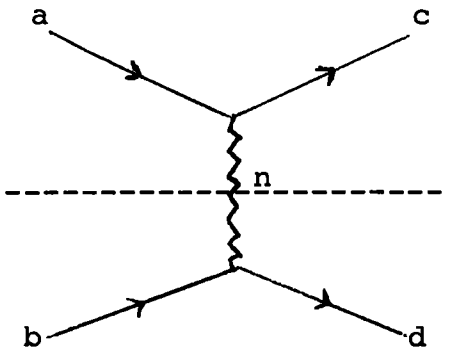

Fig.(1B.1)

into upper and lower vertex parts. It is this result which is used in reference (20), but note that the only asymptotic equality used is that in equation (1B.5) - the factorisability of the crossing matrix is <u>exact</u>.

APPENDIX 2

A. Experimental quantities

Our normalisation is such that

$$\frac{d\sigma}{dt} = \frac{0.3893}{64\pi q^2 s}\left[|A_o|^2 + |A_1|^2\right] \text{ millibarns/GeV}^2 \qquad (2A.1)$$

in the notation of Chapter 2 (A_n has units of GeV = 1). $\frac{d\sigma}{dt}$, the differential cross-section, is the reaction scattering probability per unit momentum-transfer squared[1]. With the Basle convention for the direction of the normal to the production plane, the recoil baryon polarisation is

$$P = \frac{2\ \mathrm{Im}(A_o A_1^*)}{|A_o|^2 + |A_1|^2} \qquad (2A.2)$$

If we define

$$\hat{R} = \frac{2\ \mathrm{Re}(A_o A_1^*)}{|A_o|^2 + |A_1|^2} \qquad (2A.3)$$

$$\hat{A} = \frac{|A_o|^2 - |A_1|^2}{|A_o|^2 + |A_1|^2} \qquad (2A.4)$$

then the Wolfenstein spin-correlation parameters[36,37] are

$$R = \hat{R}\sin\chi_L - \hat{A}\cos\chi_L \qquad (2A.5)$$

$$A = \hat{R}\cos\chi_L + \hat{A}\sin\chi_L$$

where χ_L, the laboratory frame baryon recoil angle, is given in equation (1A.12).

B. Absorption prescription

We follow the procedure of reference (30) whereby the partial wave exchange amplitude $f_\ell^{ex}(s)$ is modified by initial and final state absorption. Ignoring spin for the moment, the absorptive modification is

$$f_\ell(s) = f_\ell^{ex}(s) e^{2i\delta_\ell(el)} \tag{2B.1}$$

where $\delta_\ell(el)$ is the elastic phase shift which is given, in our normalisation, by

$$e^{2i\delta_\ell(el)} = 1 - \frac{iqf_\ell^{el}(s)}{4\pi\sqrt{s}} \tag{2B.2}$$

If equations (2B.1) and (2B.2) are used to modify a partial-wave decomposition of the amplitude $A^{ex}(s,t)$ we get

$$A(s,t) = A^{ex}(s,t) - \frac{iq}{4\pi\sqrt{s}} \sum_\ell (2\ell+1) P_\ell(\cos\theta)\, f_\ell^{ex}(s)\, f_\ell^{el}(s) \tag{2B.3}$$

Then, if the partial wave projection formula

$$f_\ell(s) = \frac{1}{2}\int_{-1}^{1} d(\cos\theta) P_\ell(\cos\theta) A(s,t) \tag{2B.4}$$

is substituted in equation (2B.3) and the orthogonality properties of the $P_\ell(\cos\theta)$ made use of, we get

$$A(s,t) = A^{ex}(s,t) - \frac{iq}{16\pi^2\sqrt{s}} \int d(\cos\theta_1) d\phi A^{ex}(s,\cos\theta_1) A^{el}(s,\cos\theta_2) \tag{2B.5}$$

where ϕ is some function[30] of $\cos\theta_1$ and $\cos\theta_2$ which need not concern us. The essential feature of the result (2B.5) is that absorption by partial wave modification by the relevant elastic S-matrix element gives a correction term which is a convolution integral of the exchange amplitude

and some elastic scattering amplitude which we may take to be saturated by Pomeron exchange i.e.

$$A^{el}(s,t) = -i4q^2\sigma_T e^{(A-i\pi\alpha_P^1)t/2} \qquad (2B.6)$$

A is the forward elastic peak slope width, α_P^1 the Pomeron trajectory slope and σ_T the relevant asymptotic total cross-section. In some sense (Section 3.2) the convolution integral then represents double Regge exchange, e.g. for $\pi^+p \longrightarrow K^+\Sigma^+$ this would be as shown in Figure (2B.1)

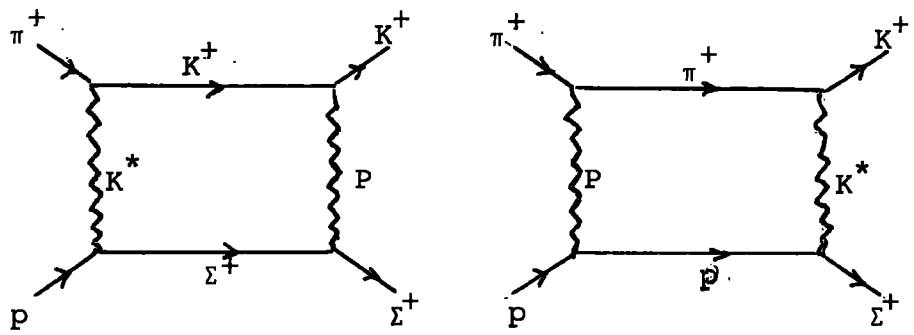

Fig. (2B.1)

The parameters A and σ_T should then be interpreted as some mean of those for π^+p and $K^+\Sigma^+$ scattering. Similarly the σ_T parameter in the correction term for $K^-p \longrightarrow \pi^-\Sigma^+$ scattering will be a mean of those for K^-p and $\pi^-\Sigma^+$ so that, treating P as an SU(3) singlet, σ_T is expected to have the same value for both line reversed reactions.

In the remainder of this Appendix we merely collect together the formulae used in Chapter 2 to calculate absorption corrections to meson baryon scattering. When spin is accounted for correctly, equation (2B.5) becomes

(equation A11b) of reference (30)).

$$A_n(s,t)=A_n^{ex}(s,t)-\frac{(-i)^n\sigma_T}{4\pi}\, e^{A't/2}\int_{-\infty}^{o}\frac{dt'}{2}\, e^{\frac{A't'}{2}}\, J_n(iA'\sqrt{(t-t_o)t'})A_n^{ex}(s,t') \tag{2B.7}$$

where

$$A' = A - i\pi\alpha'_P \tag{2B.8}$$

If A_n^{ex} is taken as

$$R_n(s,t) = \left(t_o-t\right)^{n/2} \gamma_n e^{\varepsilon n t}\left(se^{i\phi}\right)^{\alpha(t)} \tag{2B.9}$$

then

$$A_n(s,t) = R_n(s,t) + C_n(s,t) \tag{2B.10}$$

where

$$C_n(s,t)=-\left(t_o-t\right)^{n/2}\gamma_n\frac{gT}{4\pi}\left(se^{i\phi}\right)^{\alpha_o}\left(\frac{A'}{A'+B}\right)^n e^{\left(\frac{A'B}{A'+B}\right)\frac{t-t_o}{2}} e^{\frac{Bt_o}{2}} \tag{2B.11}$$

and

$$\frac{B}{2} = \varepsilon_n + \alpha'(\log s + i\phi) \tag{2B.12}$$

For the reasons outlined in Section 2.3(b) we include an enhancement factor λ_n to multiply $C_n(s,t)$ in equation (2B.10).

APPENDIX 3

A. Coupling signs in KN and πN scattering

Consider a simple pole description of KN and πN elastic scattering.

(a) KN

If P, f, ω, ρ and A_2 poles couple to K^-p scattering such that

$$A(K^-p) = P + f + \omega + \rho + A_2, \qquad (3A.1)$$

then

$$A(K^+p) = P + f - \omega - \rho + A_2 \qquad (3A.2)$$

$$A(K^-n) = P + f + \omega - \rho - A_2 \qquad (3A.3)$$

$$A(K+n) = P + f - \omega + \rho - A_2 \qquad (3A.4)$$

We assume (ω, f) and (ρ, A_2) to be EXD pairs of poles with intercepts $\alpha_o = \frac{1}{2}$ so that at $t = 0$,

$$P = i\gamma_P, \quad = \gamma_\omega (1+i), \quad A_2 = \gamma_{A2}(1-i) \text{ etc.} \qquad (3A.5)$$

where γ_i are real couplings. EXD then implies

$$\gamma_f = -\gamma_\omega, \quad \gamma\rho = -\gamma_{A2} \qquad (3A.6)$$

Then

$$A(K^+p) + A(K^+n) = 2i\gamma_P - 4\gamma_\omega \qquad (3A.7)$$

and

$$A(K^-p) + A(K^-n) = 2i\gamma_P + 4i\gamma_\omega \qquad (3A.8)$$

Using the optical theorem we obtain

$$\sigma_T(K^-p) + \sigma(K^-n) - \sigma_T(K^+p) - \sigma_T(K^+n) = 4\gamma_\omega \qquad (3A.9)$$

$$\simeq +13.6 \pm 4.4 \text{ mb}$$

at 4 GeV by inspection of the total cross-section data[114]. That is the ω + f contributions to $A(K^-p)$ in equation (3A.1)

$$\omega + f = 2i\gamma_\omega \qquad (3A.10)$$

has the same phase at t = 0 as the Pomeron contribution and therefore adds <u>constructively</u>.

(b) <u>πN</u>

We wish to calculate the relative coupling signs of P and f in πN elastic scattering. As in the KN case, the sum of the amplitudes for all charged states only involves the contribution P + f. That is if

$$A(\pi^-p) = P + f + \rho \qquad (3A.11)$$

then

$$A(\pi^+p) = P + f - \rho \qquad (3A.12)$$

so that

$$\text{Im } A(\pi^-p) + \text{Im } A(\pi^+p) = 2\text{Im}(P+f) \qquad (3A.13)$$

Unlike the KN case it is not possible to directly isolate the f contribution using EXD arguments. It is enough however to note[114] that, experimentally, the quantity $\sigma_T(\pi^-p) + \sigma_T(\pi^+p)$ <u>falls</u> to its constant Pomeron dominated value, in order to see that the P and f contributions <u>add</u> in πN scattering.

APPENDIX 4

A. Double density matrix expansion

By expanding equation (4.1.7) and substituting the inverse of equation (4.1.9) the following expression is obtained[106] for helicity-type axes,

$$3W(\theta_1,\phi_1,\theta_2,\phi_2) = 1 - 4\sqrt{\frac{\pi}{5}}\, Y_2^0(1)\, F_1 + 24\sqrt{\frac{\pi}{15}}\, \mathrm{Re}\, Y_2^1(1)\, F_2$$

$$-12\sqrt{\frac{2\pi}{15}}\, \mathrm{Re}\, Y_2^2(1) F_3 + 4\alpha\sqrt{\frac{2\pi}{3}}\, \mathrm{Im}\, Y_1^1(2) F_4 - \frac{16\pi\alpha}{\sqrt{5}}\, Y_1^0(2)\, \mathrm{Im}\, Y_2^1(1)\, F_5$$

$$+ 8\pi\alpha\sqrt{\frac{2}{5}}\, Y_1^0(2)\, \mathrm{Im}Y_2^2(1)\, F_6 - 8\pi\alpha\sqrt{\frac{2}{15}}\, \mathrm{Im}Y_1^1(2)Y_2^0(1)F_7$$

$$+ 16\pi\alpha\sqrt{\frac{2}{5}}\, \mathrm{Re}\, Y_1^1(2)\, \mathrm{Im}Y_2^1(1)F_8 + 16\pi\alpha\sqrt{\frac{2}{5}}\, \mathrm{Im}Y_1^1(2)\, \mathrm{Re}Y_2^1(1)F_9$$

$$- 16\pi\alpha\sqrt{\frac{1}{5}}\, \mathrm{Re}\, Y_1^1(2)\, \mathrm{Im}Y_2^2(1)F_{10} - 16\pi\alpha\sqrt{\frac{1}{5}}\, \mathrm{Im}Y_1^1(2)\, \mathrm{Re}Y_2^2(1)F_{11} \qquad (4A.1)$$

where

$$F_1 = \rho_{11} - \rho_{00} \qquad F_6 = \mathrm{Im}(\rho^{1-1}_{\frac{1}{2}\frac{1}{2}} - \rho^{1-1}_{-\frac{1}{2}-\frac{1}{2}})$$

$$F_2 = \mathrm{Re}\rho_{10} \qquad F_7 = \mathrm{Im}(\rho^{11}_{\frac{1}{2}-\frac{1}{2}} + \rho^{-1-1}_{\frac{1}{2}-\frac{1}{2}} - 2\rho^{00}_{\frac{1}{2}-\frac{1}{2}})$$

$$F_3 = \rho_{1-1} \qquad F_{\substack{8\\9}} = \mathrm{Im}(\rho^{10}_{\frac{1}{2}-\frac{1}{2}} \pm \rho^{10}_{-\frac{1}{2}\frac{1}{2}})$$

$$F_4 = \mathrm{Im}\rho_{\frac{1}{2}-\frac{1}{2}} \qquad F_{\substack{10\\11}} = \mathrm{Im}(\rho^{1-1}_{\frac{1}{2}-\frac{1}{2}} \pm \rho^{1-1}_{-\frac{1}{2}\frac{1}{2}})$$

$$F_5 = \mathrm{Im}(\rho^{10}_{\frac{1}{2}\frac{1}{2}} - \rho^{10}_{-\frac{1}{2}-\frac{1}{2}}) \qquad (4A.2)$$

In equation (4A.1) $Y_J^M(i)$ denotes $Y_J^M(\theta_i,\phi_i)$ and α is the lambda decay asymmetry parameter, α_Λ[98] which is about 0.65 in value. Note that in reference (106) the additional factor of ½ in the expressions given for

F_8, F_9, F_{10} and F_{11} should not be present.

B. Angular momentum functions

The $d^J_{m',m}(\theta)$ functions for $J = \frac{1}{2}$ and 1 are

$d^{\frac{1}{2}}_{m',m}$:

m' \ m	$\frac{1}{2}$	$-\frac{1}{2}$
$\frac{1}{2}$	$\cos\frac{\theta}{2}$	$-\sin\frac{\theta}{2}$
$-\frac{1}{2}$	$\sin\frac{\theta}{2}$	$\cos\frac{\theta}{2}$

(4B.1)

$d^{1}_{m',m}$:

m' \ m	1	0	-1
1	$\frac{1}{2}(1+\cos\theta)$	$-\frac{1}{\sqrt{2}}\sin\theta$	$\frac{1}{2}(1-\cos\theta)$
0	$\frac{1}{\sqrt{2}}\sin\theta$	$\cos\theta$	$-\frac{1}{\sqrt{2}}\sin\theta$
-1	$\frac{1}{2}(1-\cos\theta)$	$\frac{1}{\sqrt{2}}\sin\theta$	$\frac{1}{2}(1+\cos\theta)$

(4B.2)

The first few normalised spherical harmonic functions are

$$Y^0_0(\theta,\phi) = \frac{1}{\sqrt{4\pi}} \tag{4B.3}$$

$$Y^0_1(\theta,\phi) = \sqrt{\frac{3}{4\pi}}\cos\theta, \quad Y^{\pm 1}_1(\theta,\phi) = \mp\sqrt{\frac{3}{8\pi}}\sin\theta e^{\pm i\phi} \tag{4B.4}$$

$$Y^0_2(\theta,\phi) = \sqrt{\frac{5}{16\pi}}(3\cos^2\theta-1), \quad Y^{\pm 1}_2(\theta,\phi) = \mp\sqrt{\frac{15}{8\pi}}\cos\theta\sin\theta e^{\pm i\phi}$$

$$Y^{\pm 2}_2(\theta,\phi) = \sqrt{\frac{15}{32\pi}}\sin^2\theta e^{\pm 2i\phi} \tag{4B.5}$$

C. Maximum likelihood error estimation

We use a log-likelihood function

$$W(P) = - \log \left[L(P) \right] \tag{4C.1}$$

where

$$L(P) = \prod_{i=1}^{N} W(P;X_i)^{\omega g^i} \tag{4C.2}$$

and $W(P;X_i)$ is the angular distribution of Chapter 4. In equation (4C.2) P represents a set of parameters $p_j (j = 1,10)$ (e.g. 6 amplitude moduli and 4 phases) and X_i the set of 6 direction cosines for event i. ωg^i is a number less than 15% greater than 1 called the geometrical weight and assigned to each event(i) by the experimentalist to account for unseen neutral decays in the bubble chamber. Its motivation is, heuristically, as follows.

$W_i = W(P;X_i)$ is the probability of observing 1 event at X_i and to get the joint probability for N events we form a product. Suppose for every event actually observed at X_i there were, statistically speaking, ωg^i real events. Then the "joint" probability for this would be $W_i^{\omega g^i}$. For all N observed events the joint probability (4C.2) is then obtained.

The covariance matrix associated with the set of parameters $\bar{P}$ with maximum likelihood is[107]

$$\underline{C} = \text{cov}(\bar{P}) = \underline{H}^{-1} \underline{H}^{1} \underline{H}^{-1} \tag{4C.3}$$

where the matrices $\underline{H}$ and $\underline{H}^{1}$ are given by

$$H_{k\ell} = \frac{1}{N} \sum_{i=1}^{N} \frac{\omega_g^i}{W_i^2} \left(\frac{\partial W_i}{\partial p_k}\right) \left(\frac{\partial W_i}{\partial p_\ell}\right) \tag{4C.4}$$

$$H^1_{k\ell} = \frac{1}{N} \sum_{i=1}^{N} \frac{\omega_g^{i\,2}}{W_i^2} \left(\frac{\partial W_i}{\partial p_k}\right) \left(\frac{\partial W_i}{\partial p_\ell}\right) \tag{4C.5}$$

The estimated errors ΔP to be assigned the parameters $\bar{P}$ are got directly from the variances,

$$\Delta p_k = \sqrt{\frac{C_{kk}}{N}} \tag{4C.6}$$

For any other measureable quantity

$$m = m(\bar{P}) \tag{4C.7}$$

the estimated error is

$$\Delta m = \frac{1}{\sqrt{N}} \sqrt{\sum_{k,\ell} \frac{\partial m}{\partial p_k} \frac{\partial m}{\partial p_\ell} C_{k\ell}} \tag{4C.8}$$

References

1. (a) A.D. Martin, T.D. Spearman, 'Elementary Particle Theory' (North Holland, Amsterdam 1970).
   (b) R.J. Eden, P.V. Landshoff, D.I. Olive, J.C. Polkinghome, 'The Analytic S-Matrix' (Cambridge University Press (1966)).
2. M. Gell-Mann, Phys. Rev. 125, 1067 (1962).
3. Y. Ne'eman, Nucl. Phys. 26, 222 (1961).
4. M. Gell-Mann, Phys. Rev. 92, 833 (1953).
   K. Nishijima, Fortschr. Physik 4, 519 (1956).
5. H.J. Lipkin, Nucl. Phys. B9, 349 (1969).
6. S. Mandelstam, Phys. Rev. 112, 1344 (1958).
7. e.g. J.M. Blatt, V.F. Weisskopf, 'Theoretical Nuclear Physics' (Wiley, New York (1952)).
8. e.g. J.D. Jackson, Nuovo Cimento 34, 1644 (1964).
9. T. Regge, Nuovo Cimento 14, 951 (1959).
10. P.D.B. Collins, E.J. Squires, 'Regge Poles in Particle Physics' (Springer, Berlin (1968)).
11. E.C. Titchmarsh, 'The Theory of Functions' (Oxford University Press (1950)).
12. R. Dolen, D. Horn, C. Schmid, Phys. Rev. 166, 1768 (1968).
13. V. Barger, C. Michael, Phys. Rev. 186, 1592 (1969).
14. M. Gell-Mann, Phys. Rev. Letters 8, 263 (1962).

15. L. Bertocchi, 'Proc. Heidelberg Conf. on Elementary Particles, Sept. 1967' ed. H. Filthuth (North Holland (1968)).

16. e.g. References (22, 71).

17. G.F. Chew, S.C. Frautschi, Phys. Rev. Letters 8, 41 (1962).

18. M. Jacob, G.C. Wick, Ann. Phys. 7, 404 (1959).

19. T.L. Trueman, G.C. Wick, Ann. Phys. 26, 332 (1964).

20. G. Cohen-Tannoudji, Ph. Salin, Nuovo Cimento 55A, 412 (1968).

21. J.D. Jackson, G.E. Hite, Phys. Rev. 169, 1248 (1968).

22. G.E. Hite, Rev. Mod. Phys. 41, 669 (1969).

23. P. Bonamy et al., Phys. Letters 23B, 501 (1966).

24. V.N. Gribov, I.Y. Pomeranchuk, 'Proc. 1962 CERN Conf. on High Energy Physics'.

25. J.D. Jackson, H. Pilkuhn, Nuovo Cimento 33, 906 (1964).

26. K. Gottfried, J.D. Jackson, Nuovo Cimento 34, 735 (1964).

27. B.M. Udgaokar, M. Gell-Mann, Phys. Rev. Letters 8, 346 (1962).

28. R.C. Arnold, Phys. Rev. 153, 1523 (1967).

29. G. Cohen-Tannoudji, A. Morel, H. Navelet, Nuovo Cimento 48A, 1075(1967).

30. F. Henyey, G.L. Kane, J. Pumplin, M. Ross, Phys. Rev. 182, 1579 (1969).

31. G. Cohen-Tannoudji, A. Morel, H. Navelet, Nuovo Cimento 48A, 1075 (1967).

32. G.L. Kane, F. Henyey, D.R. Richards, M. Ross, G. Williamson, Phys. Rev. Letters 25, 1519 (1970).

33. See e.g. Reference (98).

34. H. Harari, Phys. Rev. Letters 22, 562 (1969). J.L. Rosner, Phys. Rev. Letters 22, 689 (1969).

35. J.S. Ball, G. Marchesini, Phys. Rev. 188, 2508 (1969).

36. L. Wolfenstein, Phys. Rev. 96, 1654 (1954).

37. W. Rarita, R. Ridell, C.B. Chiu, R.J.N. Phillips, Phys. Rev. 165, 1615 (1968).

38. M. Spiro, A. Derem, Lett. Nuovo Cimento 4, 593 (1970).

39. G.C. Fox, 'High Energy Collisions' (Gordon and Breach 1969)).

40. D.J. Harrison, A.C. Irving, A.D. Martin, Durham University Report, DTP/C71/5, submitted to Computer Physics Communications.

41. E.L. Berger, G.C. Fox, Nucl. Phys. B26, 1, (1971).

42. A.C. Irving, A.D. Martin, C. Michael, Nucl Phys. B32, 1 (1971).

43. $K^- p \longrightarrow \pi Y$ Data

(a) J. Badier et al., Saclay Reprint CEA-R3037 (1966).

(b) M. Haque et al., Phys. Rev. 152, 1148 (1966).

(c) L. Moscoso et al, Saclay - E.P. preprint (1970).

(d) J.S. Loos et al., Phys. Rev. 173, 1330 (1968).

(e) D. Birnbaum et al., Phys. Letters 31B, 484 (1969).

44. $K^- n \longrightarrow \pi Y$ Data

(a) R. Barloutaud et al., Nucl. Phys. B9, 493 (1969).

(b) D.J. Crennel et al., Phys. Rev. Letters 23, 1347(1969).

(c) W.L. Yen et al., Purdue preprint COO-1428-140 (1969).

45. $\overline{K}^o p \longrightarrow \pi Y$ Data

A.D. Brody et al., SLAC preprint PUB 823 (1970).

46. $\pi^+ p \longrightarrow KY$ Data

(a) S.M. Pruss et al., Phys. Rev. Letters 23, 189 (1969).

(b) H.S. Han et al., Phys. Rev. Letters 24, 1353 (1970).

(c) C.W. Akerlof et al., Michigan preprint (1970).

(d) C.W. Akerlof et al., Michigan preprint UM-HE-70-19(1971).

(e) A. Bashian et al., Stony Brook preprint (1970).

47. $\pi^- p \longrightarrow KY$ Data

(a) O.I. Dahl et al., Phys. Rev. 163, 1430 (1967).

(b) M. Abramovich et al., CERN preprint D.Ph.II/70-23(1971).

(c) R. Ehrlich et al., Phys. Rev. 152, 1194 (1966).

(d) E. Bertolucci et al., Lett. Nuovo Cimento 2, 149(1969).

(e) S. Ozaki et al., Brookhaven preprint (1970).

48. E.W. Anderson et al., Phys. Rev. Letters 20, 1929 (1968).

49. K. Wu Lai, J. Louie, Nucl. Phys. B19, 205 (1970).

50. C. Michael, R. Odorico, Phys. Letters 34B, 422 (1971)

51. D.D. Reeder, K.V.L. Sarma, Phys. Rev. 172, 1566 (1968).

52. D.P. Roy et al., Phys. Letters 34B, 512 (1971).

53. R.J.N. Phillips, Rutherford Laboratory preprint RPP/C/24 (1971).

54. e.g. V. Barger, D. Cline, 'Phenomenological Theories of High Energy Scattering' (Benjamin, New York (1969)).

55. C. Meyer, Y. Noirot, M. Rimpault, Ph. Salin, Nucl. Phys. B23, 99 (1970).

56. M. Rimpault, Ph. Salin, Nucl. Phys. B22, 235 (1970).

57. P.A. Collins et al., Nucl. Phys. B20, 381 (1970).

58. J.V. Allaby et al., Phys. Letters 30B, 500 (1969).

59. M. Borghini et al., Phys. Letters 31B, 405 (1970).

60. E. Berger, G.C. Fox, Phys. Rev. Letters 25, 1783 (1970).

61. M. Gourdin, 'Unitary Symmetries and their application to High Energy Physics' (North Holland, Amsterdam (1967)).

62. C. Michael, Springer Tracts in Modern Physics 55, 174 (1970).

63. C. Michael, Nucl. Phys. B13, 644 (1969).
C. Michael, Phys. Letters 29B, 230 (1969).

64. C. Schmid, J.K. Storrow, Nucl. Phys. B29, 219 (1971).

65. R.D. Field, J.D. Jackson, Univ. of California preprint UCRL-20287 (1971).

66. Particle Data Group, Rev. Mod. Phys. 43, No.2(1971).

67. C.W. Akerlof et al., Univ. of Michigan preprint HE-71-14 (1971).

68. H. Harari, Phys. Rev. Letters 26, 1079(1971).

69. V. Chabaud et al., Phys. Letters 38B, 445 (1972).

70. S. Mandelstam, Nuovo Cimento 30, 1127, 1148 (1963).

71. P.D.B. Collins, Phys. Reports 1C, No.4 (1971).

72. V. Gribov, Zk. Eksp. i Teor. Fiz. 53, 654 (1967).

73. G. Veneziano, Nuovo Cimento 57A, 190 (1968).

74. K. Kikkawa, B. Sakita, M. Virasovo, Phys. Rev. 184, 1701 (1969).

75. J. Finkelstein, CERN preprint TH-1306.

76. C. Lovelace, Phys. Letters 36B, 127 (1971).

77. R. Rivers, J. Scanio, Phys. Rev. 188, 2170 (1969).

78. J. Schwarz, Phys. Rev. 159, 1269 (1967).

79. e.g. J.D. Jackson, Univ. of California preprint UCRL-19205 (1969).

80. F.S. Henyey, G.L. Kane, J.J.G. Scanio, Univ. of Michigan preprint UM-HE-71-12 (1971).

81. N.W. Dean, Nucl. Phys. B7, 311 (1968).

82. R.J. Rivers, Nuovo Cimento 57A, 174 (1968).

83. C. Quigg, Univ. of California preprint UCRL-20032(1970).

84. F.D. Gault, A.D. Martin, Private Communication (1971).

85. B. Petersson, G.H. Thomas, Nucl. Phys. B20, 451 (1970).

86. C. Quigg, Nucl. Phys. B29, 67 (1971).

87. L. Stodolsky, J.J. Sakurai, Phys. Rev. Letters 11, 90 (1963).

88. A.B.B.B.H.L. Collaboration, Phys. Letters 10, 229 (1964).

89. P.J. O'Donovan, Univ. of Colorado preprint ASA-HEP-20 (1971).

90. e.g. C. Schmid, CERN preprint TH-1343.
M. Davier, H. Harari, Phys. Letters 35B, 239 (1971).
H. Harari, Ann. Phys. 63, 432 (1971).

91. A. de Lesquen et al., communication to the Amsterdam International Conference on Elementary Particles (1971).

92. F. Halzen, C. Michael, Phys. Letters 36B, 367 (1971).

93. V. Barger, R.J.N. Phillips, Phys. Rev. 187, 2210 (1969).

94. G.V. Dass, C. Michael, R.J.N. Phillips, Nucl. Phys. B9, 549 (1969).

95. H. Högaasen, C. Michael, CERN preprint TH-1442 (1971).

96. G. Fox, Cal. Inst. of Technology preprint CALT-68-334 (1971).

97. K. Gottfried, J.D. Jackson, Nuovo Cimento 33, 309 (1964).

98. J.W. Cronin, O.E. Overseth, Phys. Rev. 129, 1795 (1963).

99. H. Pilkuhn, B.E. Svensson, Nuovo Cimento 38, 518 (1965).

100. A. Kotański, Hercig Novi Summer School in Elementary Particles (1970).
A. Kotański, K. Zalewski, Nucl. Phys. B4, 559 (1968); B20, 236 (1970) (E).

101. P. Minnaert, Proceedings of the Ecole d'Eté de Physique Théorique, Les Houches (1971) to be published (Gordon and Breach, New York).

102. M. Abramovich et al., Nucl. Phys. B39, 189 (1972).

103. N. Byers, C.N. Yang, Phys. Rev. 135B, 796 (1964).

104. A. Kotański, Acta Phys. Polonica 29, 699 (1966); 30, 629 (1966).

105. M. Abramovich, A.C. Irving, A.D. Martin, C. Michael, Phys. Letters 39B, 353 (1972).

106. P.A. Schreiner, Univ. of California (UCLA) Thesis (1970).

107. W.T. Eadie et al, 'Statistical Methods in Experimental Physics' (North Holland, Amsterdam (1971)).

108. e.g. G.A. Ringland, R.L. Thews, Phys. Rev. 170, 1569 (1968).

109. R.D. Fields, Brookhaven preprint BNL-16562 (1972).

110. M. Aguilar-Benitez, S.U. Chung, R.L. Eisner, N.P. Samios, Phys. Rev. Letters 28, 574 (1972).

111. e.g. Table 4 of F.D. Gault, H.F. Jones, Nucl. Phys. B30, 68 (1971).

112. G.G. Beznogikh et al, Phys. Letters 30B, 274 (1969).

113. G.C. Fox, E. Leader, Phys. Rev. Letters 18, 628 (1967).

114. High-Energy Reactions Analysis Group, 'Compilation of Total Cross Sections,' CERN/HERA 70-1,6 (1970).

115. G. Moorhouse, Private Communication (1971).

116. D. Sutherland, Private Communication (1971).

117. K. Kajantie, J.S. Trefil, Phys. Letters 24B, 106 (1967).

118. S.Y. Lo, Glasgow Univ. preprint (April 1972).

119. A. Krzywicki, J. Tran Thanh Van, Phys. Letters 30B, 185 (1969).